Anal. Methods Environ. Chem. J. 5 (2) (2022) 5-23

AMECJ

Research Article, Issue 2
Analytical Methods in Environmental Chemistry Journal
Journal home page: www.amecj.com/ir

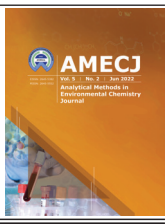

Analysis of complexation between new bidentate bis-NHC ligand and some metal cations at different temperature

Nur Rahimah Said [a], Majid Rezayi [b,c,d,*], Ninie Suhana Abdul Manan [e,f], Amirhossein Sahebkar [g,h,m,n], and Yatimah Alias [e,f,*]

[a] *School of Chemistry and Environment, Faculty of Applied Sciences, Universiti Teknologi MARA (UiTM), Cawangan Negeri Sembilan, Kampus Kuala Pilah, 72000 Kuala Pilah, Negeri Sembilan, Malaysia*
[b] *Medical Toxicology Research Center, Mashhad University of Medical Sciences, Mashhad, Iran*
[c] *Metabolic Syndrome Research Center, Mashhad University of Medical Science, Mashhad, Iran*
[d] *Department of Medical Biotechnology and Nanotechnology, School of Medicine, Mashhad University of Medical Sciences, Mashhad, Iran*
[e] *Department of Chemistry, Faculty of Science, University of Malaya Centre for Ionic Liquids, University of Malaya, 50603, Kuala Lumpur, Malaysia*
[f] *Department of Chemistry, Faculty of Science, University of Malaya, Kuala Lumpur 50603, Malaysia*
[g] *Biotechnology Research Center, Pharmaceutical Technology Institute, Mashhad University of Medical Sciences, Mashhad, Iran*
[h] *Applied Biomedical Research Center, Mashhad University of Medical Sciences, Mashhad, Iran*
[m] *School of Medicine, The University of Western Australia, Perth, Australia*
[n] *Department of Biotechnology, School of Pharmacy, Mashhad University of Medical Sciences, Mashhad, Iran.*

ARTICLE INFO:

Received 25 Jan 2022
Revised form 10 Apr 2022
Accepted 12 May 2022
Available online 28 Jun 2022

Keywords:
Analysis,
Complexation process,
Ligand,
Conductometric method,
Binary mixed solvent,
Thermodynamic parameters.

ABSTRACT

In this research, the determination and complexation process between 3,3'-(2,2'-(4-methyl-phenylenesulfonamido)bis(ethane-2,1-diyl)) bis(1-benzyl-3H-benzo[d]imidazol-1-ium)dibromide with Ni^{2+}, Zn^{2+}, Pd^{2+}, Ag^{+}, and Hg^{2+} cations in the binary mixture of methanol (MeOH) and water (H_2O) at different temperatures (15, 25, 35 and 45ºC) were studied using a conductometric method. The results show that the stoichiometry of the complexes in all binary mixed solvents for Ni^{2+}, Zn^{2+}, and Pd^{2+} were 1:1 (M:L), while in other cases 1:2 (M:L) and 2:1(M:L). The stability constants (log) of complex formation have been determined by fitting molar conductivity curves using a computer program (GENPLOT). The obtained data shows that in the pure methanol solvent system, the stability order is Ni^{2+}< Pd^{2+}<Zn^{2+}<Hg^{2+}<Ag^{+} and the complexation process seems more stable in pure methanol in most cases. The thermodynamic parameters $(\Delta G_C^o, \Delta H_C^o, \Delta S_C^o)$ were determined conductometrically. The complexes in all cases were found to be enthalpy destabilized but entropy stabilized. The experimental data was tested by using an artificial neural network (ANN) program and was in good agreement with the estimated data.

1. Introduction

In early 1968, Wanzlick and Schönherr pioneered scientists that convey N-Heterocyclic carbene (NHC) complexation to a gained general acceptance among the researchers [1]. This effort was followed by Ardueng who found the stable crystalline carbene in 1991 [2]. In the meantime, numerous studies have been reported with the various applications so far. NHCs ligands synthesized from benzimidazole and imidazole were founded as attractive ligands for complexation due to their structure variety and stability [3]. Generally, it is more stable than other types of carbenes, such as the Fisher and Schrock carbenes [4]. Furthermore, these types of ligands can bond to either hard and soft transition metal ions or atoms through strong chelation [5-9]. Several articles have described

*Corresponding Author: Nur Rahimah Said and Majid Rezayi
Email: rezaeimj@mums.ac.ir, yatimah70@um.edu.my
https://doi.org/10.24200/amecj.v5.i02.169

the interesting features of NHC ligands and their metal complexes in detail, especially on their C-C coupling catalysis activities [10-13]. Recently, its application as an anticancer activity was also reported [14-18]. Several bidentate bis-NHC ligands derived from benzimidazole and imidazole with a different bridging linker have been reported [19-23]. The types of bridging linkers play the main role in the coordination of metal complexes. Different types of bridging linkers will be offered for the different conformations of complexes. This is related to the flexibility, length, and size of linkers [5]. In addition, different cavity sizes of ligand, ionic radii of metal [24], and solvent systems are the important factors that can influence the stability of complexation formation [25].

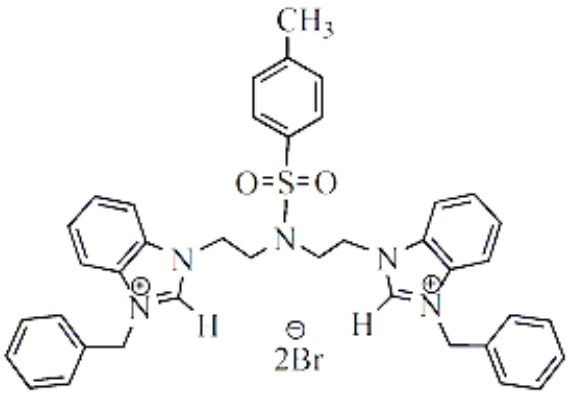

Fig. 1. 3,3'-(2,2'-(4-methyl-phenylenesulfonamido) bis(ethane-2,1-diyl))bis(1-benzyl-3H-benzo[d] imidazol-1-ium)dibromide, (NHCL)

To our certain knowledge, there have been few reports of the thermodynamic study of bidentate bis-NHC ligand complexes with different metal ions. This encouraged us to investigate the effects of pure and binary solvent mixtures on stability constants and thermodynamic parameters of complexes. In our study, bidentate bis-NHC ligand connected by sulfonamide moiety was designated and synthesized by a simple and efficient method [3, 19], namely 3,3'-(2,2'-(4-methyl-phenylenesulfonamido) bis(ethane-2,1-diyl))bis(1-benzyl-3H-benzo[d] imidazol-1-ium)dibromide (NHCL) (Fig. 1). To determine the stability, selectivity and stoichiometry of NHCL-M^{n+} complexes with different metal cations, the conductometric technique was chosen [26]. This technique has several advantages such as great sensitivity [27], low cost [28] as well as simple experimental arrangement [29] compared with other techniques such as spectrophotometry, calorimetry [30], and NMR spectroscopy [31], and potentiometry [32-35]. The sensors based on electrochemical methods have been used to measure the analyte concentrations in water samples. Hence, electroanalytical techniques such as, potentiometry, voltammetry, and conductometry have been extensively reported. Other techniques such as inductively coupled plasma mass spectrometry [36], co-precipitation [37], flame atomic absorption spectrometry (F-AAS) [38], inductively coupled plasma optical emission spectrometry (ICP-OES) [39], and electrothermal atomic absorption spectrometry (ETAAS) [40] have also been used for the determination cations in water samples after complexation process. Thus, this study can contribute to a better understanding of ligand character and behavior in coordination chemistry, and the solvent effect in its complexation process.

2. Experimental

2.1. Chemicals and Instruments

The chemicals and metal ions used, which are nickel acetate, zinc acetate, palladium acetate, silver acetate, and mercury nitrite were purchased from Sigma-Aldrich (USA) and MERCK (Germany). All chemicals were analytical grade and used without further purification. Deionized distilled water and methanol with HPLC grade available from MERCK (Germany) were used as a solvent. The conductometric measurements were carried out using a digital Thermo Scientific conductivity device in a JULABO F12 thermostat water bath with a constant temperature maintained within ±0.01ºC. A conductometric cell model Orion 013005MD with a cell constant of 0.99cm^{-1} was used throughout the studies.

2.2. Synthesis of the bidentate bis-NHC ligand, NHCL

Several steps synthesized NHCL (**4**) from the diol (**1**) are shown in Figure 2. The synthesis of compounds (**2**) and (**3**) has been reported previously [19]. NHCL (**4**) was prepared according to the modification method designated as follows [3]. Benzyl bromide (0.1710 g, 1.0 mmol) was stirred in 20 ml of 1,4-dioxane, and then compound (**3**) (0.2296 g, 0.5 mmol) was added to it. The reaction mixture was refluxed at 100 ºC for 12 hours and the pale yellow precipitated was obtained. The product was collected by filtration, washed with fresh 1,4-dioxane (2×5 mL) and diethyl ether (2×5 mL) and dried in vacuo to give a pale yellow powder (**4**).

2.3. Analysis procedure

These experimental designs were prepared according to the altered procedure [41-43] and were applied to all metal cations; Ni^{2+}, Zn^{2+}, Pd^{2+}, Hg^{2+}, and Ag^{+}. The formation constant of the complexes will be obtained by using the procedure designated as follow. A solution of the metal ion with a concentration, of 5.0×10^{-5}M was prepared and fixed in a titration cell. After that, the *L* with concentration 2.5×10^{-3}M was added to the titration cell using a micropipette. During the reaction, the desired temperature was fixed and a magnetic stir has been used to form a homogenized condition in the titration cell. The conductivity values were measured before and after each titration of ligands solution. The procedure was repeated for all metal cations in the MeOH-H_2O binary system (mol MeOH; 0.00, 9.99, 22.66, 39.73, 63.72 and 100.00%) at different temperatures (15, 25, 35 and 45ºC).

3. Results and discussion

The general reaction for complex formation (1:1) can be stated by Equation 1 and the corresponding equilibrium constant (K_f), is given by Equation 2.

$$M^{n+} + NHCL \leftrightarrow NHCLM^{n+} \qquad \text{(Eq.1)}$$

$$K_f = \frac{[NHCLM^{n+}]f_{(NHCLM^{n+})}}{[M^{n+}][NHCL]f_{(M^{n+})}f_{(NHCL)}} \qquad \text{(Eq.2)}$$

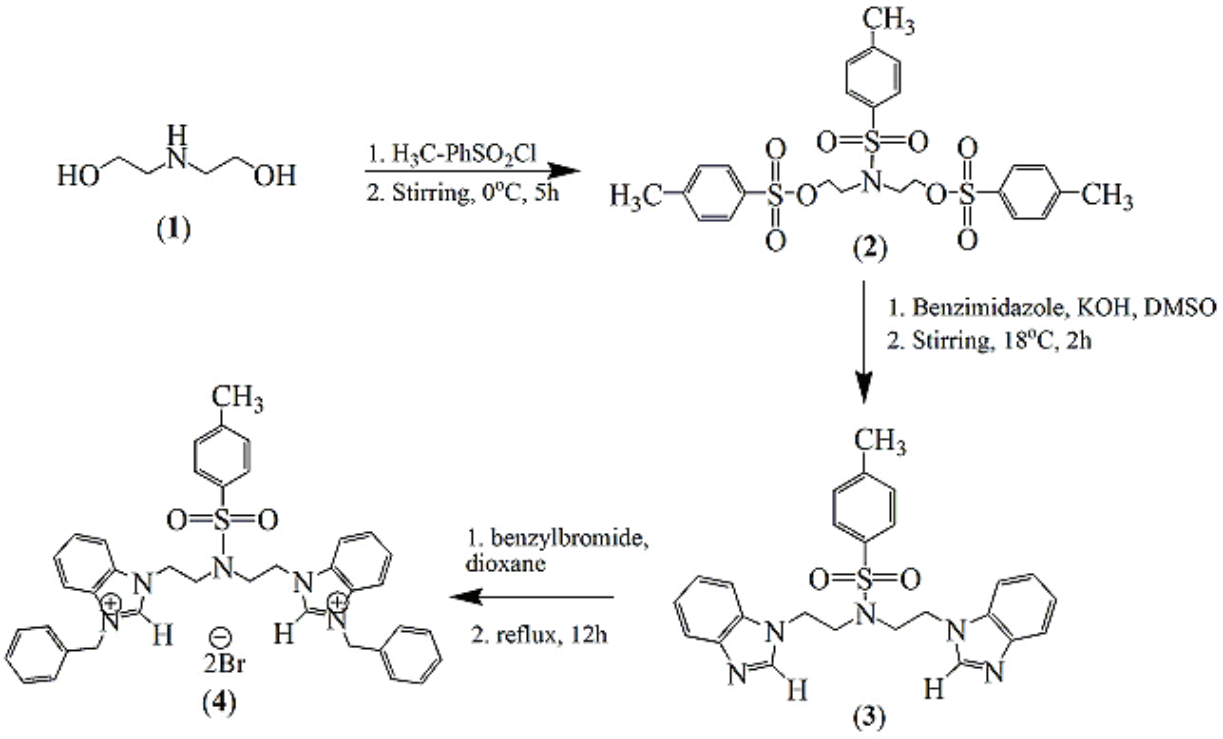

Fig. 2 . Synthesized scheme for NHCL (4).

The equation represents the equilibrium molar concentration of the complex $[NHCLM^{n+}]$, the free cation $[M^{n+}]$, the free ligand $[NHCL]$, and the activity coefficients of the species, f. Since the dilute condition was used in this work, the activity coefficient of the uncharged ligand, $f_{(NHCL)}$ is reasonably assumed to be unity. Dilute condition is where the ionic strength is less than 0.001 M. Based on the Debye-Hückel limiting law of electrolytes leads to the conclusion that $f_{(NHCLM^{n+})} \cong f_{(M^{n+})}$. Thus, the above equation can be simplified as Equation 3 [44].

$$K_f = \frac{[NHCLM^{n+}]}{[M^{n+}][NHCL]} \quad \text{(Eq.3)}$$

The specific conductivity (K) in each point of the titration process is the value of the combination of conductivity of both metal salts, $K_{(M^{n+})}$ and $NHCLM^{n+}$ complex, $K_{(NHCLM^{n+})}$ which can be seen in the following Equation 4.

$$K = K_{(M^{n+})} + K_{(NHCLM^{n+})} \quad \text{(Eq.4)}$$

Equations 5, 6 and 7 show the molar conductance of metal salt before the addition of NHC ligand, $\Lambda_{(M^{n+})}$, molar conductance of $NHCLM^{n+}$ complex, $\Lambda_{(NHCLM^{n+})}$ and observed molar conductance during titration, Λ_{Obs}.

$$\Lambda_{(M^{n+})} = \frac{K_{(M^{n+})}}{[M^{n+}]} \quad \text{(Eq.5)}$$

$$\Lambda_{(M^{n+})} = \frac{K_{(NHCLM^{n+})}}{[NHCLM^{n+}]} \quad \text{(Eq.6)}$$

$$\Lambda_{Obs} = \frac{K}{[M^{n+}]_t} \quad \text{(Eq.7)}$$

where the total analytical concentration of the metal cations $[M^{n+}]_t$ is sum of the concentration of metal salts, $[M^{n+}]$ and $NHCLM^{n+}$ complex, $[NHCLM^{n+}]$ as shown in Equation 8.

$$[M^{n+}]_t = [M^{n+}] + [NHCLM^{n+}] \quad \text{(Eq.8)}$$

By combining and simplifying the Equations 4, 5, 6 and 7, the following Equation 9 is obtained.

$$\Lambda_{Obs}[M^{n+}]_t = \Lambda_{(M^{n+})}[M^{n+}] + \Lambda_{(NHCLM^{n+})}[NHCLM^{n+}] \quad \text{(Eq.9)}$$

Then, the observed molar conductance of the solution can be represented as Equation 10 by substituting of Equation 3 to Equation 9.

$$\Lambda_{Obs}[M^{n+}]_t = \Lambda_{(M^{n+})}[M^{n+}] + \Lambda_{(NHCLM^{n+})}K_f[M^{n+}][NHCL] \quad \text{(Eq.10)}$$

The Equation 11 can be obtained by combining Equations 3 and 8.

$$[M^{n+}]_t = [M^{n+}] + K_f[NHCLM^{n+}][NHCL] = [M^{n+}](1 + K_f[NHCL]) \quad \text{(Eq.11)}$$

Thus, the observed molar conductance of solution can be simplified as Equation 12 by substituting Equation 11 into Equation 10.

$$\Lambda_{Obs} = \frac{[M^{n+}]\Lambda_{(M^{n+})} + K_f\Lambda_{(NHCLM^{n+})}[M^{n+}][NHCL]}{[M^{n+}](1 + K_f[NHCL])} = \frac{\Lambda_{(M^{n+})} + K_f\Lambda_{(NHCLM^{n+})}[NHCL]}{1 + K_f[NHCL]} \quad \text{(Eq.12)}$$

In contrast, the total concentration of NHC ligand, $[NHCL]_t$ can be described as in Equation 13.

$$[NHCL]_t = [NHCL] + [NHCLM^{n+}] \quad \text{(Eq.13)}$$

The substitution Equation 3 into Equation 13 will gave the following Equation 14.

$$[NHCL]_t = [NHCL] + K_f[M^{n+}][NHCL] = [NHCL](1 + K_f[M^{n+}])$$

(Eq.14)

Then, the combination of Equations 11 and 14 gave Equation 15:

$$[NHCL]_t = [NHCL] + \frac{K_f[M^{n+}][NHCL]}{1 + K_f[NHCL]} = \frac{[NHCL] + K_f[NHCL]^2 + K_f[NHCL][M^{n+}]_t}{1 + K_f[NHCL]}$$

(Eq.15)

Rearranging Equation 15 gave Equation 16:

$$K_f[NHCL]^2 + (1 + K_f[M^{n+}]_t - K_f[NHCL]_t)[NHCL] - [NHCL]_t = 0$$

(Eq.16)

With obtaining of $[NHCLM^{n+}]$ and $[NHCL]_t$, the values of other species involved by using the appraised amount of the formation constants at the current iteration step of the program. Refinement of the parameters is continued until the sum-of-squares of the residuals between calculated and observed values of the conductance for all experimental points is minimized. The output of the program GENPLOT comprises refined parameters, the sum-squares and the standard deviation of the data [45]. For determination of the stability constants of complex formation between the NHC ligand and various metal cations, the conductometric method has been selected as the best method in numerous studies [25, 41, 46]. To study the complexation reaction of *L* with the Ni^{2+}, Zn^{2+}, Pd^{2+}, Hg^{2+}, and Ag^{+} cations, the changes in molar conductivity (Λ_m) of the solution were supervised as a function of molar ratio $([NHCL]_t/[M^{n+}]_t)$ of the proposed complex in pure MeOH, pure H_2O and in MeOH-H_2O binary mixtures (mol%) at different temperatures (15, 25, 35 and 45ºC). The resulting Λ_m versus $([NHCL]_t/[M^{n+}]_t)$ plots for (A) Ni^{2+} in MeOH-H_2O binary system (mol% MeOH=39.73) and (B) Ag^{+} cations in MeOH-H_2O binary system (mol% MeOH= 9.90) are presented in Figure 3.

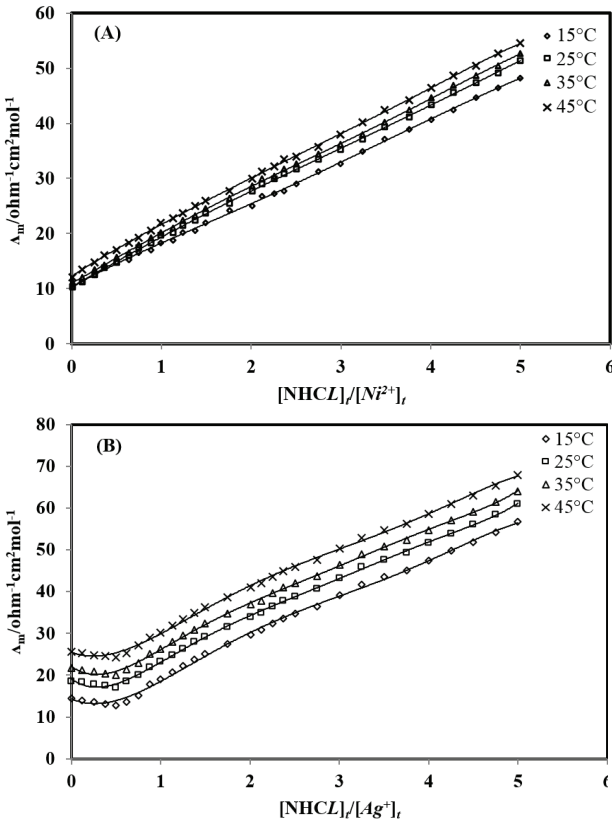

Fig.3. Molar conductance-mole ratio titration curves of (A) Ni^{2+} cation in MeOH-H_2O binary system (mol% MeOH=39.73), (B) Ag^{+} cation MeOH-H_2O binary system (mol% MeOH=9.90) with NHCL at different temperatures.

As can be seen in Figure 3 (A), the Λ_m versus $([NHCL]_t/[M^{n+}]_t)$ plots for Ni^{2+} cation show an increase in Λ_m parallel to increase of the ligand concentration. This is corresponding to the free solvated metal ion is less mobile compared to the both ligand and complex. The same cases also happened to Zn^{2+} and Pd^{2+} slope, respectively. The slope for Ni^{2+}, Zn^{2+}, and Pd^{2+} shows that the

stoichiometric for these complexation reactions was 1:1 [M:NHCL]. While, from the Λ_m versus $([NHCL]_t/[M^{n+}]_t)$ plots for Ag^+ cation, Figure 3 (B) observed a slightly decreasing in Λ_m with increasing the ligand concentration, which indicated that ligand mobility is less than free solvated metal cation. However, it shows the increment after breaking points. This is indicated that the mobility of complexes in MeOH-H_2O binary mixtures is greater than free solvated cations [46]. The Λ_m versus $([NHCL]_t/[M^{n+}]_t)$ plots for Hg^{2+} also gave the same results as Ag^+. It seems that in both complex formations, further addition of ligand to metal cation solution results in the formation of 1:2 [M:NHCL] and 2:1 [M:NHCL] complexes. Therefore, the general mechanism for all complexation processes may suggest as follows (Eq.17-Eq.19):

$$M^{n+} + NHCL \leftrightarrow NHCLM^{n+} \quad \text{(Eq.17)}$$

$$NHCLM^{n+} + NHCL \leftrightarrow NHCL_2M^{n+} \quad \text{(Eq.18)}$$

$$NHCLM^{n+} + M^{n+} \leftrightarrow NHCLM_2^{n+} \quad \text{(Eq.19)}$$

The formation constant values ($\log K_f$) of complexes for all cations were determined using a non-linear least-squares curve fitting program, GENPLOT from the corresponding Λ_m versus $([NHCL]_t/[M^{n+}]_t)$ plots at different temperatures. The obtaining data was summarized in Table 1.

The results in Table 1 show the increase of stability constants ($\log K_f$) for $NHCLM^{n+}$ complexes with an increase of temperature in most of the solvent systems. This is an indication for an endothermic complexation reaction between ligands and metal cations in the solution [36]. The obtained data shows that in the pure MeOH solvent system the stability constant is varying as $Ni^{2+} < Pd^{2+} < Zn^{2+} < Hg^{2+} < Ag^+$ and in the most cases complexation process seems more stable in pure MeOH. The results proved that the stability of the resulting complexes was influenced by the nature of the solvent system. In the reaction mixture solution, the ligand should be able to excess metal cations which are solvated by solvent molecules to form a complex. Hence, dissimilarities in the nature of the solvent system may influence in the binding properties of NHCL, and subsequently, the stability and selectivity metal complexes.

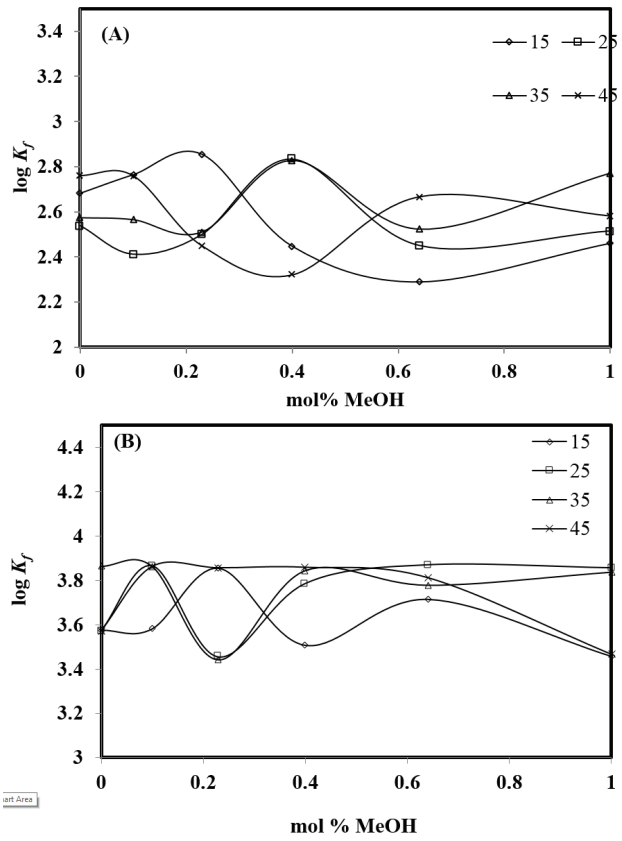

Fig. 4. Stability constant ($\log K_f$) of complexes in MeOH-H_2O binary system (mol% MeOH; 0.00, 9.99, 22.66, 39.73, 63.72 and 100.00%) at different temperature (◊ = 15ºC, □ = 25ºC, Δ =35ºC, X = 45ºC). (A) for Pd^{2+} cation and (B) for Ag^+ cation.

In the most cases, the changes in stability constant ($\log K_f$) of the complexes versus the composition of the MeOH-H_2O binary systems at various temperatures are not linear as shown in Figure 4. This pattern is probably due to solvent-solvent interaction that changed the structure of the solvent mixtures and consequently changed the solvation properties of the metal ions, ligand and the resulting complexes [25, 41]. In other cases, the increments of the stability constant value by the reducing of mol% of MeOH have been observed.

Table 1. log K_f value of $NHCLM^{n+}$ in MeOH-H_2O binary mixtures at different temperatures for the studied metals cations.

Medium[a]/ Ni^{2+}	***log K_f ± SD*[b]**			
	15ºC	25ºC	35ºC	45ºC
Pure MeOH	2.50 ± 0.14	2.43 ± 0.10	2.47 ± 0.07	2.48 ± 0.22
36.27%H_2O-63.72%MeOH	2.49 ± 0.31	2.46 ± 0.31	2.56 ± 0.27	2.40 ± 0.36
60.27%H_2O-39.73%MeOH	2.42 ± 0.19	2.57 ± 0.07	2.51 ± 0.08	2.46 ± 0.08
77.34%H_2O-22.66%MeOH	2.46 ± 0.08	2.55 ± 0.08	2.64 ± 0.07	2.45 ± 0.18
90.10%H_2O-9.90%MeOH	2.35 ± 0.31	2.60 ± 0.10	2.45 ± 0.12	2.85 ± 0.10
Pure H_2O	2.49 ± 0.08	2.56 ± 0.14	2.77 ± 0.08	2.45 ± 0.09
Medium[a]/ Zn^{2+}				
Pure MeOH	2.55 ± 0.08	2.76 ± 0.08	2.76 ± 0.08	2.75 ± 0.08
36.27%H_2O-63.72%MeOH	2.43 ± 0.14	2.40 ± 0.15	2.55 ± 0.08	2.56 ± 0.10
60.27%H_2O-39.73%MeOH	2.41 ± 0.16	2.43 ± 0.13	2.43 ± 0.15	2.45 ± 0.12
77.34%H_2O-22.66%MeOH	2.48 ± 0.11	2.42 ± 0.13	2.55 ± 0.07	2.57 ± 0.07
90.10%H_2O-9.90%MeOH	2.55 ± 0.12	2.64 ± 0.06	2.27 ± 0.32	2.86 ± 0.11
Pure H_2O	[c]	[c]	[c]	[c]
Medium[a]/ Pd^{2+}				
Pure MeOH	2.46 ± 0.21	2.51 ± 0.39	2.77 ± 0.17	2.58 ± 0.27
36.27%H_2O-63.72%MeOH	2.29 ± 0.31	2.45 ± 0.29	2.52 ± 0.17	2.67 ± 0.19
60.27%H_2O-39.73%MeOH	2.45 ± 0.21	2.83 ± 0.15	2.82 ± 0.13	2.32 ± 0.25
77.34%H_2O-22.66%MeOH	2.86 ± 0.10	2.50 ± 0.10	2.51 ± 0.09	2.45 ± 0.19
90.10%H_2O-9.90%MeOH	2.77 ± 0.08	2.41 ± 0.14	2.57 ± 0.08	2.76 ± 0.07
Pure H_2O	2.68 ± 0.17	2.54 ± 0.18	2.57 ± 0.19	2.76 ± 0.20
Medium[a]/ Hg^{2+}				
Pure MeOH	3.85 ± 0.12	3.86 ± 0.11	3.86 ± 0.12	3.85 ± 0.12
36.27%H_2O-63.72%MeOH	3.27 ± 0.35	3.42 ± 0.24	3.41 ± 0.25	3.46 ± 0.22
60.27%H_2O-39.73%MeOH	3.45 ± 0.21	3.82 ± 0.26	3.84 ± 0.21	3.84 ± 0.21
77.34%H_2O-22.66%MeOH	3.88 ± 0.12	3.45 ± 0.22	3.44 ± 0.30	3.43 ± 0.31
90.10%H_2O-9.90%MeOH	[c]	[c]	[c]	[c]
Pure H_2O	[c]	[c]	[c]	[c]
Medium[a]/ Ag^{+}				
Pure MeOH	3.46 ± 0.38	3.86 ± 0.20	3.84 ± 0.20	3.47 ± 0.40
36.27%H_2O-63.72%MeOH	3.71 ± 0.19	3.87 ± 0.22	3.78 ± 0.24	3.81 ± 0.23
60.27%H_2O-39.73%MeOH	3.51 ± 0.27	3.79 ± 0.22	3.84 ± 0.20	3.86 ± 0.17
77.34%H_2O-22.66%MeOH	3.85 ± 0.17	3.46 ± 0.32	3.44 ± 0.34	3.86 ± 0.17
90.10%H_2O-9.90%MeOH	3.86 ± 0.23	3.58 ± 0.32	3.86 ± 0.22	3.86 ± 0.22
Pure H_2O	3.58 ± 0.29	3.57 ± 0.29	3.57 ± 0.29	3.86 ± 0.22

[a]Composition of binary mixtures is expressed in mol% for solvent system,
[b]SD = Standard deviation,
[c] The data cannot be fitted to the equation in GENPLOT.

These results can be explained by the Gatmann acceptor-donor number effect. In this study binary mixture of MeOH-H_2O has been used. Pure solvent MeOH and H_2O have acceptor numbers 41.5 and 54.8 kcal mol^{-1}, respectively [47]. Therefore, the complexation in the solvent with lower acceptor ability will increase the stability constant value. This is due to the less competition of the ligand with the solvent molecules for the metal ions, thus increase the stability in the formation of complexes. The effect of a Gatmann donor number of solvents and their mixtures in this study is negligible because of their approximately equal value (DN_{Water}=18 kcal/mol; DN_{MeOH}=19 kcal/mol). By ignoring this parameter, the dielectric constant of solvents, **ε,** plays another important role in the stability constants of complexes. According to the previous studies, the interaction between the oppositely charged ions in the solvent with low dielectric constant (Methanol, ε=32.6), in compared to water (ε=81.7), would be increased and cause to form the complexes. In order to better understand the complexation proceed discussed, it is useful to consider the enthalpy and entropy contribution to these reactions. The ΔH_C^o and ΔS_C^o parameters were estimated according to the van't Hoff plots that shows the corresponded $\ln K_f$- temperature data according to the van't Hoff's equation.

All the van't Hoff plots of $\ln K_f$ versus 1000/T for all different metal cations, were constructed individually. Several cases were shown in Figure 5.

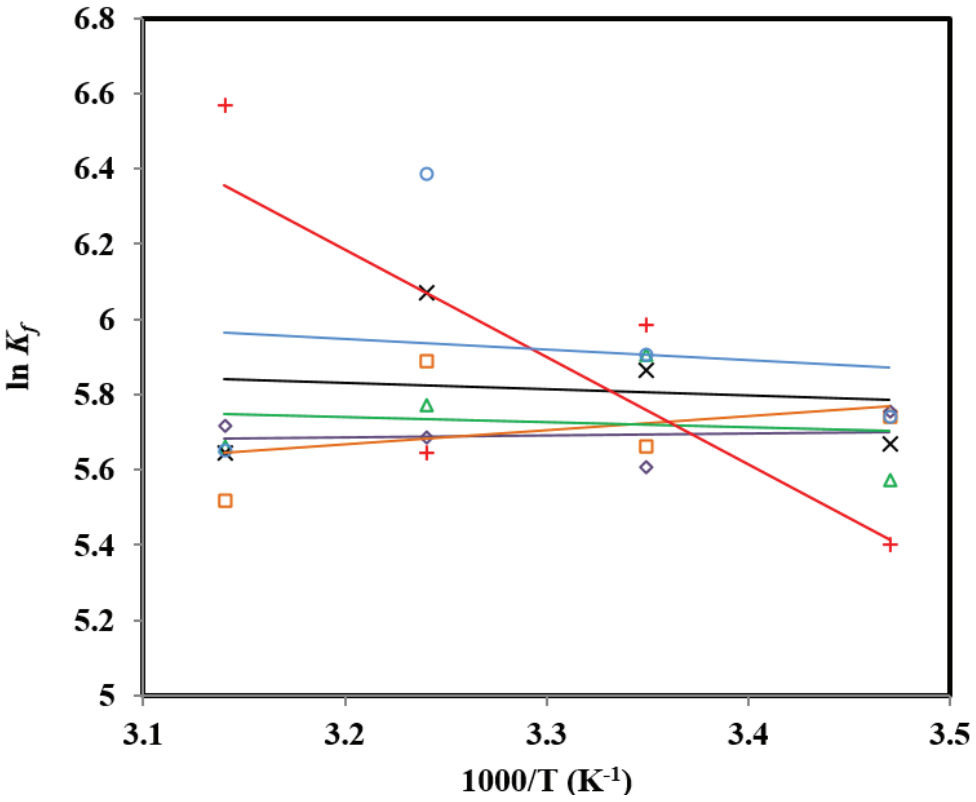

Fig. 5. Van't Hoff plot for *L*-M^{n+} with Ni^{2+} cation in MeOH-H_2O binary system (mol% MeOH; ◊ = 100, □ = 63.72, Δ = 39.73, X = 22.66, + = 9.90, ○ = 0.00) at different temperature.

The data demonstrated that these complexations process are temperature dependent. The value of standard enthalpy (ΔH_C^o) for the complexation reaction was determined from the slope of the van't Hoff plots based on van't Hoff's equation (Equation 20). Other thermodynamic parameters, the free energy of complex formation (ΔG_C^o) and the value of the standard entropy (ΔS_C^o) were obtained from thermodynamic relation Equation 21[39]. The calculated results are summarized in Table 2.

Table 2. Summary of thermodynamic parameters values of the NHCLM^{n+} complexes in MeOH-H_2O binary mixture solvent.

Medium[a] /Ni^{2+}	***log K_f ± SD[b]***		
	$\Delta G_C^o \pm SD^b$ (kJ.mol^{-1})	$\Delta H_C^o \pm SD^b$ (kJ.mol^{-1})	$\Delta S_C^o \pm SD^b$ (J.mol^{-1})
Pure MeOH	-13.9 ± 0.5	4.6 ± 1.0	62.1 ± 2.8
36.27%H_2O-63.72%MeOH	-14.04 ± 1.8	-5.6 ± 0.1	28.2 ± 1.9
60.27%H_2O-39.73%MeOH	-14.6 ± 0.4	-9.9 ± 0.3	16.0 ± 1.0
77.34%H_2O-22.66%MeOH	-14.5 ± 0.4	14.5 ± 0.4	97.3 ± 0.7
90.10%H_2O-9.90%MeOH	-14.8 ± 0.6	28.7 ± 0.3	146.1 ± 4.4
Pure H_2O	-14.6 ± 0.8	23.2 ± 7.4	127.0 ± 2.5
Medium[a] /Zn^{2+}			
Pure MeOH	-15.8 ± 0.5	11.0 ± 6.3	89.9 ± 2.0
36.27%H_2O-63.72%MeOH	-13.7 ± 0.9	7.3 ± 2.2	70.4 ± 6.9
60.27%H_2O-39.73%MeOH	-13.8 ± 0.7	1.1 ± 0.9	50.0 ± 1.6
77.34%H_2O-22.66%MeOH	-13.8 ± 0.7	5.5 ± 0.3	64.7 ± 2.2
90.10%H_2O-9.90%MeOH	-15.1 ± 0.4	17.9 ± 1.7	110.7 ± 5.6
Pure H_2O	[c]	[c]	[c]
Medium[a] /Pd^{2+}			
Pure MeOH	-14.4 ± 2.2	6.9 ± 0.7	71.4 ± 7.0
36.27%H_2O-63.72%MeOH	-14.0 ± 1.7	21.0 ± 1.9	117.4 ± 3.3
60.27%H_2O-39.73%MeOH	-16.2 ± 0.8	32.3 ± 8.0	162.7 ± 6.3
77.34%H_2O-22.66%MeOH	-14.3 ± 0.6	-4.5 ± 4.0	32.9 ± 1.9
90.10%H_2O-9.90%MeOH	-13.8 ± 0.8	31.6 ± 2.9	152.3 ± 9.4
Pure H_2O	-14.7± 1.0	16.5 ± 4.0	104.6 ± 6.9
Medium[a] /Hg^{2+}			
Pure MeOH	-22.0 ± 0.6	-1.2 ± 0.2	69.8 ± 2.0
36.27%H_2O-63.72%MeOH	-19.5 ± 1.4	11.1 ± 0.9	102.6 ± 3.6
60.27%H_2O-39.73%MeOH	-21.8 ± 1.5	24. 6 ± 7.6	155.6 ± 5.0
77.34%H_2O-22.66%MeOH	-19.7 ± 1.3	-2.3 ± 0.5	58.4 ± 4.0
90.10%H_2O-9.90%MeOH	[c]	[c]	[c]
Pure H_2O	[c]	[c]	[c]
Medium[a] /Ag^{+}			
Pure MeOH	-21.9 ± 1.1	32.1 ± 9.2	181.1 ± 6.4
36.27%H_2O-63.72%MeOH	-22.1 ± 1.8	21.7 ± 8.3	146.9 ± 7.3
60.27%H_2O-39.73%MeOH	-21.6 ± 1.3	28.3 ± 9.8	167.4 ± 3.7
77.34%H_2O-22.66%MeOH	-19.3 ± 1.9	35.9 ± 3.5	185.1 ± 8.4
90.10%H_2O-9.90%MeOH	-20.4 ± 1.3	-0.2 ± 0.1	67.8 ± 4.2
Pure H_2O	-20.4 ± 1.3	-4.8 ± 4.5	52.3 ± 4.5

[a]Composition of binary mixtures is expressed in mol% for solvent system,
[b]SD = Standard deviation,
[c] The data cannot be fitted to equation.

$$\ln K_f = \frac{\Delta_f S_C^o}{R} - \frac{\Delta_f H_C^o}{RT}$$

(Eq.21)

$$\Delta G_{C,298.15}^o = \Delta H_{C,298.15}^o - T\Delta S_C^o$$

(Eq.21)

The results reveal, in the most cases the changes in ΔH_C^o for the complexation process is negligible, whereas the change in ΔS_C^o is significant. Therefore, the formation of complexes between ligand (NHCL) and all cations in MeOH-H_2O binary solvent mixtures are enthalphy destabilized but entropy stabilized. Additionally, the different solvent-solvent interaction in all solvent system and changes in flexibility of ligand during complexation contribute to change in entropy. The calculated value of ΔG_C^o in all cases shows negative values. This is an evidences that the ability of the ligand to form stable complexes with metal cations and the process were spontaneous [42]. However, The exitance of such a compensating e-ect between ΔH_C^o and ΔS_C^o values for all studied binary systems is shown in Figure 6. It is clear that the observed increase or decrease in ΔH_C^o value which is depending on the nature of the metal ion will be compensated by an increase (or decrease) in the corresponding ΔS_C^o value. Then the small changes of ΔG_C^o values will be resulted due to this compensating e-ect for ΔH_C^o and ΔS_C^o, independently.

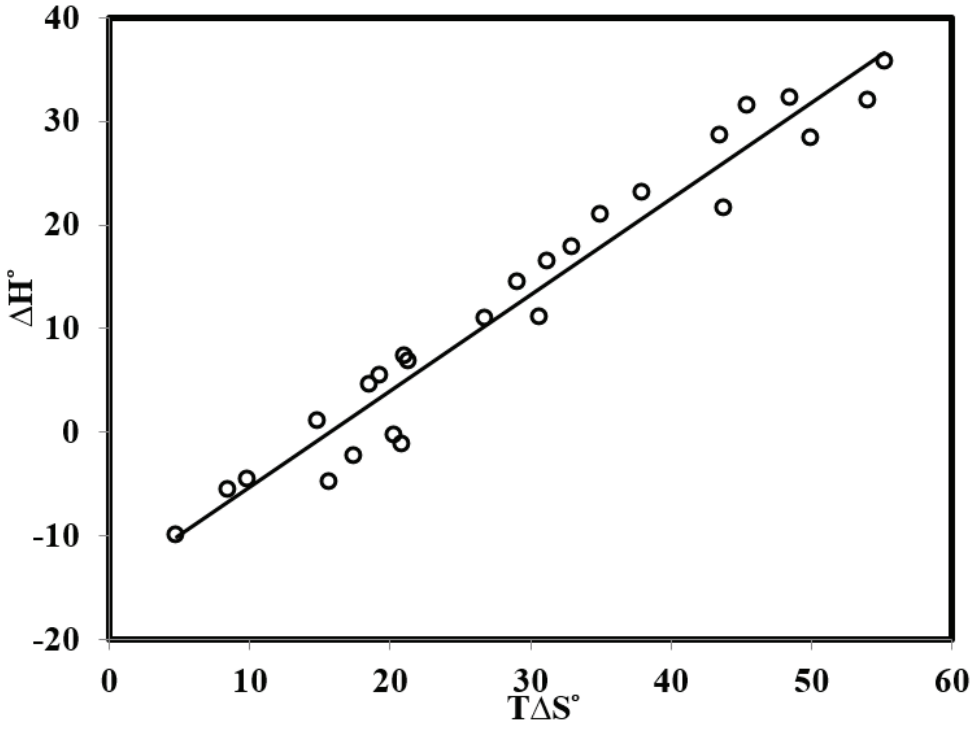

Fig. 6. Plot of ΔH_C^o (kJmol^{-1}) versus $T\Delta S_C^o$ (kJmol^{-1}) for NHCLM^{n+} (M= Ni^{2+}, Pd^{2+}, Zn^{2+}, Hg^{2+} and Ag^{+}) in different MeOH-H_2O systems (R^2=0.9537).

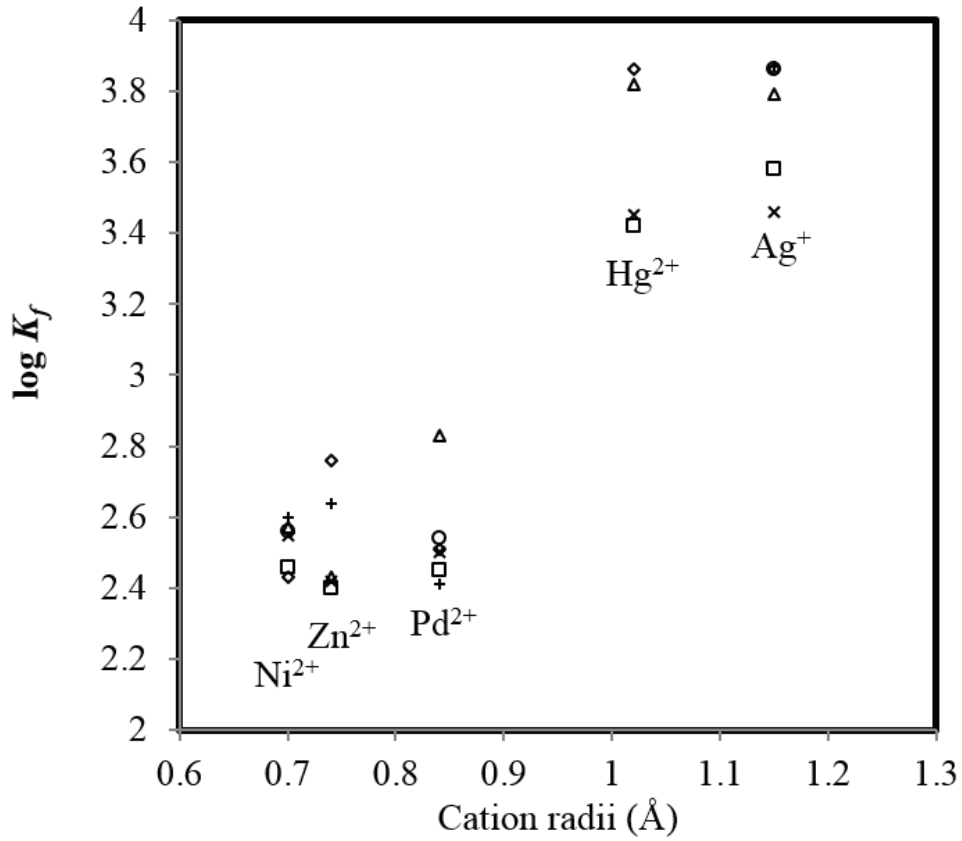

Fig. 7. Changes of stability constant (log K_f) of NHCL-M^{n+} with all metal cation in MeOH-H_2O binary system (mol% MeOH; ◊ = 100, □ = 63.72, Δ = 39.73, X = 22.66, + = 9.90, ○ = 0.00) at 25ºC.

The variation of log K_f for all complex cases in contrast with cationic radius for studied cations in MeOH-H_2O binary mixture at 25ºC were presented in Figure 7. As it is seen in Figure 7, the stability constant of complexes increase as the size of a metal cation increases from Ni^{2+} to Ag^{+}. These results can be explained due to solvent system effect. Usually the small metals cations will be more solvated than the bigger metals cations in a same solvent system and decrease its mobility. Consequently, the competition ligand with solvent molecules was increase and resulted in the decreasing of stability constant [44].

3.1. Computational study

With the purpose to elucidate the obtained experimental results, a density functional theory (DFT) study was conducted. The DFT calculations were carried out with the GAUSSIAN 09 software package, with the B3LYP/LANL2DZ basis set. The binding energy ΔE in the complexation between NHCL and M^{n+} in MeOH pure solvent is defined by the following formula, Equation 22:

$$\Delta E = E_{NHCLM^{n+}} - (E_{M^{n+}} + E_{NHCL}) \qquad \text{(Eq.22)}$$

Where $\Delta E, E_{NHCLM^{n+}}, E_{M^{n+}}$ and E_{NHCL} are binding energy, NHCLM^{n+} complex energy, free metal ion energy and NHCL energy, respectively [48]. The optimized structure of free and complexes NHCL with Zn^{2+} and Ag^{+} was shown in Figure 8(A, B, C), respectively. While the calculated results of binding energies for all complexes in MeOH pure solvent were listed in Table 3.

It is clear from Table 3 that the binding energy

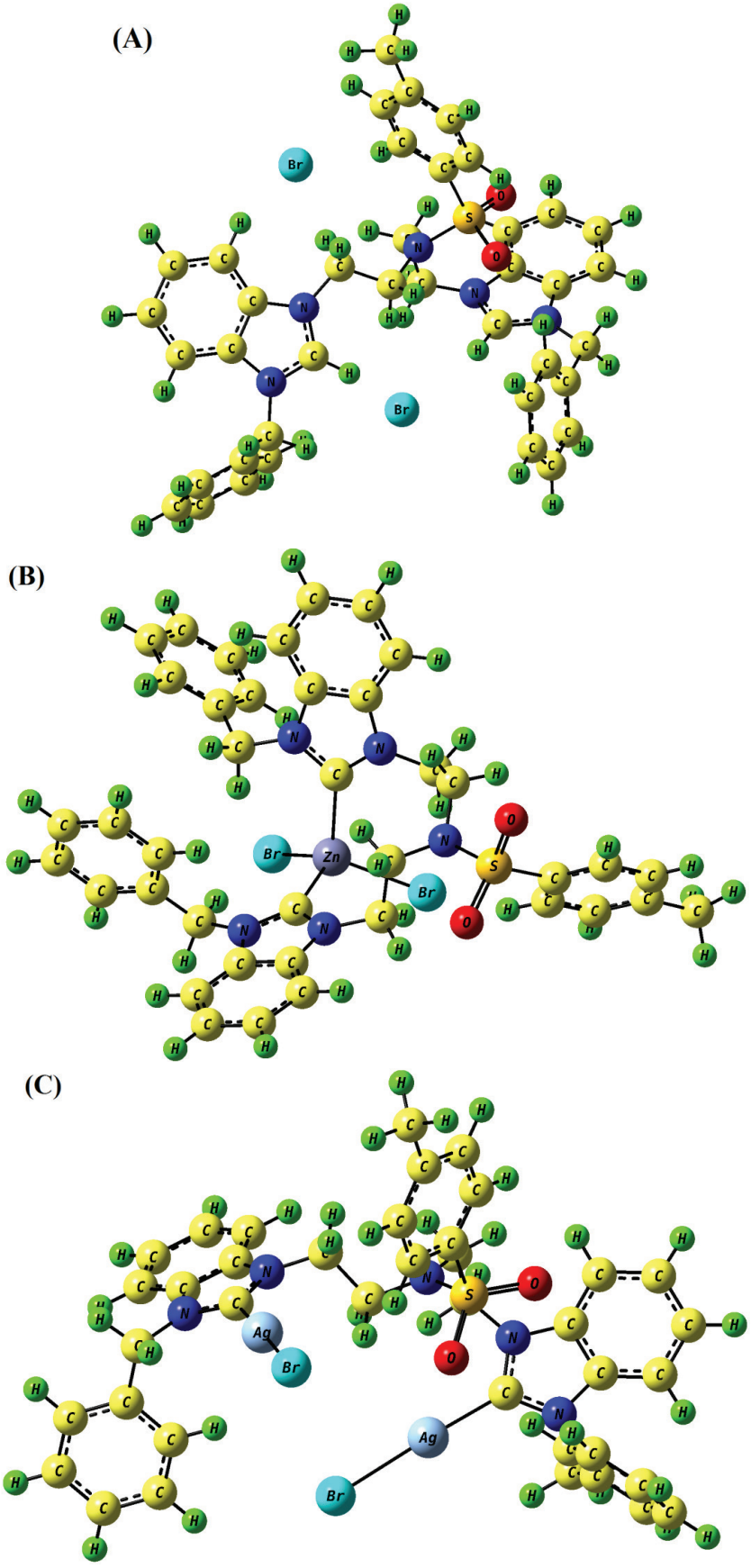

Fig. 8. Optimized structure of NHC ligand

Table 3. The calculated binding energies ΔE, in the formation of $NHCLM^{n+}$ by DFT method, where E_{NHCL} is -1969.8454 (Hartree).

M^{n+}	$E_M{}^{n+}$ (Hartree)	$E_{NHCL-M}{}^{n+}$ (Hartree)	ΔE (Hartree)	ΔE (kJ mol^{-1})
Ni^{2+}	-168.8263978	-2138.0707	0.66742646	1752.327917
Zn^{2+}	-65.30191723	-2034.37409	0.83955559	2204.252883
Pd^{2+}	-126.2368438	-2095.515285	0.63328753	1662.696169
Ag^{+}	-145.6275022	-2114.513658	1.02557279	2692.64097
Hg^{2+}	-42.5030206	-2011.502124	0.91262536	2396.097536

increases monotonically with increasing the size of studied cations. Therefore the binding energy of Ag^{+} is much larger than other cations, showing prominent affinity to NHCL in the MeOH solvent. The obtained experimental data in MeOH pure solvent (Table 1) shows the same trends. As discussed before, small cations such as Ni^{2+} and Pd^{2+} have high solvation free energy with MeOH that causes them to be more solvalized in the solution, and have less interaction with free NHCL ligand.

3.2. Mathematical Modeling

Artificial neural network (ANN) as a mathematical (or computational) model that is inspired by the structure and function of biological neural networks in the brain, is one of the most successful technologies in the last two decades [49-52]. In this research work, the ANN was applied for the simulation of property parameters correlation, and a good agreement in the experimental and predicted value is obtained. A 4-11-1 (input layer-hidden layer-output layer) network structure was used as shown in Figure 9. The effect of four parameters (cationic radii, temperature, molar percentage of MeOH in the media and molar percentage of water in the media) for the determining of complex formation (K_f) was the input layer matrix of the network. 59 training examples, 26 testing examples and 20 validating examples (10 times of each node) were prepared for training, testing and validating the network, respectively.

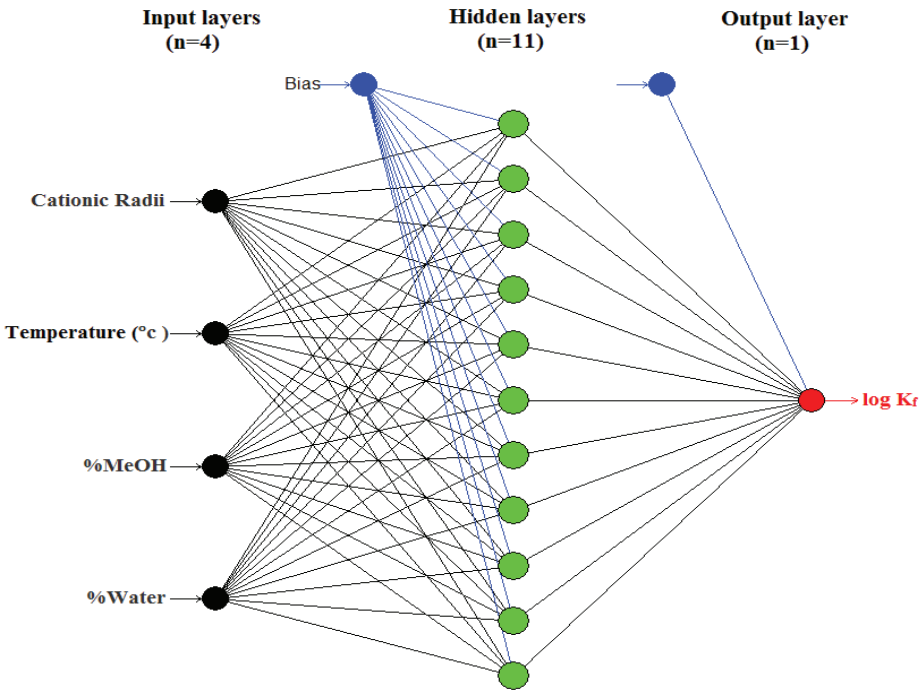

Fig. 9. Structure of neural network adopted in this study.

The model training based on the quick prob (QP) learning algorithm was carried out to test the data set and determine the minimum value of RMSE as an error function. The regression coefficient of determination (R^2) showed a fairly good correlation between estimated and experimental data sets for both train (0.959) and test data sets (0.943) (Figure 10 (A) and (B)).

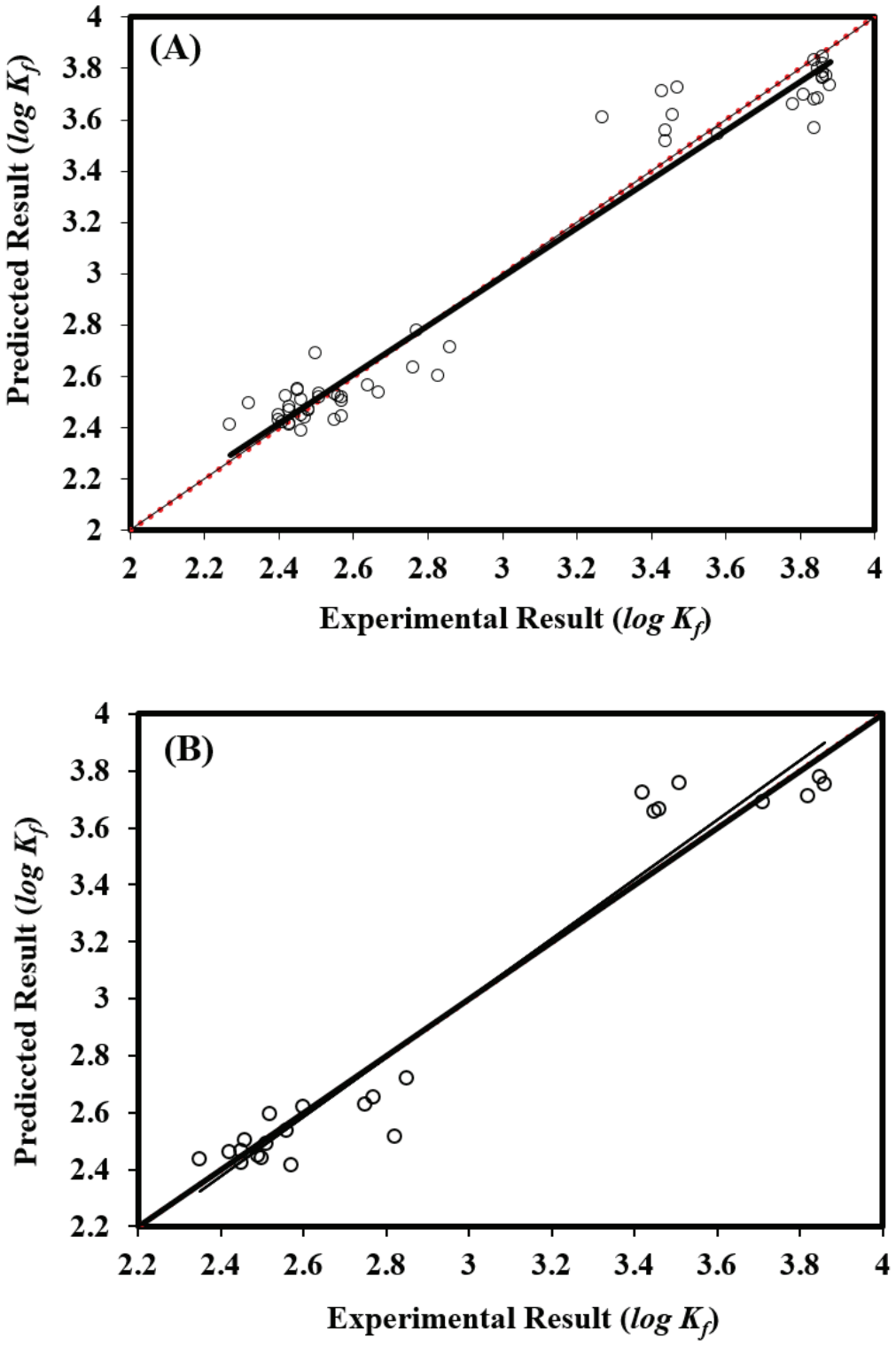

Fig. 10. Comersion of estimated logKf with experimental data (a) training data set and (b) test data set.

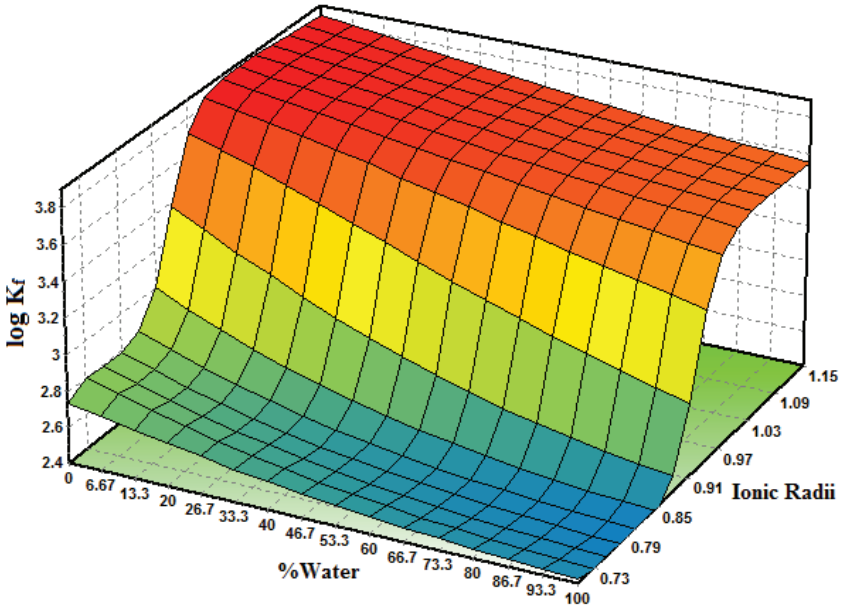

Fig. 11. Surface and contour plots of the stability constant (log K_f) as a function of the mol% of water and ionic radius of cations (Ni^{2+}, Pd^{2+}, Zn^{2+}, Hg^{2+} and Ag^{+})

The obtained constant formations of complex reactions between all metal studied cations and the proposed ligand using the various mole percentages of water in H_2O-MeOH binary media system at different temperatures were visualized in Figure 11 by drawing surface and contour plots of the stability constant (log K_f) for the complex formation as a function of the mol% of H2O in the binary mixtures and different studied cationics radius.

As seen in Figure 11, increasing of mol% of water and cationic radius causes a decrease and an increase in the constant stability of complexes (log K_f). The maximum constant formation of complexes was obtained in zero mol percentage of water (100% of MeOH) and the highest amount of cationic radii related to Ag^{+} cation (1.15Å).This result indicated that this model is valid for the estimation of constant stability of complexes of Ni^{2+}, Pd^{2+}, Zn^{2+}, Hg^{2+} and Ag^{+} in MeOH-Water binary mixtures at different temperatures. The estimated results based on the ANN program were in a good agreement with obtaining experimental results.

4. Conclusion

According to the obtained results, the complexation of Ni^{2+}, Zn^{2+}, Pd^{2+}, Hg^{2+} and, Ag^{+} cations with NHC ligand can be explained in terms of the size-fit concept, where the NHC ligand forms a most stable complex with a cation having a size which fits best with its cavity size. The obtained data shows that in the pure MeOH solvent system the stability constant is varying as $Ni^{2+}< Pd^{2+}<Zn^{2+}<Hg^{2+}<Ag^{+}$ and the complexations process seems more stable in pure MeOH and pure H_2O.The result also showed that in most cases, the $NHCLM^{n+}$ complexes was enthalpy destabilizer but entropy stabilizer. The stoichiometry of complexes for Ni^{2+}, Zn^{2+}, and Pd^{2+} are 1:1[M:NHCL]. While, for Hg^{2+} and Ag^{+}, they have two stoichiometry which is 1:2[M:NHCL] and 2:1[M:NHCL]. The changes in the stability constant of the complex versus the composition of the MeOH-H_2O binary system at various temperatures are not linear in most cases. However, some results have shown that increment in stability is constant with the decrease of mol% MeOH in the solvent system. The effects of mole% of water and cationic radii of studied cations on the complexation reactions were investigated and high correlation between experimental data and ANN kinetic model was obtained which is a proof of the high performance of conductometric method for the complex formation study.

5. Acknowledgement

This research was supported by AUA-UAEU Joint Research Grant Project (IF016-2021 and G00003485), University Malaya Centre for Ionic Liquid (UMCiL) and Mashhad University of Medical Sciences, Mashhad Iran. The author gratefully acknowledge to Universiti Teknologi MARA Cawangan Negeri Sembilan,Kampus Kuala Pilah to pursue postgraduate studies.

6. References

[1] H.W. Wanzlick, H.J. Schönherr, Direct synthesis of a mercury salt-carbene complex, Angewandte Chemie International Edition in English, 7 (1968) 141-142. https://doi.org/10.1002/anie.196801412

[2] A.J. Arduengo, R.L. Harlow, M. Kline, A stable crystalline carbene, J. Am. Chem.Soc., 113 (1991) 361-363. https://doi.org/10.1021/ja00001a054

[3] R.A. Haque, A. Washeel Salman, New N-heterocyclic carbene mercury(II) complexes: Close mercury–arene interaction, J. Organometal. Chem., 696 (2011) 3507-3512. https://doi.org/10.1016/j.jorganchem.2011.07.032

[4] C.M. Crudden, D.P. Allen, Stability and reactivity of N-heterocyclic carbene complexes, Coor. Chem. Rev., 248 (2004) 2247-2273. https://doi.org/10.1016/j.ccr.2004.05.013

[5] S. Budagumpi, R.A. Haque, A.W. Salman, Stereochemical and structural characteristics of single- and double-site Pd(II)–N-heterocyclic carbene complexes: Promising catalysts in organic syntheses ranging from CC coupling to olefin polymerizations, Coord. Chem. Rev., 256 (2012) 1787-1830. https://doi.org/10.1016/j.ccr.2012.04.003

[6] M. Rezayi, Y.H. Lee, M.M. Abdi, N.M.D. Noran, C. Esmaeili, S. B. Tavakoly Sany, A. Salleh, L. Narimani, N. Saadati, F. Tajalli, A thermodynamic study on the complex formation between tris (2-Pyridyl) methylamine (tpm) with Fe II, Fe III, Cu II and Cr III cations in water, acetonitrile binary solutions using the conductometric method, Int. J. Electrochem. Sci., 8 (2013) 6922-6932. http://www.electrochemsci.org/

[7] M. Y. Khorasani, H. Langari, S.B. Tavakoly Sany, M. Rezayi, A. Sahebkar, The role of curcumin and its derivatives in sensory applications, Mater. Sci. Eng. C, 103 (2019) 109792. https://doi.org/ 10.1016/j.msec.2019.109792

[8] S.B. Tavakoly Sany, R. Hashim, A. Salleh, M. Rezayi, O. Safari, Ecological quality assessment based on macrobenthic assemblages indices along West Port, Malaysia coast. Environ. Earth Sci., 74 (2015) 1331-1341. https://doi.org/10.1007/s12665-015-4122-3

[9] S.B. Tavakoly Sany, R. Hashim, M. Rezayi, M.A.Rahman, B.B.M. Razavizadeh, E. Abouzari-lotf, D.J. Karlen, Integrated ecological risk assessment of dioxin compounds. Environ. Sci. Pollut. Res., 22 (2015) 11193-11208. https://doi.org/ 10.1007/s11356-015-4511-x

[10] J. Houghton, G. Dyson, R.E. Douthwaite, A.C. Whitwood, B. Kariuki, Structural variation, dynamics, and catalytic application of palladium(II) complexes of di-N-heterocyclic carbene-amine ligands, Dalton Trans, 28 (2007) 3065-73. https://doi.org/10.1039/b703248j

[11] C.Y Liao, K.T. Chan, J.Y. Zeng, C.H. Hu, C.Y. Tu, H.M. Lee., Nonchelate and chelate complexes of Palladium (II) with N-heterocyclic carbene ligands of amido functionality, Organometallics, 26 (2007) 1692-1702. https://doi.org/10.1021/om0610041

[12] Q.X. Liu, L.X. Zhao, X.J. Zhao, Z.X. Zhao, Z.Q. Wang, A.H. Chen, X.G. Wang, Silver (I), palladium (II) and mercury (II) NHC complexes based on bis-benzimidazole salts with mesitylene linker: Synthesis, structural studies and catalytic activity, J. Organomet. Chem., 731(2013) 35-48. https://doi.org/10.1016/j.jorganchem.2013.01.026

[13] S.B. Tavakoly Sany, R. Hashim, A. Salleh, O. Safari, A. Mehdinia, M. Rezayi, Risk assessment of polycyclic aromatic hydrocarbons in the West Port semi-enclosed basin (Malaysia), Environ. Earth Sci., 71 (2014) 4319-4332. https://doi.org/10.1007/s12665-013-2826-9

[14] R.A. Haque, M.A. Iqbal, M.B Khadeer Ahamed, A.M.S. Abdul Majid, Z.A Abdul Hameed. Design, synthesis and structural studies of meta-xylyl linked bis-benzimidazolium salts: Potential anticancer agents against'human colon cancer, Chem. Cent. J., 6 (2012) 68. https://doi.org/10.1186/1752-153X-6-68

[15] K.A. Abu-Safieh, A.S. Abu-Surrah, H.D. Tabba, H.A. AlMasri, R.M. Bawadi, F.M. Boudjelal, L.H. Tahtamouni, Novel palladium(II) and platinum(II) complexes with 1H-benzimidazol-2-ylmethyl-N-(4-bromo-phenyl)-amine: structural studies and anticancer activity, Eur. J. Med. Chem., 47 (2012) 399-411. https://doi.org/10.1016/j.ejmech.2011.11.008

[16] R.A. Haque, M.Z. Ghdhayeb, S. Budagumpi, A.W. Salman, M.B. Khadeer Ahamed, A.M.S Abdul Majid, Non-symmetrically substituted N-heterocyclic carbene–Ag(I) complexes of benzimidazol-2-ylidenes: Synthesis, crystal structures, anticancer activity and transmetallation studies, Inorg. Chim. Acta, 394 (2013) 519-525. https://doi.org/10.1016/j.ica.2012.09.013

[17] M. Darroudi, M. Gholami, M. Rezayi, M. Khazaei, An overview and bibliometric analysis on the colorectal cancer therapy by magnetic functionalized nanoparticles for the responsive and targeted drug delivery, J. Nanobiotechnol., 19 (2021) 1-20. https://doi.org/10.1186/s12951-021-01150-6

[18] B. Hatamluyi, R. Sadeghian, S.B. Tavakoly Sany, I. Alipourfard, M. Rezayi, Dual-signaling electrochemical ratiometric strategy for simultaneous quantification of anticancer drugs, Talanta, 234 (2021) 122662. https://doi.org/10.1016/j.talanta.2021.122662

[19] N. N. Al-Mohammed, Y. Alias, Z. Abdullah, R.M. Shakir, E.M. Taha, A. Abdul Hamid, Synthesis and antibacterial evaluation of some novel imidazole and benzimidazole sulfonamides, Molecules, 18 (2013) 11978-95. https://doi.org/10.3390/molecules181011978.

[20] R.E. Douthwaite, J. Houghton, B.M. Kariuki, The synthesis of a di-N-heterocyclic carbene-amido complex of palladium(II), Chem. Commun. (Camb), 10 (2004) 698-9. https://doi.org/10.1039/b314814a

[21] D.J. Nielsen, K.J. Cavell, B. Skelton, A. White, A pyridine bridged dicarbene ligand and its silver (I) and palladium (II) complexes: synthesis, structures, and catalytic applications, Inorg. Chim. Acta, 327(2002) 116-125. https://doi.org/10.1016/S0020-1693(01)00677-6

[22] F.J.B Dit Dominique, H. Gornitzka, A Sournia-Saquet, C. Hemmert, Dinuclear gold(I) and gold(III) complexes of bridging functionalized bis(N-heterocyclic carbene) ligands: synthesis, structural, spectroscopic and electrochemical characterizations, Dalton Trans, (2009) 340-52. https://doi.org/10.1039/b809943j

[23] U.J. Scheele, S. Dechert, F. Meyer, Bridged dinucleating N-heterocyclic carbene ligands and their double helical mercury(II) complexes, Inorg. Chim. Acta, 359 (2006) 4891-4900. https://doi.org/10.1016/j.ica.2006.08.048

[24] B.A. Shah, F.A. Christy, P.S. Shrivastav, M. SanyalShah, Study on complex formation of dicyclohexyl-18-crown-6 with Mg^{2+}, Ca^{2+} and Sr^{2+} in acetonitrile-water binary mixtures by conductometry, J. Phys. Chem. Sci., 1 (2014) 215777300. https://doi.org/10.15297/JPCS.V1I2.02

[25] M. Joshaghani, M.B. Gholivand, F. Ahmadi, Spectrophotometric and conductometric study of complexation of salophen and some transition metal ions in nonaqueous polar solvents, Spectrochim. Acta A, Mol. Biomol.

Spect., 70 (2008) 1073-1078. https://doi.org/10.1016/j.saa.2007.10.015

[26] A. Nezhadali, G.Taslimi, Thermodynamic study of complex formation between 3,5-di iodo-hydroxy quinoline and Zn^{2+}, Ni^{2+} and Co^{2+} cations in some binary solvents using a conductometric method, Alexandria Eng. J., 52 (2013) 797-800. htpps://doi.org/10.1016/j.aej.2013.08.007

[27] M. Rezayi, S. Ahmadzadeh, A. Kassim, L.Y. Heng, Thermodynamic studies of complex formation between Co (Salen) ionophore with chromate (II) ions in AN-H_2O binary solutions by the conductometric method, Int. J. Electrochem. Sci, 6 (2011) 6350-6359. http://www.electrochemsci.org/

[28] E. R. Enemo, T.E. Ezenwa, E.C. Nleonu, Determination of formation constants and thermodynamic Parameters of chromium (III) ions with some ligands by conductometry, IOSR J. Appl. Chem., 12 (2019) 54-58. htpps://doi.org/ 10.9790/5736-1210015458

[29] M. Rezayi ,Y. Alias, M.M. Abdi, K. Saeedfar, N. Saadati, Conductance studies on complex formation between c-methylcalix[4]resorcinarene and titanium (III) in acetonitrile-H(2)O binary solutions, Molecules, 18 (2013) 12041-12050. https://doi.org/10.3390/molecules181012041

[30] L. Rao, G. Tian, Thermodynamic study of the complexation of uranium(VI) with nitrate at variable temperatures, J. Chem. Thermodyn., 40 (2008) 1001-1006. https://doi.org/10.1016/j.jct.2008.02.013

[31] S. Jaubert, G. Maurer, Quantitative NMR spectroscopy of binary liquid mixtures (aldehyde+alcohol) Part I: Acetaldehyde+(methanol or ethanol or 1-propanol), J. Chem. Thermodyn., 68 (2014) 332-342. https://doi.org/10.1016/j.jct.2013.03.022

[32] B. Ghalami-Choobar, N. Mahmoodi, P. Mossayyebzadeh-Shalkoohi, Thermodynamic properties determination of ternary mixture (NaCl+Na_2HPO_4+water) using potentiometric measurements, J. Chem. Thermodyn., 57 (2013) 108-113. https://doi.org/10.1016/j.jct.2012.08.011

[33] M. Rezayi, L.Y. Heng, A. Kassim, S. Ahmadzadeh, Y. Abdollahi, H. Jahangirian, Immobilization of ionophore and surface characterization studies of the titanium (III) ion in a PVC-membrane sensor, Sensors, 12 (2012) 8806-8814. https://doi.org/10.3390/s120708806

[34] M. Rezayi, L.Y. Heng, A. Kassim, S. Ahmadzadeh, Y. Abdollahi, H. Jahangirian, Immobilization of tris (2 pyridyl) methylamine in PVC-membrane sensor and characterization of the membrane properties, Chem. Cent. J., 6 (2012) 40. https://doi.org/10.1186/1752-153X-6-40

[35] M. Rezayi, M. Ghasemi, R. Karazhian,M. Sookhakian, Y. Alias, Potentiometric chromate anion detection based on Co (SALEN)2 ionophore in a PVC-membrane sensor, J. Electrochem. Soc., 161 (2014) B129-B136. https://doi.org/10.1149/2.051406jes

[36] A. Zhuravlev, A. Zacharia, M. Arabadzhi, C. Turetta, G. Cozzi, C. Barbante, Comparison of analytical methods: ICP-QMS, ICP-SFMS and FF-ET-AAS for teh determination of V, Mn, Ni, Cu, As, Sr, Mo, Cd and Pb in ground natural waters, Int. J. Environ. Anal. Chem., 96 (2016) 332–352. https://doi.org/10.1080/03067319.2016.1160380

[37] B. Feist, B. Mikula, Preconcentration of some metal ions with lanthanum-8-hydroxyquinoline co-precipitation system, Food Chem., 147 (2014) 225-229. https://doi.org/10.1016/j.foodchem.2013.09.149

[38] A. Habibiyan, M. Ezoddin, N. Lamei, K. Abdi, M. Amini, M. Ghazi-khansari, Ultrasonic assisted switchable solvent based on liquid phase microextraction combined with micro sample injection flame atomic absorption spectrometry for determination of some heavy metals in water, urine and tea infusion samples, J. Mol. Liq., 242 (2017) 492–496. https://doi.org/10.1016/j.molliq.2017.07.043

[39] Q. Xiong, Y. Lin, W. Wu, J. Hu, Y. Li, K. Xu, Chemometric intraregional discrimination of Chinese liquors based on multi-element determination by ICP-MS and ICP-OES, Appl. Spectrosc. Rev., 56 (2021) 115-127. https://doi.org/10.1080/05704928.2020.1742729.

[40] EH. Evans, J. Pisonero, C.M. Smith, R.N. Taylor, Atomic spectrometry update: review of advances in atomic spectrometry and related techniques, J. Anal. At. Spectrom., 35 (2020) 830–851. https://doi.org/10.1039/d0ja90015j

Electronic Supplementary Material
(ESM: References 41-51)

Anal. Methods Environ. Chem. J. 5 (2) (2022) 24-38

AMECJ

Research Article, Issue 2
Analytical Methods in Environmental Chemistry Journal
Journal home page: www.amecj.com/ir

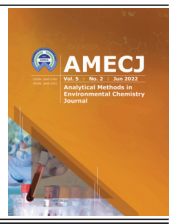

Adsorption of diazinon using Cd-MOF nanoparticles before determination by UV-Vis spectrometer: isotherm, kinetic and thermodynamic study

Faeze Khakbaz [a], Mohamad Mahani[b*] and Mehdi Yoosefian[b]

[a] *Department of Chemistry, Shahid Bahonar University, Kerman, Iran*

[b] *Department of Chemistry, Faculty of Chemistry and Chemical Engineering, Graduate University of Advanced Technology, Kerman, 7631818356, Iran.*

ARTICLE INFO:

Received 15 Feb 2022

Revised form 20 Apr 2022

Accepted 25 May 2022

Available online 29 Jun 2022

Keywords:

Cadmium Metal–Organic Fameworks,
Diazinon,
UV-Vis spectrometer,
Adsorption kinetic,
Adsorption thermodynamic,
Pesticides

ABSTRACT

In this work, cadmium metal–organic frameworks (Cd-MOF) has been prepared using a hydrothermal method and characterized by the SEM, elemental mapping, XRD, EDS, and BET analysis. The diazinon stability has been investigated in various pH (4-8) and temperature (298°K – 323°K) using UV-Vis spectrometer in the range of 230 – 280 nm, at its main absorption peak at 247 nm. Adsorption behaviors of diazinon on the Cd MOF were considered in different conditions. UV-Vis spectroscopy was used to monitor the removal of diazinon using the Cd MOF. The adsorption capacity of 138 mg g^{-1} was obtained. The effect of temperature (298°K -323°K), pH (4-8), adsorbent dose (1-7 mg), initial concentration (4-12 mg L^{-1}), stirring speed (0-500 rpm), and adsorption kinetics were studied using batch rout. All the studied parameters have shown significant effects on the efficiency of removal of diazinon by the Cd MOF. The adsorption thermodynamic was investigated in the temperature range of 298°K to 323°K and it has shown the endothermic nature of adsorption of diazinon using prepared Cd MOF. The adsorption isotherm follows by the Langmuir isotherm model. It was demonstrated that synthesized adsorbent could be effectively used for the removal of diazinon from water.

1. Introduction

The use of pesticides in agriculture to control unwanted insects and disease carriers increases food production. Widespread use of pesticides in agriculture and public health programs endangers public health with issues such as acute human poisoning and environmental pollution [1]. According to the World Health Organization (WHO), the number of acute pesticide poisonings in developing countries is increasing every year. In 1982, it was estimated that while developing countries accounted for only 15% of global pesticide use, more than 50% of pesticide poisoning occurred in those countries due to misuse [2]. Organophosphates, phosphorus-containing compounds which are derived from phosphoric acid, are generally used as insecticides among pesticides and are usually the most toxic insecticides to vertebrates. Residual amounts of organophosphates pesticides have been identified in cereals, vegetables, water bodies, soil, water, and other agricultural products [3]. Due to the widespread use of pesticides, their toxic effects have been observed in humans [4]. The mechanism of action is based on the inhibition of acetylcholinesterase activity by

*Corresponding Author: Mohamad Mahani
Email: mohmahani@gmail.com
https://doi.org/10.24200/amecj.v5.i02.175

covalently binding to its serine residues, thereby stopping nerve impulses that lead to death [5]. The lipophilic nature of organophosphates, facilitates their interaction with the cell membrane and led to disrupts the bilayer structure of phospholipids in visceral organs [6]. Acute poisoning by organophosphates stimulates muscarinic receptors, and diarrhea, abdominal pain, sweating, excessive salivation, and other symptoms are appeared [7]. In addition, stimulation of nicotine receptors in skeletal muscle neuromuscular connections by organophosphates cause weakness, involuntary contraction, and paralysis [8]. These pesticides have many adverse effects on the reproductive system , urinary system and human immune system [9]. Among the most commonly used organophosphates pesticides, O,O-Diethyl O- [4-methyl-6- (ppropane2-yl)pyrimidin-2-yl][10] phosphorothioate, INN - Dimpylate (diazinon) is a synthetic chemical that is used worldwide in agriculture to control insects in crops, vegetables, fruits, grass, and ornamental plants [11]. Diazinon is classified as a moderately dangerous organophosphate class II insecticide and can be absorbed through the gastrointestinal tract, skin, or respiratory tract upon inhalation [12]. Diazinon also leads to hyperglycemia, and depletion of glycogen from the brain and peripheral tissues along with increased glycogen phosphorylase activity in the brain and liver [13]. Recently, the removal of diazinon from water using adsorption methods has attracted much attention. For determining percentages of removal various methods such as simulation, spectroscopy, and chromatography have been used [14, 15]. Various materials such as multi-walled carbon nanotubes [16], activated carbon [17], bismuth oxide-fullerene nanoparticles [18], mesoporous silica [19] and , metal-organic frameworks [20] and other porous materials [21] have been used as adsorbents. Metal-organic framework, which is composed of metal ions or clusters of organic linkers, are crystalline materials that have a variety of applications in the removal of contaminants [22] drug delivery [23], catalysis [24] separation [19], electronic devices [25] gas storage [26], and sensors [27]. Due to the adjustable porosity, high surface area, adsorptive properties, and variety of structures MOFs are effective agents for the removal of pesticides from water. MOFs are synthesized using many methods such as ionothermal [28], solvent evaporation [29], self-assembly of primary building blocks [30], mechanochemical [31], electrochemical [32], ultrasonic [33], microwave [34], solvothermal [35] and hydrothermal [20, 36] methods.

In this work, Cd MOF was prepared using a hydrothermal route. The synthesized porous nanomaterial was used for the removal of diazinon from water. The temperature, pH, contact time, amount of adsorbent, stirring speed effect, adsorption isotherms, and adsorption kinetics were investigated.

2. Experimental

2.1. Materials and apparatus

Cadmium (II) nitrate tetrahydrate (CAS N.: 10022-68-1; Sigma, Germany), fumaric acid (CAS N.: 110-17-8; Sigma, Germany), and diazinon (CAS N.: 333-41-5: Merck, Germany) were used without any purification. The chemical structure of diazinon is shown in Figure 1. The sample pH was adjusted with hydrochloric acid (CAS N.: 7647-01-0: Merck, Germany) and sodium hydroxide (CAS N.: 1310-73-2; Merck, Germany). The absorption spectra were obtained by using an Agilent Cary 50 UV-Vis spectrometer, with 1.0 cm quartz cells. The crystal structure of Cd MOF was analyzed by Bruker Advance-D8 equipped with Cu Kα radiation (Bruker, Germany). The morphology was obtained by an S-4800 HITACHI scanning electron microscope at 10 kV, 100 mA (Hitachi, Japan). The pore volume and surface area of the Cd MOF were determined by BET method using Sorptomatic 1990 after degassing at 150^{o}C (Thermo Fisher Scientific, USA.)

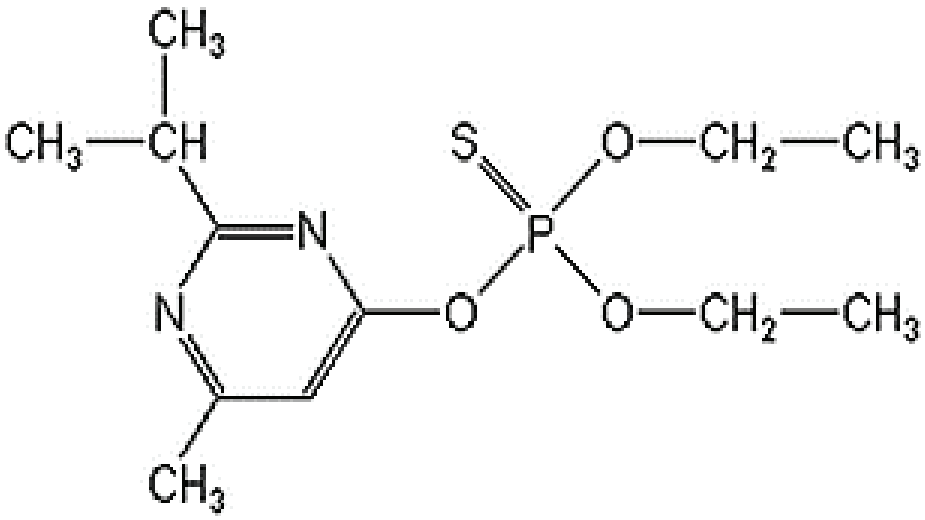

Fig.1. Chemical structure of diazinon

2.2. Synthesis of the Cd-MOF

Cd MOF was synthesized according to the previous reports with minor modifications [20]. 8.9 g $Cd(NO_3)_2.4H_2O$, 5.22 g fumaric acid, and 3.6 g NaOH were dispersed in 50 mL ultrapure water and were stirred for 30 minutes. The solution was transferred into a 100 ml Teflon-lined hydrothermal reactor and incubated in 180°C for 48 h (Scheme 1). The autoclave was cooled to room temperature for 12 h. The product was centrifuged at 10000 g for 15 minutes, washed several times with distilled water, and dried at 50°C overnight.

Scheme1. Synthesis of Cd MOF

2.3. Adsorption study procedure

Removal studies of diazinon by the Cd MOF were carried out in the batch procedure. UV-Vis spectroscopy was used to monitor equilibrium concentrations of diazinon. The calibration curve was plotted for different concentrations of diazinon and their corresponding absorbance at 248 nm. After the removal process, the residual concentration of diazinon was deducted from the calibration curve. The uptake capacity and removal efficiency were determined by comparing the concentration of diazinon before and after adsorption, according to the following equation 1 and 2:

$$\text{Removal efficiency (\%)} = (C_i - C_e) / C_i \times 100 \quad \text{(Eq. 1)}$$

$$\text{Uptake capacity Qe (mg g}^{-1}) = (C_i - C_e) \times V/m \quad \text{(Eq. 2)}$$

Qe is the amount of diazinon adsorbed on the surface of MOF. Where C_i and C_e are the initial and equilibrium concentration of diazinon solution, V is the volume of diazinon solution, and m is the weight of MOF. In the batch procedure, the influence of effective parameters such as contact time, adsorbent dose, initial concentration of insecticides, temperature, pH, and the stirring speed was investigated.

3. Results and discussion

3.1. characterization of Cd MOF

Figure 2a shows the XRD pattern of the synthesized Cd MOF. The pattern exhibited diffraction peaks that were similar to the plan of Cd (No. 01-085-0989). The crystal size of the Cd MOF was calculated using the Debye-Scherrer equation at about 21 nm.

The morphology of Cd MOF was characterized by SEM, which is shown in Figure 2b. The obtained SEM images show that the prepared Cd MOF are cubic and have uniform size distributions. The energy-dispersive X-ray spectroscopy (EDS) has been used to characterize the chemical composition of synthesized nanocrystals. Figure 2c and 2d show the chemical elemental mapping and EDS of the Cd MOF. The EDS results are revealed that the synthesized nanocrystals have composed of Cd, O, and C. In addition, the elemental mapping shows that the elements are homogeneously distributed through the MOFs. The specific surface area of the prepared Cd MOFs is explained using Brunaur-Emmett-Teller (BET) method. The mean pore diameter, surface area, and total pore volume of the nanocrystals were calculated at about 15.5 nm, 0.4 m^2 g^{-1}, and 0.0014 cm^3 g^{-1}, respectively.

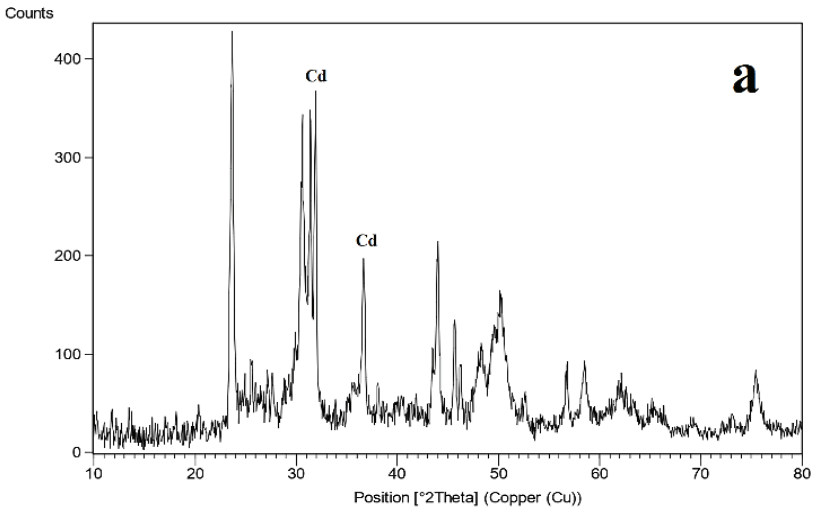

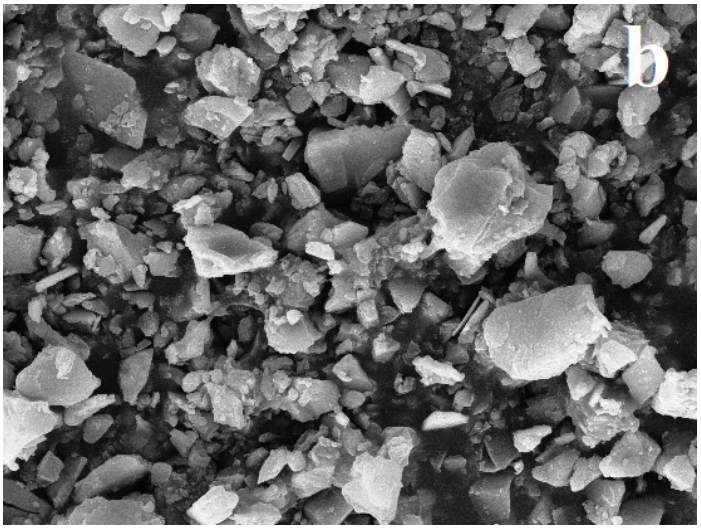

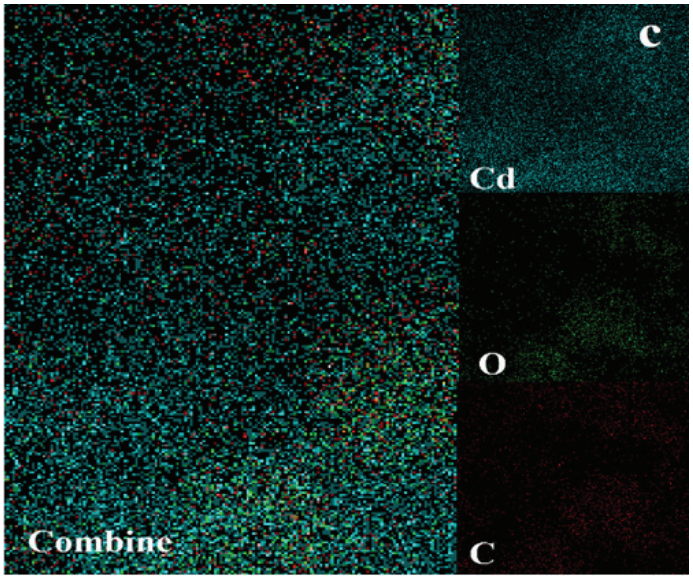

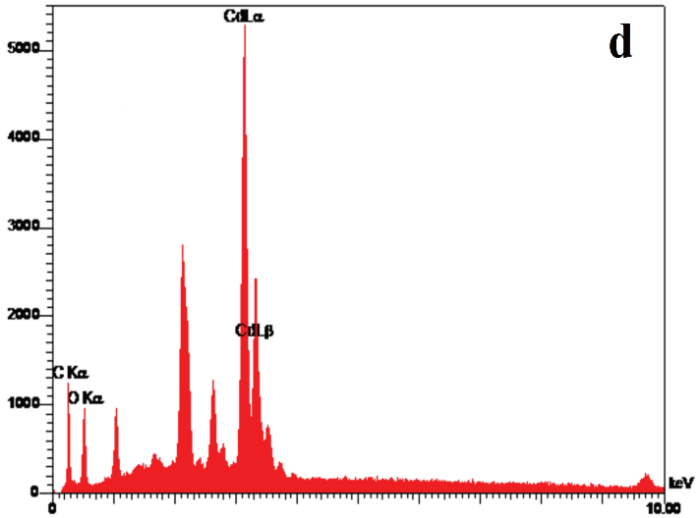

Fig. 2. Characterization of Cd MOF, a) The XRD pattern, b) The SEM image, c) The elemental mapping, and d) The EDS analysis of Cd MOF

3.2. Adsorption of diazinon onto Cd MOF

3.2.1.Optical stability of diazinon

Diazinon stability was studied in various pH and temperature conditions. As shown in Figure 3, temperature and pH changes of the diazinon solution don't have significant effects on the absorption intensity at 248 nm. Therefore, it can be said that diazinon is stable at the studied temperature and pH values.

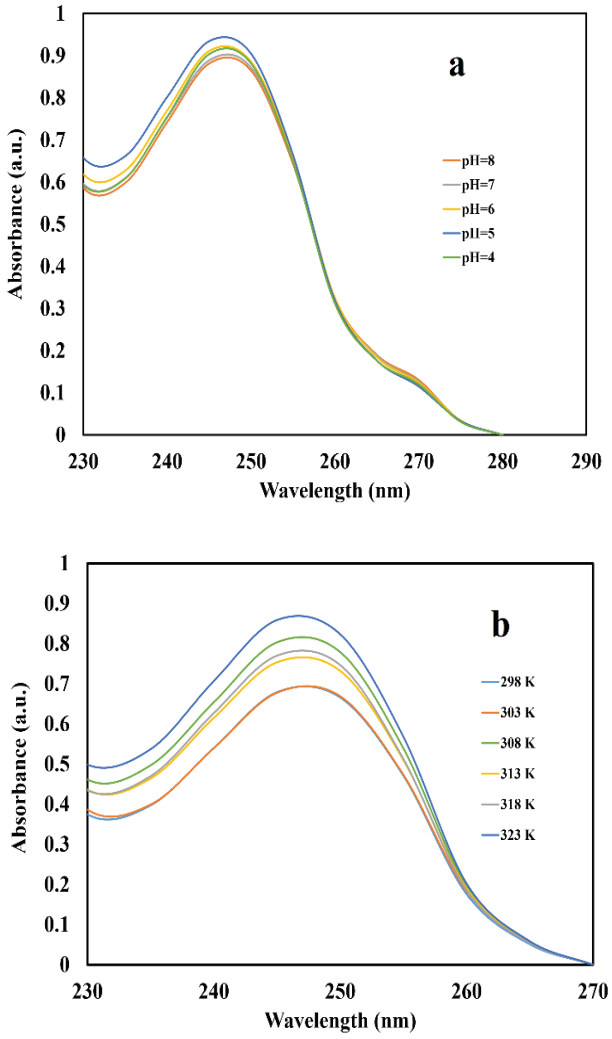

Fig. 3. Effect of various (a) pH and (b) temperature on diazinon absorption spectra

3.2.2.Effect of adsorbent dose

For investigation the optimized mass of Cd MOF in adsorption process, various amounts (1-7 mg) of adsorbent were added to the constant volume (30 ml) of 12-ppm diazinon solution under the same conditions and stirred at 300 rpm. The absorption spectra of solutions were recorded at a specific time. Figure 4 shows the removal efficacy and uptake capacity of different amounts of Cd MOF in various periods. It can be seen that the removal intensity of diazinon was increased from 37% to 95% with increasing the adsorbent dose from 1 to 7 mg at 15 minutes as the contact times. This increase is clearly due to the increase in surface area and adsorption sites. 3 mg of Cd MOF was chosen as the optimal amount of adsorbent for further experiments.

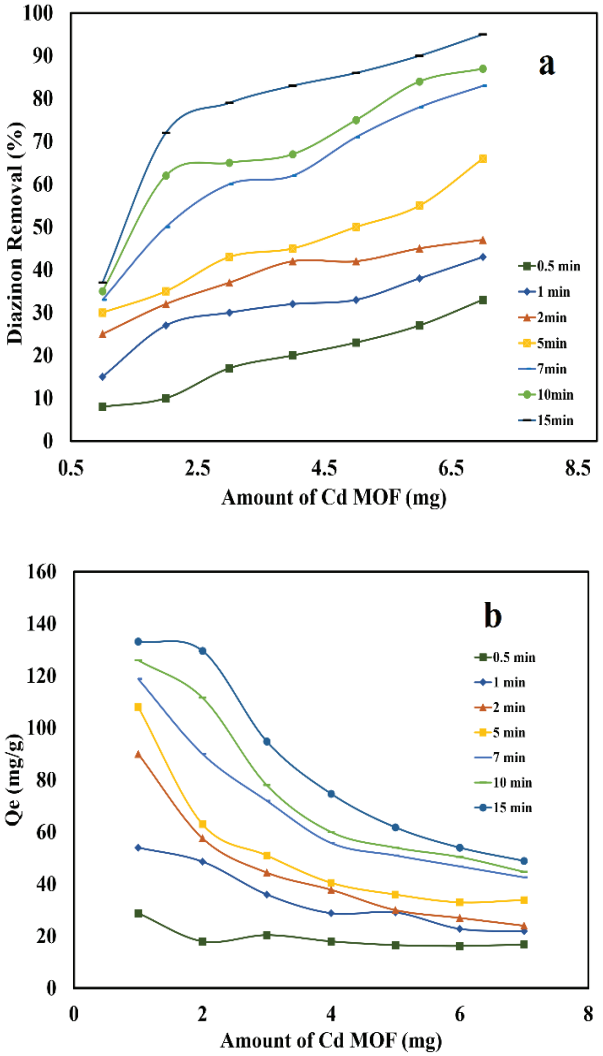

Fig. 4. Effect of adsorbent dose on (a) removal efficiency and (b) uptake capacity of Cd MOF (diazinon concentration = 12 ppm, natural pH, room temperature)

3.2.3.Effect of diazinon concentration

The plot of uptake capacities vs. initial diazinon concentrations in presence of 3 mg Cd MOF as the optimal amount of adsorbent and at various contact time were shown in Figure 5. It was shown that after 15 minutes, with increasing the initial diazinon concentration from 4 to 12 ppm, the uptake capacity increased from 42 To 95 mg g^{-1}. The increase of uptake capacity is probably due to increase in the mass gradient between the diazinon solution and Cd MOF with increasing the insecticide concentration.

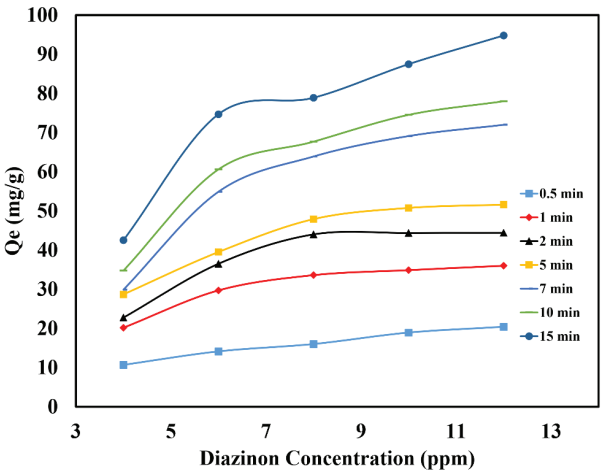

Fig. 5. Effect of initial diazinon concentration on uptake capacity of Cd MOF in various contact times (amount of adsorbent = 3 mg, natural pH, room temperature)

3.2.4.Effect of contact time

Figure 6 shows the plot of uptake capacity vs. contact time in presence of various amounts of Cd MOF (the diazinon concentration of 12 ppm), and different concentrations of diazinon (adsorbent dose of 3 mg) at natural pH and room temperature. According to the results, the diazinon is rapidly adsorbed and the optimal removal efficacy is obtained at 7 minutes. A large number of empty sites at the Cd MOF surface in the early minutes causes high adsorption efficacy. With time and occupied the active sites with diazinon molecules, the adsorption speed decreased impressively.

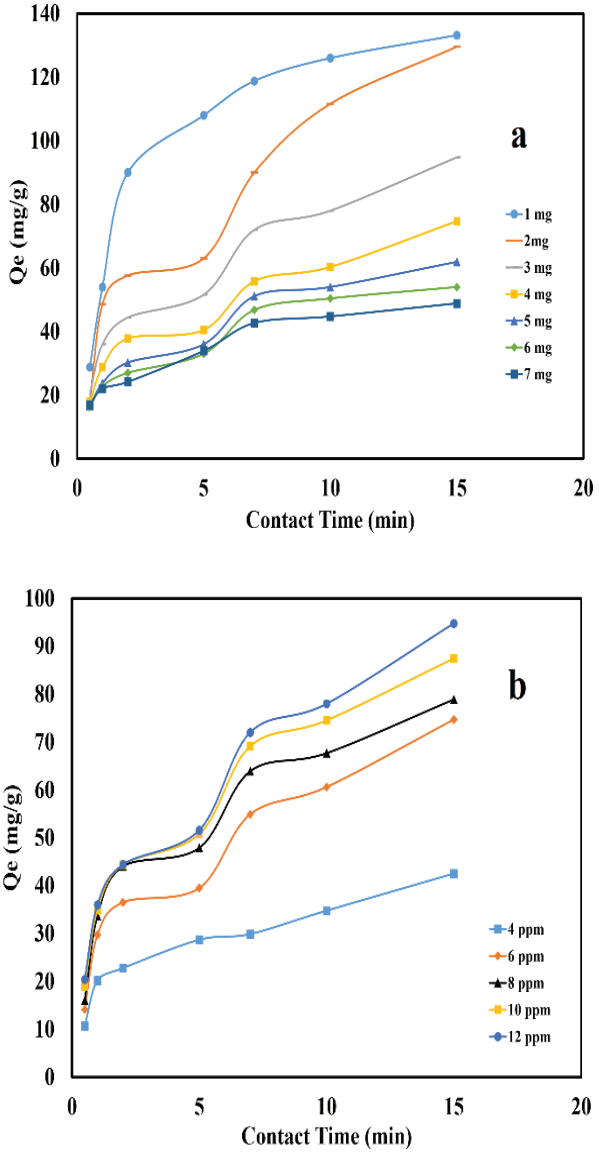

Fig. 6. Effect of contact time on uptake capacity of Cd MOF in (a) various amounts of adsorbent (diazinon concentration = 12 ppm, natural pH, and room temperature) (b) various concentrations of diazinon (amount of adsorbent = 3 mg, natural pH, and room temperature)

3.2.5.Effect of pH

The adsorption of diazinon onto Cd MOF was investigated in a pH range of 4-8 at room temperature. 3 mg of Cd MOF was added to 30 ml of 12 ppm diazinon solution and stirred at 300 rpm for 0.5 to 10 minutes. According to Figure 7, the removal efficiency of diazinon by Cd MOF was increased with an increase in pH. Figure

7b clearly shows increasing the uptake capacity from 43 to 58 mg g^{-1} by increasing the pH from 4 to 8. The desirable removal at higher pH can be due to the cationic nature of diazinon. The presence of excess, H^+ in acidic solution cause to decrease in the negative adsorbent site and it is not favored for positively charged diazinon ions. An increasing number of negative sites on the adsorbent can enhance the adsorption of diazinon at high pH.

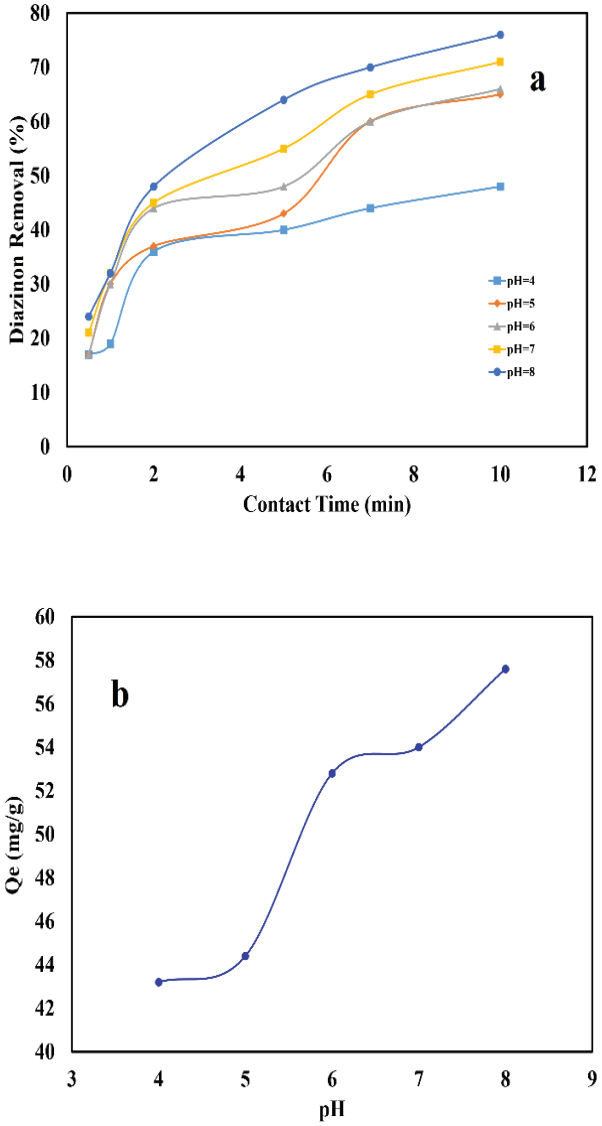

Fig. 7. Effect of pH on (a) removal efficiency of diazinon using Cd MOF at various contact times, (b) uptake capacity of Cd MOF at 7 minutes (diazinon concentration = 12 ppm, amount of adsorbent = 3 mg, and room temperature)

3.2.6.Effect of temperature

Removal of the diazinon was studied at various temperatures from 298 to 323 K in the presence of 3 mg of Cd MOF at different times. As shown in Figure 8, the adsorption efficiency has been increased with increasing in temperature. The increase of removal efficiency can be due to the endothermic nature of the adsorption process.

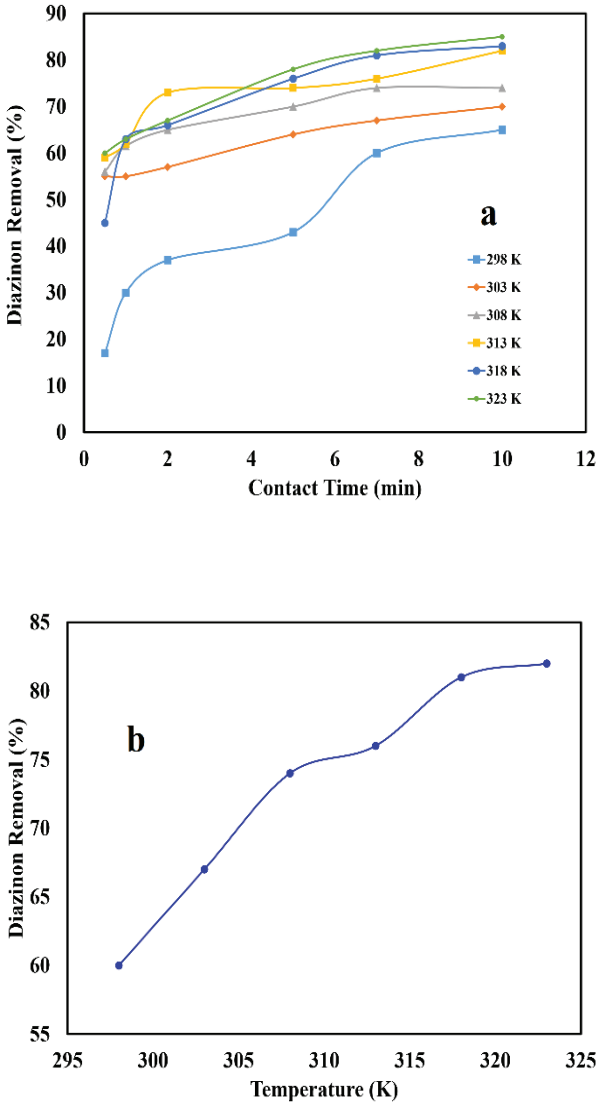

Fig. 8. Effect of temperature on removal efficiency of diazinon (a) at various times, (b) at 7 minutes as optimum time (dye concentration = 12 ppm, amount of adsorbent = 3 mg, and natural pH)

3.2.7.Effect of stirring speed

The effect of stirring speed on the removal of diazinon was studied at various stirring speeds (0 -

500 rpm) in identical conditions (natural pH, room temperature, 12 ppm initial diazinon concentration, 7 minutes as contact time). According to Figure 9, the stirring speed shows significant effect on removal rate in the removal process of diazinon.

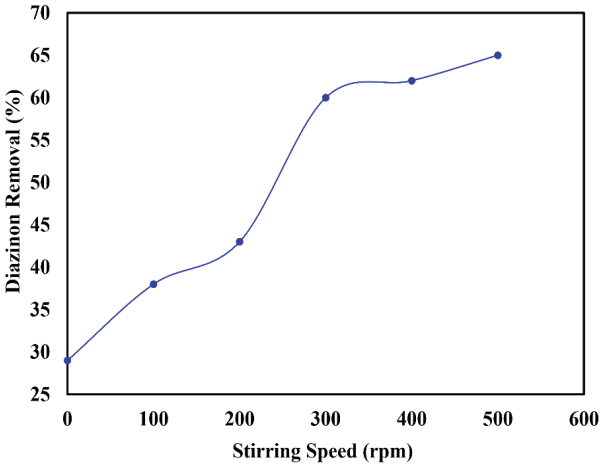

Fig. 9. Effect of stirring speed on removal efficiency of diazinon (diazinon concentration = 12 ppm, amount of adsorbent = 3 mg, contact time = 7 minutes, natural pH, and room temperature)

3.3. Adsorption isotherm

The adsorption isotherm can be used to study, estimation of the affinity between Cd MOF and diazinon, the adsorption mechanism and predict the maximum adsorption capacity of the Cd MOF. Here, three isotherm models (Temkin, Freundlich, and Langmuir isotherm) were applied. The Freundlich isotherm is applicable to the non-uniform adsorption processes of adsorbed molecules occurring on heterogeneous adsorbent surfaces. Multilayer adsorption is considered in this isotherm [37]. Temkin isotherm considers for accounting the effects of indirect adsorbate/adsorbate interactions on the adsorption process. It shows that there are various energetical sites on the adsorbent surface, in which adsorption of adsorbate occurs on the energetic sites at first. It is supposed that by increasing the surface coverage, the heat of absorption of the molecules in the layer decreases linearly. The Temkin isotherm model is reliable just for the intermediate range of dye concentrations [38]. The Langmuir adsorption isotherm takes into describes the homogenous surface that a single surface site of adsorbent is occupied by a single adsorbate molecule. The Langmuir isotherm assumes that there is not any lateral interaction between the adsorbed molecules [39]. Langmuir, Temkin, and Freundlich isotherm represent according to the following Equations (3-5):

$$Ce / Qe = 1/K_L Q_L + Ce/Q_L \quad \text{Langmuir isotherm} \quad \text{(Eq. 3)}$$

$$Qe = (RT/b_T) \ln K_T + (RT/b_T) \ln Ce \quad \text{Temkin isotherm} \quad \text{(Eq. 4)}$$

$$Ln\ Qe = \ln K_f + (1/n) \ln Ce \quad \text{Freundlich isotherm} \quad \text{(Eq. 5)}$$

Where Ce (mg L^{-1}) is the equilibrium concentration of diazinon solution, Qe (mg g^{-1}) is the amount of diazinon adsorbed by Cd MOF at equilibrium. R is gas constant (8.314 J $mol^{-1}K^{-1}$) and T is temperature (K) that room temperature was taken into account. K_L and Q_L (the Langmuir monolayer adsorption capacity), b_T and K_T, K_f (adsorption capacity), and 1/n (adsorption intensity and adsorption capacity), are empirical constants parameters that affecting the adsorption process for Langmuir, Temkin, and Freundlich isotherms respectively [40].

As shown in Figure 10 the plots of Qe vs. ln Ce, ln Qe vs. ln Ce, and Ce/Qe vs. Ce were used to calculate the constant parameters of Temkin, Freundlich, and Langmuir isotherms respectively. All parameters and correlation coefficient are listed in Table 1. The Langmuir isotherm gave the highest correlation coefficient, which was 0.98 at room temperature revealing that the adsorption of diazinon on the Cd MOF is perfectly described by this model.

3.4. Thermodynamic

The thermodynamic parameters of the

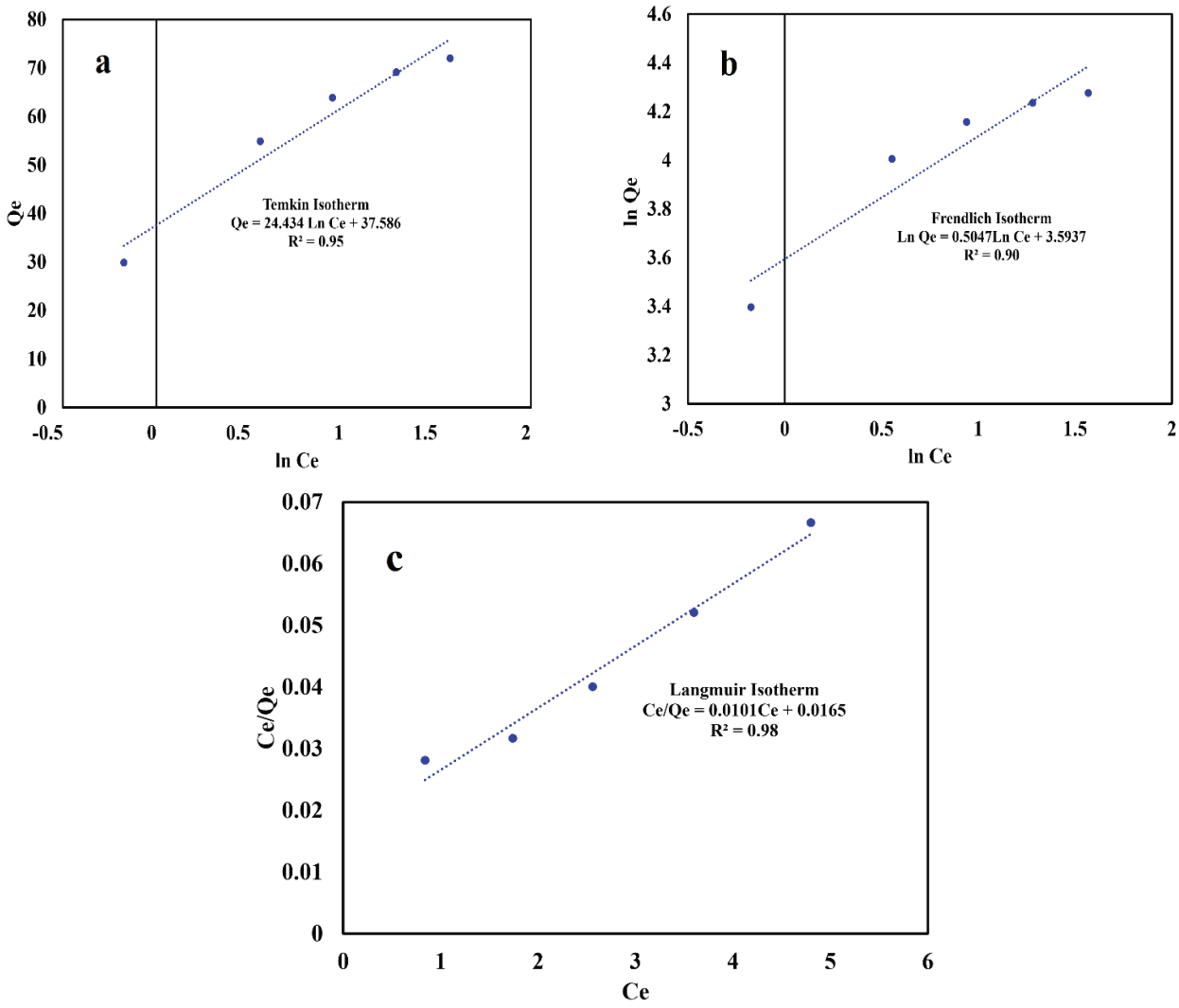

Fig. 10. Linear plot of (a) Temkin, (b) Frendlich, and (c) Langmuir isotherm

Table 1. Isotherm parameters for diazinon adsorption on Cd MOFs

Diazinon concentration (ppm)		Q_e (mg g^{-1})	Langmuir isotherm			Temkin isotherm			Freundlich isotherm		
C_0	C_e		Q_L	K_L	R^2	b_T	K_T	R^2	n	K_f	R^2
4	0.84	29.88									
6	1.74	54.9									
8	2.56	63.9	100	0.6	0.98	101.4	4.66	0.95	1.98	36.23	0.9
10	3.6	69.12									
12	4.8	72									

adsorption process were used to determine the spontaneity of the adsorption process at various temperatures. Change in enthalpy ΔH (kJ mol^{-1}), entropy ΔS (J mol^{-1} K^{-1}), and Gibbs free energy ΔG (kJ mol^{-1}) was calculated using the following equations 6 and 7:

$$Ln\ (Q_e/C_e) = \Delta S/R - \Delta H/RT \quad \text{(Eq. 6)}$$

$$\Delta G = \Delta H - T\Delta S \quad \text{(Eq. 7)}$$

ΔH and ΔS can be provided from the slope (ΔH/R) and intercept (ΔS/ R) of the plot of ln (Q_e/C_e) vs. 1/T (Fig. 11). The calculated values of thermodynamic parameters are shown in table 2. The negative amount of ΔG indicates that the feasibility of the adsorption process and its spontaneous nature. The positive value of ΔH describes that the adsorption of diazinon by the Cd MOF is endothermic.

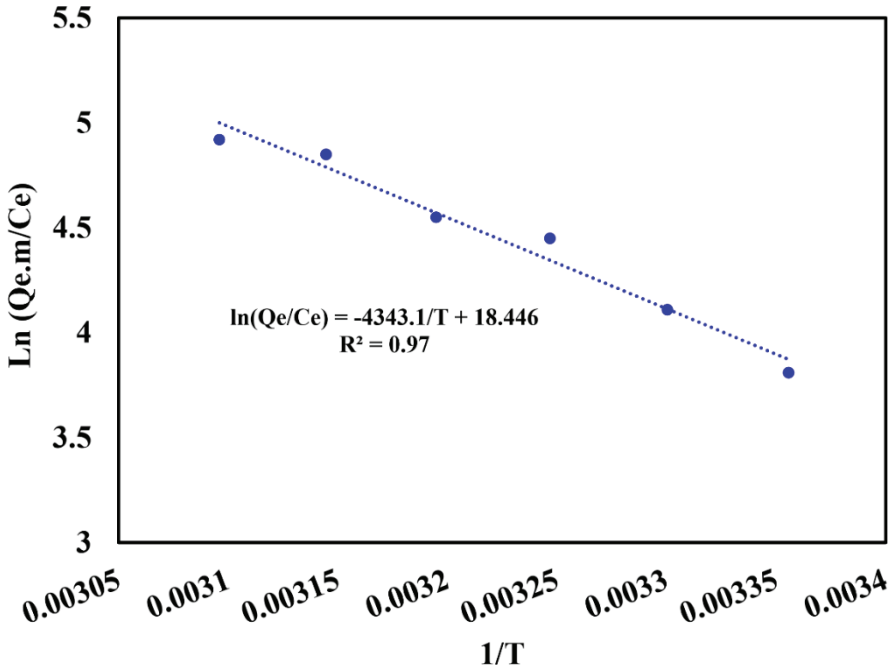

Fig. 11. Plot of ln(Qe.m/Ce) vs. 1/T to give thermodynamic parameters

Table 2. Thermodynamic parameters for adsorption of diazinon on Cd MOF

Diazinon concentration (ppm)	**ΔH** (KJ mol^{-1})	**ΔS** (KJ $mol^{-1}K^{-1}$)	**ΔG** (KJ mol^{-1}) 298 K	**ΔG** (KJ mol^{-1}) 303 K	**ΔG** (KJ mol^{-1}) 308 K	**ΔG** (KJ mol^{-1}) 313 K	**ΔG** (KJ mol^{-1}) 318 K	**ΔG** (KJ mol^{-1}) 323 K
12	36.11	0.15	-81.8	-82.6	-83.3	-84.1	-84.9	-85.6

3.5. Kinetic

Adsorption kinetics of diazinon removal were studied using Pseudo-first-order, pseudo-second-order and intrapacticle diffusion models to identify the rapid initial phase of adsorption, chemisorptions and intra- particle diffusion. The linear forms of kinetic models are given as Equation 8-10:

$$\ln (Q_e - Q_t) = \ln Q_e - k_1 t \quad \text{(Pseudo first order kinetics)} \quad \text{(Eq. 8)}$$

$$t/Q_t = t/Q_e + 1/k_2 Q_e^2 \quad \text{(Pseudo second-order kinetics)} \quad \text{(Eq. 9)}$$

$$Q_t = k_i t^{1/2} + C \quad \text{(Intraparticle diffusion)} \quad \text{(Eq. 10)}$$

Where, Q_t (mg g^{-1}) and Q_e (mg g^{-1}) refer to the amount of diazinon adsorbed at time t (min) and equilibrium respectively. k_1 (min^{-1}), k_2 (g $mg^{-1}min^{-1}$), and k_i (mg $g^{-1}min^{1/2}$) are rate constant of adsorption for pseudo-first order, pseudo second order and intraparticle diffusion respectively. In intraparticle diffusion, constant C reflects the boundary layer effect [39].

Table 3 shows a list of kinetic parameters for various initial concentrations of diazinon. Compared to the pseudo-first-order and intraparticle diffusion, the pseudo-second-order model showed a higher regression coefficient and was selected as the model for the absorption kinetics of diazinon removal.

4. Conclusion

In this work, Cd based metal organic frameworks (Cd MOFs) were synthesized by a simple and cost-effective hydrothermal route using fumaric acid as a linker. The prepared Cd MOF used for removal of diazinon from water. The absorbent dose, pH, temperature, diazinon concentration, contact time and stirring speed were optimized as affecting parameters and the best condition was reported in this paper. Various isotherm and kinetic models were investigated for the removal of diazinon using the prepared Cd MOF and the Langmuir isotherm and pseudo-second -order kinetic model was suggested for uptake of diazinon on the Cd MOFs through an endothermic process. According to results, Cd MOF can act as an effective adsorbent for removal the pesticides from water through a fast, cost-effective and simple route.

Table 3. Kinetic parameters for adsorption of diazinon on Cd MOF

Qi (mg g^{-1})	Q_e (mg g^{-1})	Pseudo First order			Pseudo Second order			Intraparticle		
		Q_e	K_1	R^2	Q_e	K_2	R^2	C	K_i	R^2
4	29.88	1.24	0.58	0.98	43.01	0.032	0.99	6.59	10.44	0.86
6	54.9	1.18	0.18	0.7	46.51	0.027	0.98	10.59	14.45	0.72
8	63.9	1.31	0.21	0.74	58.14	0.018	0.98	10.37	18.67	0.76
10	69.12	1.34	0.19	0.82	60.24	0.019	0.99	11.91	18.9	0.82
12	72	1.35	0.18	0.81	60.24	0.02	0.99	13.35	18.48	0.84

5. References:

[1] M. Abdollahi, S. Mostafalou, S. Pournourmohammadi, S. Shadnia, Oxidative stress and cholinesterase inhibition in saliva and plasma of rats following subchronic exposure to malathion, Comparative Biochemistry and Physiology Part C: Toxicol. Pharmacol., 137 (2004) 29-34. https://doi.org/10.1016/j.cca.2003.11.002

[2] M.D. Shah, M. Iqbal, Diazinon-induced oxidative stress and renal dysfunction in rats, Food Chem. Toxicol., 48 (2010) 3345-3353. https://doi.org/10.1016/j.fct.2010.09.003

[3] E. Noroozian, Solid phase microextraction of organochlorine pesticides in water using MWCNTs-doped polypyrrole coated on steel fiber, Anal. Methods Environ. Chem. J., 3 (2020) 40-51. https://doi.org/10.24200/amecj.v3.i04.117

[4] R. Kamanyire, L. Karalliedde, Organophosphate toxicity and occupational exposure, Occup. Med., 54 (2004) 69-75. https://doi.org/10.1093/occmed/kqh018

[5] I.B. Obinna, E.C. Ebere, A review: Water pollution by heavy metal and organic pollutants: Brief review of sources, effects and progress on remediation with aquatic plants, Anal. Methods Environ. Chem. J., 2 (2019) 5-38. https://doi.org/10.24200/amecj.v2.i03.66

[6] S. Selmi, S. El-Fazaa, N. Gharbi, Oxidative stress and cholinesterase inhibition in plasma, erythrocyte and brain of rats' pups following lactational exposure to malathion, Environ. Toxicol. Pharmacol., 34 (2012) 753-760. https://doi.org/10.1016/j.etap.2012.09.012

[7] M.E. Buyukokuroglu, M. Cemek, Y. Yurumez, Y. Yavuz, A. Aslan, Antioxidative role of melatonin in organophosphate toxicity in rats, Cell Biol. Toxicol., 24 (2008) 151-158. https://doi.org/10.1007/s10565-007-9024-z

[8] M.E. Büyükokuroğlu, M. Cemek, M. Tosun, Y. Yürümez, O. Baş, Y. Yavuz, Dantrolene may prevent organophosphate-induced oxidative stress and muscle injury, Pesticide Biochem. Physiol., 92 (2008) 156-163. https://doi.org/10.1016/j.pestbp.2008.07.012

[9] A. Mitra, M. Sarkar, C. Chatterjee, Modulation of immune response by organophosphate pesticides: Mammals as potential model, Proceedings of the Zoological Society, Springer, 2019, pp. 13-24. https://doi.org/10.1007/s12595-017-0256-5

[10] M.K. Mahani, A.R. Khanchi, M. Heidari, A. Ahmadi, A novel inductively coupled plasma atomic emission spectrometry method for uranium isotope ratio measurements using chemometric techniques, J. Anal. Atom. Spect., 25 (2010) 1659-1660. https://doi.org/10.1039/C004761A

[11] P. Sharma, A. Sharma, N.D. Jasuja, S.C. Joshi, Organophosphorous compounds and oxidative stress: a review, Toxicol. Environ. Chem., 96 (2014) 681-698. https://doi.org/10.1080/02772248.2014.972045

[12] M. Kushwaha, S. Verma, S. Chatterjee, Profenofos, An acetylcholinesterase-inhibiting organophosphorus pesticide: a short review of its usage, Toxicity, and Biodegradation, J. Environ. Quality, 45 (2016) 1478-1489. https://doi.org/10.2134/jeq2016.03.0100

[13] S. Karami-Mohajeri, M. Abdollahi, Toxic influence of organophosphate, carbamate, and organochlorine pesticides on cellular metabolism of lipids, proteins, and carbohydrates: a systematic review, Human Exp. Toxicol., 30 (2011) 1119-1140. https://doi.org/10.1177/0960327110388959

[14] M.K. Mahani, M.G. Maragheh, Simultaneous determination of sodium, potassium, manganese and bromine in tea by standard addition neutron activation analysis, Food Anal. Methods, 4 (2011) 73-76._https://doi.org/10.1007/s12161-009-9120-1

[15] H. Sepehrian, S. Waqif-Husain, J. Fasihi, M.K. Mahani, Adsorption behavior of molybdenum on modified mesoporous zirconium silicates, Sep. Sci. Technol., 45 (2010) 421-426. https://doi.org/10.1080/01496390903423519

[16] E. Zolfonoun, Solid phase extraction and determination of indium using multiwalled carbon nanotubes modified with magnetic nanoparticles, Anal. Methods Environ. Chem. J., 1 (2018) 5-10. https://doi.org/10.24200/amecj.v1.i01.14

[17] A. Zarei, M. Arjomandi, Synthesis and performance of graphene and activated carbon composite for absorption of three-valance arsenic from wastewater, Anal. Methods Environ. Chem. J., 2 (2019) 63-72. https://doi.org/10.24200/amecj.v2.i01.53

[18] C. Jamshidzadeh, H. Shirkhanloo, A new analytical method based on bismuth oxide-fullerene nanoparticles and photocatalytic oxidation technique for toluene removal from workplace air, Anal. Methods Environ. Chem. J., 2 (2019) 73-86. https://doi.org/10.24200/amecj.v2.i01.55

[19] M. Gou, B.B. Yarahmadi, Separation and determination of lead in human urine and water samples based on thiol functionalized mesoporous silica nanoparticles packed on cartridges by micro column fast micro solid-phase extraction, Anal. Methods Environ. Chem. J., 2 (2019) 39-50. https://doi.org/10.24200/amecj.v2.i03.72

[20] S. Fakhraie, A. Ebrahimi, Facile synthesis of a modified HF-free MIL-101 (Cr) nanoadsorbent for extraction nickel in water and wastewater samples, Anal. Methods Environ. Chem. J., 3 (2020) 59-73. https://doi.org/10.24200/amecj.v3.i02.103

[21] M.H. Mokari-Manshadi, M. Mahani, Z. Hassani, D. Afzali, E. Esmaeilzadeh, Synthesis of Mesoporous Molybdenum Disulfide (MoS2): A Photocatalyst for Removal of Methylene Blue, J. Nanosci. Nanotechnol., 17 (2017) 8864-8868. https://doi.org/10.1166/jnn.2017.14317

[22] F. Khakbaz, M. Mirzaei, M. Mahani, Enhanced adsorption of crystal violet using Bi^{3+}–intercalated Cd-MOF: isotherm, kinetic and thermodynamic study, Particulate Sci. Technol., (2022) 1-13. https://doi.org/10.1080/02726351.2022.2032890

[23] J. Cao, X. Li, H. Tian, Metal-organic framework (MOF)-based drug delivery, Curr. Med. Chem., 27 (2020) 5949-5969. https://doi.org/10.2174/0929867326666190618152518

[24] V. Stavila, R. Parthasarathi, R.W. Davis, F. El Gabaly, K.L. Sale, B.A. Simmons, S. Singh, M.D. Allendorf, MOF-based catalysts for selective hydrogenolysis of carbon–oxygen ether bonds, ACS Catal., 6 (2016) 55-59. https://doi.org/10.1021/acscatal.5b02061

[25] S. Roy, S. Halder, M.G. Drew, P.P. Ray, S. Chattopadhyay, Fabrication of an active electronic device using a hetero-bimetallic coordination polymer, ACS Omega, 3 (2018) 12788-12796. https://doi.org/10.1021/acsomega.8b02025

[26] V.O.N. Njoku, C. Arinze, I.F. Chizoruo, E.N. Blessing, A Review: Effects of air, water and land dumpsite on human health and analytical methods for determination of pollutants, Anal. Methods Environ. Chem. J., 4 (2021) 80-106. https://doi.org/10.24200/amecj.v4.i03.147

[27] M.G. Campbell, M. Dincă, Metal–organic frameworks as active materials in electronic sensor devices, Sensors, 17 (2017) 1108. https://doi.org/10.3390/s17051108

[28] Z.-H. Zhang, L. Xu, H. Jiao, Ionothermal synthesis, structures, properties of cobalt-1, 4-benzenedicarboxylate metal–organic frameworks, J. Solid State Chem., 238 (2016) 217-222. https://doi.org/10.1016/j.jssc.2016.03.028

[29] S.J. Yang, T. Kim, K. Lee, Y.S. Kim, J. Yoon, C.R. Park, Solvent evaporation mediated preparation of hierarchically porous metal organic framework-derived carbon with controllable and accessible large-scale porosity, Carbon, 71 (2014) 294-302. https://doi.org/10.1016/j.carbon.2014.01.056

[30] N.M. Kazemi, A novel sorbent based on metal–organic framework for mercury separation from human serum samples by ultrasound assisted-ionic liquid-solid phase

microextraction, Anal. Methods Environ. Chem. J., 2 (2019) 67-78. https://doi.org/10.24200/amecj.v2.i03.68

[31] L.S. Germann, A.D. Katsenis, I. Huskić, P.A. Julien, K. Uzarevic, M. Etter, O.K. Farha, T. Friscic, R.E. Dinnebier, Real-time in situ monitoring of particle and structure evolution in the mechanochemical synthesis of UiO-66 metal–organic frameworks, Cryst. Growth Des., 20 (2019) 49-54. https://doi.org/10.1021/acs.cgd.9b01477

[32] A.M. Antonio, J. Rosenthal, E.D. Bloch, Electrochemically Mediated Syntheses of Titanium (III)-Based Metal–Organic Frameworks, J. Am. Chem. Soc., 141 (2019) 11383-11387. https://doi.org/10.1021/jacs.9b05035

[33] N. Motakef kazemi, Zinc based metal–organic framework for nickel adsorption in water and wastewater samples by ultrasound assisted-dispersive-micro solid phase extraction coupled to electrothermal atomic absorption spectrometry, Anal. Methods Environ. Chem. J., 3 (2020) 5-16. https://doi.org/10.24200/amecj.v3.i04.123

[34] M. Taddei, D.A. Steitz, J.A. van Bokhoven, M. Ranocchiari, Continuous-Flow Microwave Synthesis of Metal–Organic Frameworks: A Highly Efficient Method for Large-Scale Production, Chem. A Euro. J., 22 (2016) 3245-3249. https://doi.org/10.1002/chem.201505139

[35] C. McKinstry, R.J. Cathcart, E.J. Cussen, A.J. Fletcher, S.V. Patwardhan, J. Sefcik, Scalable continuous solvothermal synthesis of metal organic framework (MOF-5) crystals, Chem. Eng. J., 285 (2016) 718-725. https://doi.org/10.1016/j.cej.2015.10.023

[36] F. Pourbahman, A. Monzavi, Z. Khodadadi, S.S. Homami, Reusable and sustainable graphene oxide/metal–organic framework-74/Fe3O4/polytyramine nanocomposite for simultaneous trace level quantification of five fluoroquinolones in egg samples by high performance liquid chromatography, Anal. Methods Environ. Chem. J., 4 (2021) 5-24. https://doi.org/10.24200/amecj.v4.i02.135

[37] N. Ayawei, A.N. Ebelegi, D. Wankasi, Modelling and interpretation of adsorption isotherms, J. Chem., 2017 (2017). https://doi.org/10.1155/2017/3039817

[38] H. Shahbeig, N. Bagheri, S.A. Ghorbanian, A. Hallajisani, S. Poorkarimi, A new adsorption isotherm model of aqueous solutions on granular activated carbon, World J. Model. Simul., 9 (2013) 243-254. http://doi.org/10.1.1.571.6718.

[39] B. Kaith, J. Sharma, Sukriti, S. Sethi, T. Kaur, U. Shanker, V. Jassal, Fabrication of green device for efficient capture of toxic methylene blue from industrial effluent based on K2Zn3 [Fe (CN) 6] 2· 9H2O nanoparticles reinforced gum xanthan-psyllium hydrogel nanocomposite, J. Chin. Adv. Mater. Soc., 4 (2016) 249-268. https://doi.org/10.1080/22243682.2016.1214923

[40] A. Mohammadi, A. Alinejad, B. Kamarehie, S. Javan, A. Ghaderpoury, M. Ahmadpour, M. Ghaderpoori, Metal-organic framework Uio-66 for adsorption of methylene blue dye from aqueous solutions, Int. J. Environ. Sci. Technol., 14 (2017) 1959-1968. https://doi.org/10.1016/j.cca.2003.11.002

Anal. Methods Environ. Chem. J. 5 (2) (2022) 39-50

AMECJ

Research Article, Issue 2
Analytical Methods in Environmental Chemistry Journal
Journal home page: www.amecj.com/ir

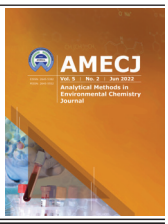

Response surface modeling for the treatment of methylene blue from aqueous media using electro-Fenton process before determination by UV-Vis spectrometer: Kinetic and degradation mechanism

Sara Zahedi [a], Ali Asadipour [b], Maryam Dolatabadi [c], Saeid Ahmadzadeh [d, e, *]

[a] *Student Research Committee, Kerman University of Medical Sciences, Kerman, Iran.*
[b] *Department of Medicinal Chemistry, Faculty of Pharmacy, Kerman University of Medical Sciences, Kerman, Iran.*
[c] *Environmental Science and Technology Research Center, Department of Environmental Health Engineering, School of Public Health, Shahid Sadoughi University of Medical Sciences, Yazd, Iran.*
[d] *Pharmaceutics Research Center, Institute of Neuropharmacology, Kerman University of Medical Sciences, Kerman, Iran.*
[e] *Pharmaceutical Sciences and Cosmetic Products Research Center, Kerman University of Medical Sciences, Kerman, Iran*

ARTICLE INFO:

Received 3 Mar 2022
Revised form 29 Apr 2022
Accepted 16 May 2022
Available online 29 Jun 2022

Keywords:
Electro-Fenton process,
UV-Vis spectrometer,
Methylene blue,
Response surface methodology,
Degradation,
Kinetic

ABSTRACT

In the present study, response surface methodology was employed to investigate the effects of main variables, including the initial MB concentration, hydrogen peroxide dosage, current density, and electrolysis time on the removal efficiency of MB using the electro-Fenton (EF) process. The MB concentration determination by UV-Vis spectrometer**.** The EF process degrades the MB contaminant molecules by the highly oxidizing species of the ·OH. A quadratic regression model was developed to predict the removal of MB, where the R^2 value was found to be 0.9970, which indicates the satisfactory accuracy of the proposed model. ANOVA analysis showed a non-significant lack of fit value (0.0840). Moreover, the predicted correlation coefficient values (R^2=0.9915) were reasonably in agreement with the adjusted correlation coefficient value (R^2=0.9958), demonstrating a highly significant model for MB dye removal. In addition, the obtained results showed 95.8% MB was removed in the optimum removal efficiency, including the initial MB concentration of 20 mg L^{-1}, H_2O_2 dosage of 400 µL, and the current density of 7.0 mA cm^{-2}, and electrolysis time of 10 min which was agreed with the predicted removal efficiency of 98.3%. Electrical energy consumption was found to be 0.163 kWh m^{-3}. The constant rate value of K_{app} at the optimum operating condition was 0.3753 min^{-1}.

1. Introduction

Due to the increasing use of tens of thousands of various types of dyes, which are employed in plastic products, cosmetics, leather, and food industries, and their release of about over 100 tons into the aqueous environments, a severe global concern has been raised for efficient removal of such organic micropollutants before releasing the industrial wastewater into the environmental medium [1, 2]. The adverse effects of toxic dyes on human beings, biota, microorganisms, and environmental health, even at deficient concentrations on the one hand, and their high resistance to photochemical and biological degradation, on the other hand, the

*Corresponding Author: Saeid Ahmadzadeh
Email: saeid.ahmadzadeh@kmu.ac.ir
https://doi.org/10.24200/amecj.v5.i02.178

necessity has required to eliminate the synthetic dyes contaminant from effluents [3-5]. Among the high-consumption dyes, methylene blue (MB), a derivative of phenothiazine, is widely used as a redox indicator, biological staining reagent, medication to treat methemoglobinemia, and adjunct employed in endoscopic polypectomy. Besides, it is used extensively in textiles dyeing industries of cotton, wool, and silk. Exposure of methylene blue to the eyes causes irreversible damage of partial blindness [6, 7]. Moreover, its inhalation causes respiratory problems. Its ingestion orally causes a burning sensation in the gastrointestinal tract and induces nausea, vomiting, profuse sweating, as well as mental confusion, and methemoglobinemia [8-11]. There are many techniques such as UV-VIS spectrometer, gas chromatography, and liquid chromatography for determining MB, dye, tyrosine kinase, toluene, benzene, and organic materials in different matrixes [12-17]. During the last decades, several treatments techniques, including coagulation, adsorption, and filtration processes, have been developed for the removal of dye contaminants which suffered from the disadvantages such as high operational costs due to the production of a massive amount of sludge or solid waste and transferring the dyes to another phase by concentrating them rather than eliminating them [18, 19]. The advanced oxidation processes (AOPs) as an economical and high efficient approach provide a valuable opportunity to overcome the limitations of the conventional treatment process by generating a robust oxidative agent of hydroxyl radicals, which degrade and mineralize the dye molecules into their less-toxic forms and harmless inorganic products such as water or carbon dioxide [20-22]. As seen from the proposed reaction in Equation 1, Fenton's reagent of Fe^{2+} and H_2O_2 generates the oxidative agents of hydroxyl radicals under the acidic medium of solution pH less than 3. The Fe^{2+} species are generated from the oxidation of iron anode electrode and reduction of Fe^{3+} ions through cathodic reaction as described by Equation 2 [23, 24].

$$Fe^{2+} + H_2O_2 \rightarrow Fe^{3+} + OH^- + HO^\bullet$$

(Fenton's reaction) (Eq. 1)

$$Fe^{3+} + e^- \rightarrow Fe^{2+} \ (E^\circ = 0.77 \text{ V/SHE})$$ (Eq. 2)

In the current work, response surface methodology (RSM) was employed as a computational approach to optimize the removal efficiency of MB using the EF process. The effect of main operational variables, including electrolysis time, MB initial concentration, H_2O_2 dosage, and current density throughout the treatment process, were evaluated, and the kinetics of the process were studied.

2. Material and methods

2.1. Chemical

All chemicals used in the MB removal study are analytical (high purity) grade without further purification. $C_{16}H_{18}ClN_3S$ (Methylene blue), H_2O_2 (30%, v/v), Na_2SO_4, H_2SO_4, and NaOH were obtained from Merck® Co. $(CH_3)_3COH$, and CH_3OH were obtained from Sigma Aldrich® Co. The investigation samples in this study were prepared in double-distilled water (DDW).

2.2. EF process system

The Pyrex cylindrical reactor with dimensions of 9.0 cm (height) × 7.0 cm (diameter) and a volume capacity of 300 mL was used to carry out MB removal studies using the EF process. The iron electrodes with a thickness of 0.1 cm and an immersed area of 12 cm^2 were used as cathode and anode electrodes. The distance between electrodes (anode and cathode) was considered constant and equal to 3.0 cm. In a typical run, MB solution was degraded in the reactor with 50 mM Na_2SO_4 as the supporting electrolyte. The pH of the MB solution was adjusted to 3.0 by 0.01 M of H_2SO_4. The rotation speed was kept at 200 rpm during the experiment.

2.3. Analytical methods

The MB concentration of samples before and after the treatment process was measured by a UV-

Vis spectrometer (OPTIZEN 3220 model) at 670 nm [1]. Evaluations for the degradation and MB removal efficiency and total amount of electrical energy consumption (kWh m^{-3}) were calculated from the Equation (3) and (4) [25-27]:

$$\text{Removal MB (\%)} = \frac{C_0 - C_t}{C_0} \times 100 \quad \text{(Eq. 3)}$$

$$EEC = \left(\frac{UIt}{V}\right) \quad \text{(Eq. 4)}$$

where C_0 (MB concentration before EF process; mg L^{-1}), Ct (MB concentration after EF process; mg L^{-1}), U (applied voltage; V), I (electrical current; A), t (electrolysis time; h), and V (volume of sample;L).

2.4. Application of Response Surface Methodology

Response Surface Methodology (RSM) is a widely used mathematical and statistical approach employed to model, design, and evaluate the relationship between several independent variables and responses of the proposed model. The goal is to optimize the applied reaction in a short time and reduce the costs of the process. Unlike conventional methods for data analysis, RSM analyzes data using simple techniques based on the mathematical model. In the RSM, to optimize the studied variables, a polynomial function (often a quadratic polynomial model) can be used, as given in Equation 5 [27, 28]

$$Y = \beta_0 + \sum_{i=1}^{k} \beta_i X_i + \sum_{i=1}^{k} \beta_{ii} X_i^2 + \sum_{i=1}^{n-1} \sum_{j=i+1}^{k} \beta_{ij} X_i X_j \quad \text{(Eq. 5)}$$

where Y is the predicted response (MB removal %), k is the number of independent factors, β_0, β_i, β_{ii}, and β_{ij} are the constant, linear, quadratic, and interaction model coefficients, respectively, also, X_i, X_j, and ε are the independent factors and the error. Analysis of variance (ANOVA) with a 95% confidence interval was used to determine the significance of the parameters. In the current study, the RSM approach was used to investigate four variables' effects (initial MB concentration, H_2O_2 dosage, current density, and electrolysis time) and identify the optimal condition for MB removal using the EF process employing Design-Expert Software Version 11.0.4.0.

3. Result and discussion

3.1. Development of models and analysis of variance (ANOVA) using RSM

Table 1 describes the experimental condition of 30 runs designed by RSM and the obtained responses of the developed model in each run summarized. The mentioned removal efficiencies of MB are the averages of duplicate runs in each experimental condition.

Some valuable parameters, including lack of fit of the model, the significance of linear and interaction effects of operating variables, and coefficient of determination, were evaluated by analysis of variance (ANOVA). As seen in Table 2, the *p*-value less than 0.0001 corresponds to the significant coefficients.

As seen, the obtained results from ANOVA analysis confirmed that the developed quadratic regression model was satisfactorily fitted to the removal efficiency of the treatment process with the F-value of 858. Since the calculated *p*-value of the Lack of Fit was less than 0.05, it confirmed that the lack of fit was insignificant, corresponding to the pure error. The predicted and adjusted R^2 of 0.9915 and 0.9958 are in reasonable agreement. Furthermore, the fitted model's prediction ability over the experimental condition range is acceptable due to the obtained predicted R^2 of about 100%. The normality of the residuals was analyzed and demonstrated in Figure 1(a). As seen, all the demonstrated data are relatively near to a straight line with the R^2 of 0.9970. Moreover, the association between the obtained values of actual removal efficiencies and predicted removal efficiencies were revealed in Figure 1(b). As seen, since the residual results were distributed near the diagonal line, it can be concluded that the proposed treatment model successfully predicted the removal efficiencies.

Table 1. Experimental values for the removal efficiency of MB from the CCD.

Run order	Actual values				Coded values				Removal (%)
	A (mg L^{-1})	B (µL)	C (mA cm^{-2})	D (min)	X_1	X_2	X_3	X_4	
1	40	387	8.2	5.2	+1	+1	+1	-1	70.6
2	30	275	6.5	8.5	0	0	0	0	82.9
3	30	275	6.5	8.5	0	0	0	0	84.1
4	20	387	4.7	11.7	-1	+1	-1	+1	85.2
5	20	162	8.2	11.7	-1	-1	+1	+1	71.0
6	40	387	4.7	11.7	+1	+1	-1	+1	64.0
7	20	162	8.2	5.2	-1	-1	+1	-1	66.6
8	30	275	10.0	8.5	0	0	+2	0	67.2
9	20	387	4.7	5.2	-1	+1	-1	-1	82.3
10	10	275	6.5	8.5	-2	0	0	0	99.8
11	30	500	6.5	8.5	0	+2	0	0	77.1
12	30	50	6.5	8.5	0	-2	0	0	41.3
13	30	275	6.5	8.5	0	0	0	0	84.5
14	40	162	8.2	11.7	+1	-1	+1	+1	59.3
15	20	162	4.7	11.7	-1	-1	-1	+1	63.3
16	40	387	8.2	11.7	+1	+1	+1	+1	75.2
17	50	275	6.5	8.5	+2	0	0	0	69.8
18	30	275	3.0	8.5	0	0	-2	0	47.1
19	40	162	4.7	11.7	+1	-1	-1	+1	49.7
20	20	387	8.2	11.7	-1	+1	+1	+1	95.7
21	40	162	4.7	5.2	+1	-1	-1	-1	45.5
22	30	275	6.5	8.5	0	0	0	0	84.1
23	40	162	8.2	5.2	+1	-1	+1	-1	56.1
24	20	162	4.7	5.2	-1	-1	-1	-1	58.6
25	20	387	8.2	5.2	-1	+1	+1	-1	90.9
26	30	275	6.5	8.5	0	0	0	0	83.7
27	30	275	6.5	2.0	0	0	0	-2	67.5
28	30	275	6.5	15.0	0	0	0	+2	79.2
29	40	387	4.7	5.2	+1	+1	-1	-1	61.3
30	30	275	6.5	8.5	0	0	0	0	84.4

Table 2. ANOVA of the fitted polynomial model.

Source	Sum of Squares	Degree of freedom (df)	Mean square	F-value	p-value
Model	6580	8	822	858	< 0.0001
X_1	1535	1	1535	1602	< 0.0001
X_2	2142	1	2142	2237	< 0.0001
X_3	555	1	555	579	< 0.0001
X_4	125	1	125	130	< 0.0001
X_1X_2	72	1	72	76	< 0.0001
X_2^2	1087	1	1087	1135	< 0.0001
X_3^2	1276	1	1276	1332	< 0.0001
X_4^2	204	1	204	214	< 0.0001
Residual	20	21	0.96	-	-
Lack of Fit	18	16	1.15	3.54	0.0840
Pure Error	1.6	5	0.33	-	-
Core Total	6600	29	-	-	-
Mean: 71.65				R^2: 0.9970	
Coefficient of Variance: 1.37%				Adj.R^2: 0.9958	
Standard Deviation: 0.98				Pred. R^2: 0.9915	

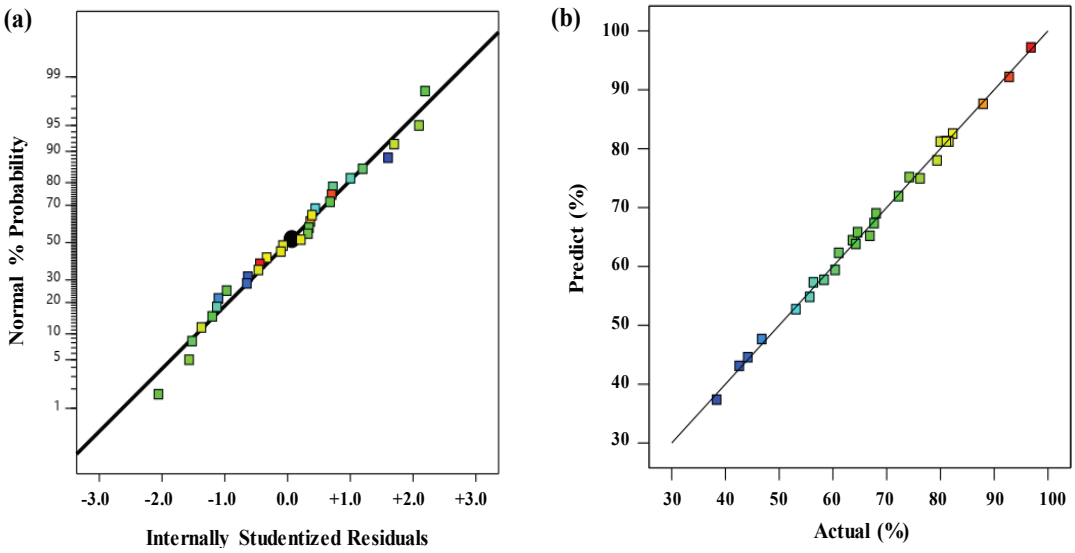

Fig. 1. **(a)** Normal probability plot of studentized residuals, **(b)** Predicted removal efficiencies *vs.* experimental removal efficiencies.

The regression model developed for the removal efficiency of MB is represented in Equation 6. The proposed second-order model in the term of coded factors by eliminating the insignificant terms is expressed as follows (6):

$$MB\ removal\ (\%) = 84.2 - 8.9X_1 + 9.45X_2 + 4.81X_3 + 2.29X_4 - 2.13X_1X_2 - 6.23X_2^2 - 6.75X_3^2 - 2.71X_4^2 \quad \text{(Eq. 6)}$$

Here, X_1 represents initial MB concentration, X_2 is H_2O_2 dosage, X_3 is current density, and X_4 is electrolysis time. As seen, the intensity of each particular variable on the removal efficiency as the response of the proposed model is identified by the related magnitude of each variable's coefficient. Each coefficient's positive or negative value indicates the synergistic or antagonistic effect of the related variable on the response. As seen, the coefficients

of X_2 (H_2O_2 dosage), X_3 (current density), and X_4 (electrolysis time) are all positive. Moreover, it can be concluded that the variables of X_1 and X_2 with much larger coefficients play more significant roles in MB's removal efficiency as the model's response.

3.2. Effect of parameter on the MB removal efficiency

In the present study, the effect of initial MB dye concentration on removal efficiency using the EF process was investigated. As Figure 2 shows, the initial MB dye concentration is inversely related to the MB removal efficiency, when increasing the initial MB dye concentration from 10 mg L-1 to 500 mg L^{-1}, and removal efficiency decreases from 99.8% to 68.2%. This phenomenon can be due to the decrease in the ratio of oxidant agents to MB dye molecules. For example, if all the parameters studied in the EF process, are constant (at high MB dye concentrations), the number of dye molecules is greater than the oxidizing agents. Therefore, the number of oxidizing agents is insufficient to remove high concentrations of the dye molecule, and consequently, the removal efficiency decreases [29, 30].

Optimizing the amount of H_2O_2 in all treatment methods in which H_2O_2 plays a key role is very important because it affects the removal efficiency, the management of the treated effluent, and the cost. The effects of H_2O_2 dosage in the range of 50-500 µL on MB removal were investigated at the initial MB concentration of 30 mg L^{-1}, the current density of 6.5 mA cm^{-2}, and electrolysis time of 8.5 min, the result is shown in Figure 3 the obtained results show that the increase in degradation percentage from 40.7% to 78.1% whenever H_2O_2 increased from 50 to 500 µL, at the initial MB concentration of 30 mg L^{-1}, the current density of 6.5 mA cm^{-2}, and electrolysis time of 8.5 min.

Excess concentration of H_2O_2 causes the spontaneous auto composition of $H_2O_2$to H_2O and O_2 molecules through Equation(7), as well as the decomposition of $^{\bullet}OH$, produced during the EF reaction to radicals with lower oxidation strength ($HO_2^{\bullet}$ ions) according to Equation (8) and (9) which reduces the removal efficiency [31, 32].

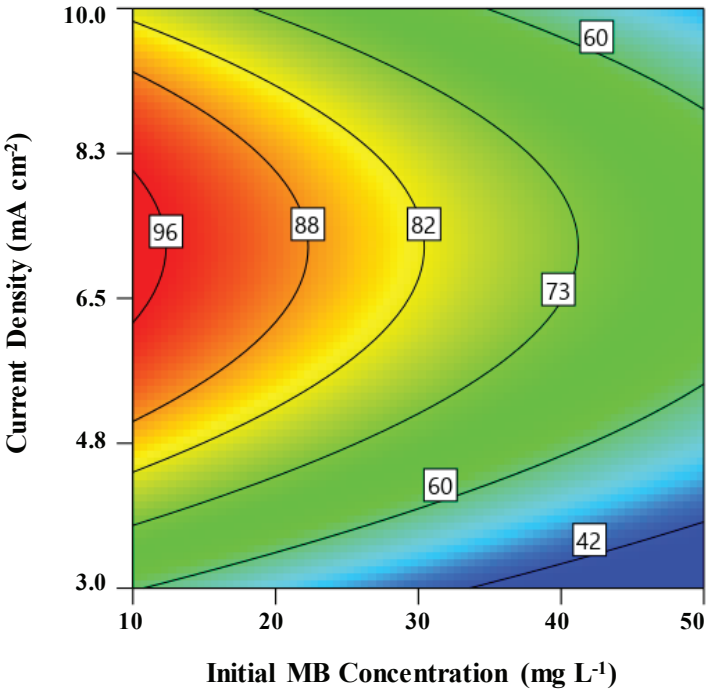

Fig. 2. Contour plots of the initial MB concentration and current density.

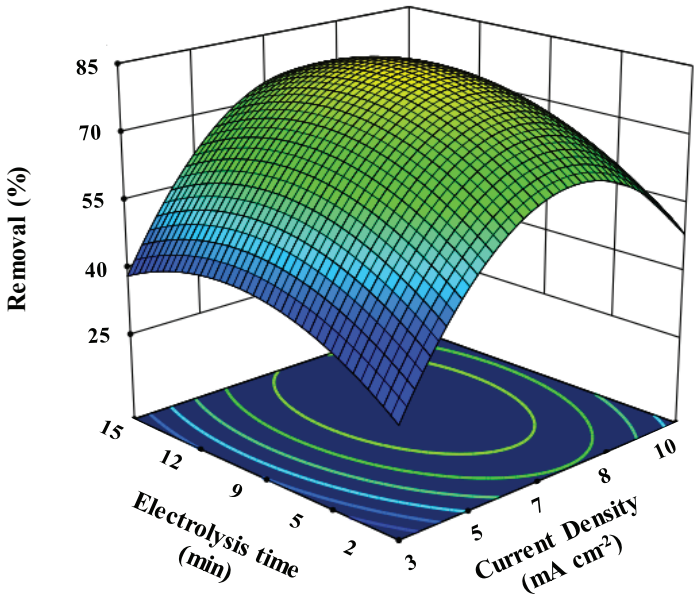

Fig. 3. 3Dplot of the initial MB concentration and H_2O_2 dosage.

$$2\,H_2O_2 \rightarrow 2H_2O + O_2 \quad \text{(Eq. 7)}$$

$$H_2O_2 + HO^{\bullet} \rightarrow HO_2^{\bullet} + H_2O \quad \text{(Eq. 8)}$$

$$HO_2^{\bullet} + HO^{\bullet} \rightarrow H_2O + O_2 \quad \text{(Eq. 9)}$$

Current density is one of the most effective parameters that affects the kinetic rate and removal efficiency. Increasing the current density more than the optimal value causes more electrical energy consumption and heat generation and consequently adverse effects on the removal process, so its value must be optimized. Due to the importance and influence of current density in the EF process, the effect of applied current density was studied in the range of 3-10 mA cm^{-2}. The removal of MB dye depended on the current density.

The increase in current density from 2 to 5.5 mA cm^{-2} offered faster MB dye degradation (MB removal efficiency of 47.5% to 66.9%). Increasing the dye removal efficiency with increasing current density can be attributed to the fact that increasing the current density increases the amount of iron generated by the anode electrode. The increase in removal and degradation rates from 3 mA cm^{-2} to the optimum value of 7.0 mA cm^{-2} can be related to the acceleration of Fenton's Reaction (Equation1). Therefore, increasing the concentration of Fe^{2+} produced could lead to an increase in $^{\bullet}OH$ generated through (Equation 1). These $^{\bullet}OH$ generated reacts immediately with the MB dye, increasing the MB removal efficiency.

However, more than the optimal value of current density leads to a decrease in the MB removal efficiency in the EF reactor. This negative effect is due to the role of Fe^{2+} as the scavenger of $^{\bullet}OH$ (Equation 10) [32, 33]. Hence, 7.0 mA cm^{-2} was selected as the optimal value of current density.

$$Fe^{2+} + HO^{\bullet} \rightarrow Fe^{3+} + OH^{-} \quad \text{(Eq. 10)}$$

The effect of electrolysis time in the range of 2-15 min on MB removal was studied (Fig. 4). According to the results; MB removal efficiency was directly related to electrolysis time, so with increasing electrolysis time, the removal efficiency increases. From the start EF process until 9 min after electrolysis time, due to in presence of sufficient H_2O_2 and Fe^{2+}, a large number of hydroxyl radicals ($^{\bullet}OH$) are generated according to the Fenton's reaction, which

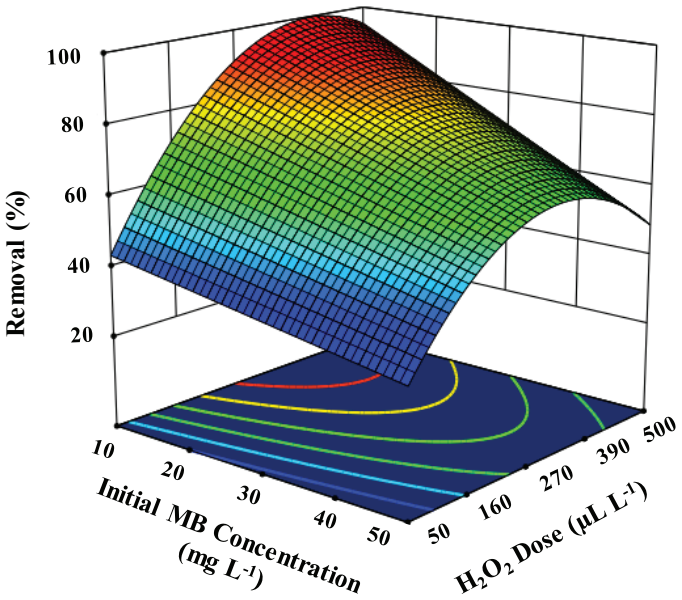

Fig. 4. The 3D plot of the current density and electrolysis time effects on the MB removal efficiency

subsequently leads to the MB dye degradation and increased removal efficiency. As the electrolysis time increases, the concentration of H_2O_2 in the electrochemical reactor decreases until the reactor is free of H_2O_2, consequently, the Fenton's reaction slows down and eventually stops [34].

3.3. Optimization process

The optimization process was carried out over the upper to lower limits of each operating parameter's value to determine the best treatment condition for maximum MB removal at a reasonable cost. The highest MB removal efficiency of 98.3% was predicted at the optimum condition of initial MB concentration of 20 mg L^{-1}, H_2O_2 dosage of 400 µL, the current density of 7.0 mA cm^{-2}, and electrolysis time of 10 min, which was in good accordance with the obtained experimental MB removal efficiency.

3.4. Kinetic model of hydroxide radical assisted EF process

The kinetic studies of the treatment process revealed that hydroxyl radical reaction with MB contaminant follows the pseudo-first-order reaction, which indicates that •OH directly attacked the contaminant molecules. The hydroxyl radicals are generated and consumed continuously at a similar rate to provide a steady-state concentration of active radicals throughout the treatment process. The apparent constant rate of K_{app} could be evaluated by the pseudo-first-order reaction equation and corresponds to the slope of demonstrated plot in Figure 5, with the value of 0.3753 min^{-1} [35]. Figure 5 revealed the variation of Ln (C_0/C_t) in the function of time during the 15 min treatment process with the initial concentration of MB 20 mg L^{-1}, the current density of 7.0 mA cm^{-2}, and H_2O_2 dosage of 400 µL L^{-1}.

4. Conclusion

Herein, to achieve an economical treatment process for the efficient removal of MB, the response surface methodology was employed. The analysis of variance (ANOVA) at the confidence level of 95% was carried out to evaluate the significance of the independent variables and their interactions. The obtained results revealed that the initial MB concentration and H_2O_2 dosage affected the removal efficiency significantly. The obtained experimental removal efficiency of 95.8% by the EF process was in satisfactory agreement with the predicted removal efficiency of 98.3% by the

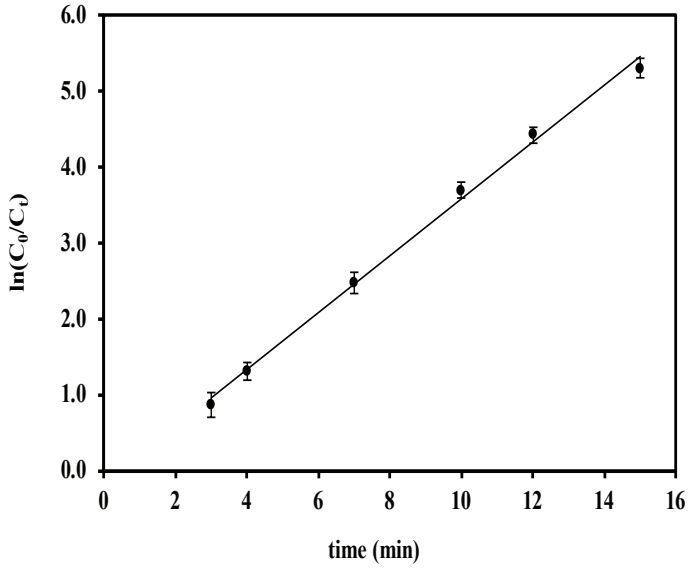

Fig. 5. Pseudo-first-order Kinetic model of MB degradation.

developed quadratic regression treatment model. The kinetic analysis showed that the applied treatment process followed a pseudo-first-order model.

5. Acknowledgements

The authors would like to express their appreciation to the student research committee of Kerman University of Medical Sciences [Grant number 400000747] for supporting the current work.

Funding: This work received a grant from the Kerman University of Medical Sciences [Grant number 400000747].

Conflict of interest: The authors declare that they have no conflict of interest regarding the publication of the current paper.

Ethical approval: The Ethics Committee of Kerman University of Medical Sciences approved the study (IR.KMU.REC.1400.510).

6. References

[1] S. Soni, P. Bajpai, J. Mittal, C. Arora, Utilisation of cobalt doped Iron-based MOF for enhanced removal and recovery of methylene blue dye from waste water, J. Mol. Liq., 314 (2020) 113642. https://doi.org/10.1016/j.molliq.2020.113642.

[2] H.N. Bhatti, Y. Safa, S.M. Yakout, O.H. Shair, M. Iqbal, A. Nazir, Efficient removal of dyes using carboxymethyl cellulose/alginate/polyvinyl alcohol/rice husk composite: adsorption/desorption, kinetics and recycling studies, Int. J. Biol. Macromol., 150 (2020) 861-870. https://doi.org/10.1016/j.ijbiomac.2020.02.093.

[3] J.-C. Lee, H.-J. Kim, H.-W. Kim, H. Lim, Iron-impregnated spent coffee ground biochar for enhanced degradation of methylene blue during cold plasma application, J. Ind. Eng. Chem., 98 (2021) 383-388. https://doi.org/10.1016/j.jiec.2021.03.026.

[4] I. Khan, K. Saeed, I. Zekker, B. Zhang, A.H. Hendi, A. Ahmad, S. Ahmad, N. Zada, H. Ahmad, L.A. Shah, Review on methylene blue: its properties, uses, toxicity and photodegradation, Water, 14 (2022) 242. https://doi.org/10.3390/w14020242.

[5] S.A. Almodaresi, M. Mohammadrezaei, M. Dolatabadi, M.R. Nateghi, Qualitative analysis of groundwater quality indicators based on Schuler and Wilcox diagrams: IDW and Kriging models, J. Environ. Health . Sustain. Dev., 4 (2019) 903 -912. https://doi.org/10.18502/jehsd.v4i4.2023

[6] M.B. Yeamin, M.M. Islam, A.-N. Chowdhury, M.R. Awual, Efficient encapsulation of toxic dyes from wastewater using several biodegradable natural polymers and their composites, J. Clean. Prod., 291 (2021) 125920. https://doi.org/10.1016/j.jclepro.2021.125920.

[7] M. Vakili, M. Rafatullah, B. Salamatinia, A.Z. Abdullah, M.H. Ibrahim, K.B. Tan, Z. Gholami, P. Amouzgar, Application of chitosan and its derivatives as adsorbents for dye removal from water and wastewater: A review, Carbohydrate polymers, 113 (2014) 115-130. https://doi.org/10.1016/j.carbpol.2014.07.007.

[8] A. Kirchon, P. Zhang, J. Li, E.A. Joseph, W. Chen, H.-C. Zhou, Effect of isomorphic metal substitution on the fenton and photo-fenton degradation of methylene blue using Fe-based metal–organic frameworks, ACS Appl. Mater. Interfaces, 12 (2020) 9292-9299. https://doi.org/10.1021/acsami.9b21408.

[9] A. Kausar, S.U. Rehman, F. Khalid, A. Bonilla-Petriciolet, D.I. Mendoza-Castillo, H.N. Bhatti, S.M. Ibrahim, M. Iqbal, Cellulose, clay and sodium alginate composites for the removal of methylene blue dye: Experimental and DFT studies, Int. J. Biol. Macromol., 209 (2022) 576-585. https://doi.org/10.1016/j.ijbiomac.2022.04.044.

[10] A. Bukhari, M. Atta, A. Nazir, M.R. Shahab, Q. Kanwal, M. Iqbal, H. Albalawi, N. Alwadai, Catalytic degradation of MO and MB dyes under solar and UV light irradiation using ZnO fabricated using Syzygium Cumini leaf extract, Zeitschrift für Physikalische Chem., 236 (2022) 659-671. https://doi.org/10.1515/zpch-2021-3096.

[11] A. Syafiuddin, M.A. Fulazzaky, Decolorization kinetics and mass transfer mechanisms of Remazol Brilliant Blue R dye mediated by different fungi, Biotechnol. Reports, 29 (2021) e00573. https://doi.org/10.1016/j.btre.2020.e00573.

[12] M. Ghazaghi, HZ. Mousavi, H. Shirkhanloo, A. Rashidi, Ultrasound assisted dispersive micro solid-phase extraction of four tyrosine kinase inhibitors from serum and cerebrospinal fluid by using magnetic nanoparticles coated with nickel-doped silica as an adsorbent, Microchim. Acta, 183 (2016) 2779-2789. https://doi.org/10.1007/s00604-016-1927-z

[13] H. shirkhanloo, M. Osanloo, Nobel method for toluene removal from air based on ionic liquid modified nano-graphen, Int. J. Occup. Hyg., 6 (2014) 1-5. https://ijoh.tums.ac.ir/index.php/ijoh/article/view/89

[14] M.B.H. Abadi, H. Shirkhanloo, J. Rakhtshah, Air pollution control: The evaluation of TerphApm@ MWCNTs as a novel heterogeneous sorbent for benzene removal from air by solid phase gas extraction, Arab. J. Chem., 13 (2020) 1741-1751. https://doi.org/10.1016/j.arabjc.2018.01.011

[15] A. Faghihi-Zarandi, H. Shirkhanloo, C. Jamshidzadeh, A new method for removal of hazardous toluene vapor from air based on ionic liquid-phase adsorbent, Int. J. Environ. Sci. Technol., 16 (2019) 2797-2808. https://doi.org/10.1007/s13762-018-1975-5

[16] C. Jamshidzadeh, H. Shirkhanloo, A new analytical method based on bismuth oxide-fullerene nanoparticles and photocatalytic oxidation technique for toluene removal from workplace air, Anal. Methods Environ. Chem. J., 2 (2019) 73-86. https://doi.org/10.24200/amecj.v2.i01.55

[17] R. Ashouri, H Shirkhanloo, AM Rashidi, SAH Mirzahosseini, N. Mansouri, Dynamic and static removal of benzene from air based on task-specific ionic liquid coated on MWCNTs by sorbent tube-headspace solid-phase extraction procedure, Int. J. Environ. Sci. Technol., 18 (2021) 2377-2390. https://doi.org/10.1007/s13762-020-02995-4

[18] F. Jamali-Behnam, A.A. Najafpoor, M. Davoudi, T. Rohani-Bastami, H. Alidadi, H. Esmaily, M. Dolatabadi, Adsorptive removal of arsenic from aqueous solutions using

magnetite nanoparticles and silica-coated magnetite nanoparticles, Environ. Prog. Sustain. Energy, 37 (2018) 951-960. https://doi.org/10.1002/ep.12751.

[19] A. Najafpoor, H. Alidadi, H. Esmaeili, T. Hadilou, M. Dolatabadi, A. Hosseinzadeh, M. Davoudi, Optimization of anionic dye adsorption onto Melia azedarach sawdust in aqueous solutions: effect of calcium cations, Asia-Pacific J. Chem. Eng., 11 (2016) 258-270. https://doi.org/10.1002/apj.1962.

[20] I. Sirés, E. Brillas, M.A. Oturan, M.A. Rodrigo, M. Panizza, Electrochemical advanced oxidation processes: today and tomorrow. A review, Environ. Sci. Pollut. Res., 21 (2014) 8336-8367. https://doi.org/10.1007/s11356-014-2783-1.

[21] M. Rezayi, L.Y. Heng, A. Kassim, S. Ahmadzadeh, Y. Abdollahi, H. Jahangirian, Immobilization of tris (2 pyridyl) methylamine in a PVC-Membrane Sensor and Characterization of the Membrane Properties, Chem. Cent. J., 6 (2012) 1-6. https://doi.org/10.1186/1752-153X-6-40.

[22] S. Ata, M. Feroz, I. Bibi, I.-u. Mohsin, N. Alwadai, M. Iqbal, Investigation of electrochemical reduction and monitoring of p-nitrophenol on imprinted polymer modified electrode, Synthetic Metals, 287 (2022) 117083. https://doi.org/10.1016/j.synthmet.2022.117083.

[23] Y. Zhu, R. Zhu, Y. Xi, J. Zhu, G. Zhu, H. He, Strategies for enhancing the heterogeneous Fenton catalytic reactivity: a review, Appl. Catal. B: Environ., 255 (2019) 117739. https://doi.org/10.1016/j.apcatb.2019.05.041.

[24] Y.S. Woo, M. Rafatullah, A.F.M. Al-Karkhi, T.T. Tow, Removal of Terasil Red R dye by using Fenton oxidation: a statistical analysis, Desalination Water Treat., 52 (2014) 4583-4591. https://doi.org/10.1080/19443994.2013.804454.

[25] M. Dolatabadi, M.T. Ghaneian, C. Wang, S. Ahmadzadeh, Electro-Fenton approach for highly efficient degradation of the herbicide 2, 4-dichlorophenoxyacetic acid from agricultural wastewater: Process optimization, kinetic and mechanism, J. Mol. Liq., 334 (2021) 116116. https://doi.org/10.1016/j.molliq.2021.116116.

[26] A. Talaiekhozani, M.R. Mosayebi, M.A. Fulazzaky, Z. Eskandari, R. Sanayee, Combination of TiO2 microreactor and electroflotation for organic pollutant removal from textile dyeing industry wastewater, Alexandria Eng. J., 59 (2020) 549-563. https://doi.org/10.1016/j.aej.2020.01.052.

[27] R.A. Khera, M. Iqbal, A. Ahmad, S.M. Hassan, A. Nazir, A. Kausar, H.S. Kusuma, J. Niasr, N. Masood, U. Younas, Kinetics and equilibrium studies of copper, zinc, and nickel ions adsorptive removal on to Archontophoenix alexandrae: conditions optimization by RSM, Desalination Water Treat., 201 (2020) 289-300. https://doi.org/10.5004/dwt.2020.25937.

[28] M. Dolatabadi, H. Naidu, S. Ahmadzadeh, A green approach to remove acetamiprid insecticide using pistachio shell-based modified activated carbon; economical groundwater treatment, J. Clean. Prod., 316 (2021) 128226. https://doi.org/10.1016/j.jclepro.2021.128226.

[29] M. López-Guzmán, M.A. Flores-Hidalgo, L. Reynoso-Cuevas, Electrocoagulation process: An approach to continuous processes, reactors design, pharmaceuticals removal, and hybrid systems—A Review, Processes, 9 (2021) 1831. https://doi.org/10.3390/pr9101831.

[30] P. Nidheesh, R. Gandhimathi, Trends in electro-Fenton process for water and wastewater treatment: an overview, Desalination, 299 (2012) 1-15. https://doi.org/10.1016/j.desal.2012.05.011.

[31] E. Brillas, S. Garcia-Segura, Benchmarking recent advances and innovative technology approaches of Fenton, photo-Fenton, electro-Fenton, and related processes: A review on the relevance of phenol as model molecule, Sep.

Purif. Technol., 237 (2020) 116337. https://doi.org/10.1016/j.seppur.2019.116337.

[32] J. Casado, Towards industrial implementation of Electro-Fenton and derived technologies for wastewater treatment: A review, J. Environ. Chem. Eng., 7 (2019) 102823. https://doi.org/10.1016/j.jece.2018.102823.

[33] H. Monteil, Y. Pechaud, N. Oturan, M.A. Oturan, A review on efficiency and cost effectiveness of electro-and bio-electro-Fenton processes: application to the treatment of pharmaceutical pollutants in water, Chem. Eng. J., 376 (2019) 119577. https://doi.org/10.1016/j.cej.2018.07.179.

[34] J.J. Rueda-Márquez, I. Levchuk, M. Manzano, M. Sillanpää, Toxicity reduction of industrial and municipal wastewater by advanced oxidation processes (Photo-Fenton, UVC/H2O2, Electro-Fenton and Galvanic Fenton): a review, Catalysts, 10 (2020) 612. https://doi.org/10.3390/catal10060612.

[35] A. Chmayssem, S. Taha, D. Hauchard, Scaled-up electrochemical reactor with a fixed bed three-dimensional cathode for electro-Fenton process: Application to the treatment of bisphenol A, Electrochim. Acta, 225 (2017) 435-442. https://doi.org/10.1016/j.electacta.2016.12.183.

Anal. Methods Environ. Chem. J. 5 (2) (2022) 51-59

AMECJ

Research Article, Issue 2
Analytical Methods in Environmental Chemistry Journal
Journal home page: www.amecj.com/ir

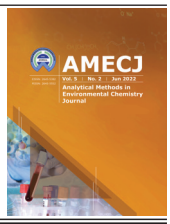

Application of pipette-tip solid-phase extraction technique for fast determination of levofloxacin from wastewater sample using cobalt metal-organic framework

Mohammad Abbaszadehbezi [a], Mohammad Reza Rezaei Kahkha [a,*], Alireza Khammar[a] and Morteza Mehdipour Rabouri [b]

[a] *Faculty of Health, Zabol University of Medical Sciences, Zabol, Iran*
[b] *Occupational Health Engineering Department, Kerman University of Medical Sciences, Kerman, Iran*

ARTICLE INFO:

Received 19 Feb 2022
Revised form 26 Apr 2022
Accepted 20 May 2022
Available online 30 Jun 2022

Keywords:
Cobalt metal-organic framework,
Levofloxacin,
Pipette tip,
Preconcentration,
Solid-phase extraction,
High-performance liquid chromatography

ABSTRACT

In this research, a miniaturized solid-phase extraction method based on pipette tip solid-phase extraction (PT-SPE) was employed for the determination of levofloxacin. Cobalt metal-organic framework (CoMOF) was used as an adsorbent. Levofloxacin was determined using high-performance liquid chromatography and UV detection (HPLC-UV). Important parameters that influence the extraction efficiency (*i.e.* pH, amount of adsorbent, extraction time, volumes of sample, and eluting solvent) were tested and optimized. Results indicated that the proposed method was validated over the range of 0.70 - 150.0 µg L^{-1}. The relative standard deviation (RSD%) was below 2.75% for the levofloxacin. The limit of detection (LOD) of this method is 0.041 µg L^{-1}. The preconcentration factor (PF) was obtained at 200 and the analysis time was around 10 min that confirming the reliability and accuracy of this method for extraction of levofloxacin. The PT-SPE procedure based on CoMOF adsorbent was efficiently extracted for levofloxacin more than 95%. In a static system, the adsorption capacity of CoMOF adsorbent for levofloxacin was obtained at 156.7 mg g^{-1} (n=10). The validation of results was successfully obtained for levofloxacin values based on the spiking real samples before determination by the HPLC technique.

1. Introduction

Antibiotics are among the drugs that are widely used in medicine and veterinary medicine and through various routes such as agricultural runoff, direct discharge from municipal wastewater treatment plants, human waste, direct disposal of medical waste, veterinary, and industry[1, 2]. As a result, their presence has been observed in local streams and around the world, especially in streams that directly receive treated wastewater[3]. Large amounts of these compound residues remain in agricultural soils after being applied, which leach into the groundwater and can also be found in run-off waters[4]. Due to the mentioned toxicological effects, sensitive and reliable analytical methods are needed for the determination of trace amounts of these compounds[5]. Levofloxacin is a broad-spectrum antibiotic that prevents the growth of bacteria, so it is classified as a bacteriostatic[5, 6]. It is widely used in the treatment of patients with Covid-19 in recent two years[7]. Several methods have been applied for determining levofloxacin residues

*Corresponding Author: Mohammad Reza Rezaei Kahkha
Email: m.r.rezaei.k@gmail.com
https://doi.org/10.24200/amecj.v5.i02.185

in aqueous samples, including, solid-phase microextraction (SPME)[8, 9], dispersive-solid phase extraction[10, 11], molecularly imprinted polymer (MIP)[12, 13]and other techniques based on microextraction principles[14, 15]. The pipette tip (PT) is a micro-scale of SPE that is used for the separation and extraction of environmental pollutant samples[16]. This method used small volume and low consumption of any solvents that satisfied by green chemistry rules. It differs from common SPE in that a small amount of sorbent is inserted into a pipet tip, and it is relatively inexpensive without a special auxiliary device for extraction. In general terms, an advantage of pipet tips for sample preparation is that extraction can be carried out faster and more facile than conventional SPE cartridges. Many SPE methods based on adsorbents (silver nanoparticles (AgNPs) coating on micro glassy balls (MGB), graphene oxide-packed micro-column, magnetic nanoparticles, cadmium Sulfide Nanoparticles, amine-functionalized bimodal mesoporous silica nanoparticles) were used for extraction heavy metals, organic materials and drugs in different matrixes such as, water, human, vegetable, food and drug samples [17-22]. In recent years, many types of research have been focused on the synthesis and application of metal-organic framework (MOF) compounds. The MOFs are one of major approaches for making sorbents with large surface area. MOFs are a new class of porous compounds consisting of organic linkers coordinated to inorganic metal nodes[23]. Thermal and chemical stability, porosity, their tailorable structures and properties are some advantages of MOFs for several purposes such as separation, sensing drug delivery and the removal of toxic materials from air and water[24, 25]. In this work we used cobalt metal-organic framework(Co-MOF) for the preparation of a novel solid-phase adsorbent. Then pipette–tip solid-phase extraction methods were used and developed for preconcentration and extraction of levofloxacin.

2. Material and methods

2.1. Reagents

All chemicals were of analytical grade. Cobalt nitrate ($Co(NO_3)_2.6H_2O$) and pyridine 2,6-dicarboxylic acid (98%) were purchased from Aldrich (Millipore-Sigma, USA). Ethanol and N,N-dimethyl formamide (DMF) were obtained from Merck KGaA (Germany). Other reagents such as the hydrochloric acid (HCl, CAS N: 7647-01-0,), the sulphuric acid (H_2SO_4, CAS N: 7664-93-9) with high purity were purchased from Sigma, Germany. The pH of the samples is tuned by the sodium acetate (CH_3COONa/ CH_3COOH), the sodium phosphate (HPO_4^{2-}/ NaH_2PO_4 -) and the ammonium buffer for pH of 4-5, 5-8 and pH 8-10, respectively. All the plastic and glass tubes were put on the HNO_3 solution (0.5 M, v/v) for at least 2 days and then washed with DW many times.

2.2. Instrumental analysis

The chromatographic analysis was carried out on Cecil HPLC system (Cecil, England), equipped with a UV detector. A reverse-phase ACE-C18 column (250 mm × 4.6 mm i.d.) was used for separation of the analyte. The mobile phase was a mixture of trimethylamine phosphate buffer (1%, Ph=4.30) and acetonitrile (12/88, v/v) at a flow rate of 1.0 mL min-1. The column temperature was kept at 30oC and the detection wavelength was set at 280 nm. The injection volume was 10 µL.

2.3. Synthesize of Co-MOF

Synthesize of adsorbent was described in one of our previously reported works[26]. First, 1.85 mmol of pyridine 2,6-dicarboxylic acid and 5.62 mmol of cobalt nitrate were dissolved in 14 mL of ethanol. After this, the solution was transferred into a Teflon reactor with a tight cap and kept for 7 hours at 85oC. The products were washed with dimethyl formamide (DMF). After mixing and dissolving the reactants, the clear solution radiated in the ultrasound bath for 13 min at working conditions of 160 W, 1 kJ and 21 kHz. Synthesized Co-MOF was stored at 4 oC.

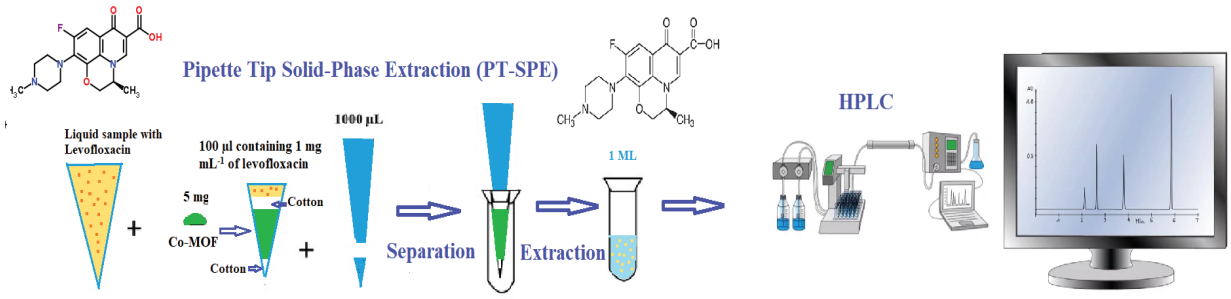

Fig. 1. The levofloxacin determination based on Co-MOF adsorbent by pipette tip solid-phase extraction procedure (PT-SPE)

2.4. Pipette- tip solid phase extraction procedure

5 mg of Co-MOF was put into the pipette-tip. The extraction of levofloxacin was performed by attaching this pipette-tip extractor to a variable pipette. Then 100 µl of the aqueous standard solution containing 1 mg mL-1 of levofloxacin in a 5 mL glass test tube was withdrawn into the sorbent and dispensed back into the same tube. Before the optimization of the number of draw/ eject cycles, the extraction was optimized with 10 cycles. The adsorbed levofloxacin on the surface of the Co-MOF was eluted with 1000 µl of a mixture of methanol-acetonitrile (90:10, v/v) into a 2-mL glass vial, also with 10 aspirating/ dispensing cycles (Fig.1). So, the levofloxacin was determined based on Co-MOF adsorbent by pipette tip solid-phase extraction procedure (PT-SPE).

3. Results and discussion

3.1. Optimization of extraction conditions

For achieving the highest extraction efficiency, several parameters that influenced the extraction procedure were investigated and optimized as follows.

3.1.1.Type of eluting solvent

Several solvents including, methanol, acetonitrile, deionized water, mixture of water- acetonitrile and mixture of methanol- acetonitrile were investigated for obtaining the best extraction efficiency. With different polarities were evaluated to desorb levofloxacin from the Co-MOF sorbent. Experiments showed that the levofloxacin was completely desorbed by a mixture of methanol and acetonitrile (90:10, v/v)

3.1.2.Effect of pH

The effect of sample pH on the recovery of levofloxacin was investigated between 2.0 and 10.0, using a one molar NaOH or HCl. As shown in Figure 2, a pH value of 7.0 has highest extraction efficiency. However; in stronger acidic and basic media, extraction efficiency was decreased.

3.1.3.Effect of amount of sorbent

To obtain high extraction efficiency with good recoveries of levofloxacin, the amount of sorbent for pipette-tip extraction was changed between 1-5 mg. The adsorption ability of Co-MOF was increased by increasing amount of nanocomposite up to 2 mg. After that, the extraction recovery became constant and hence, amount of adsorbent was optimized at 2 mg (Fig. 3).

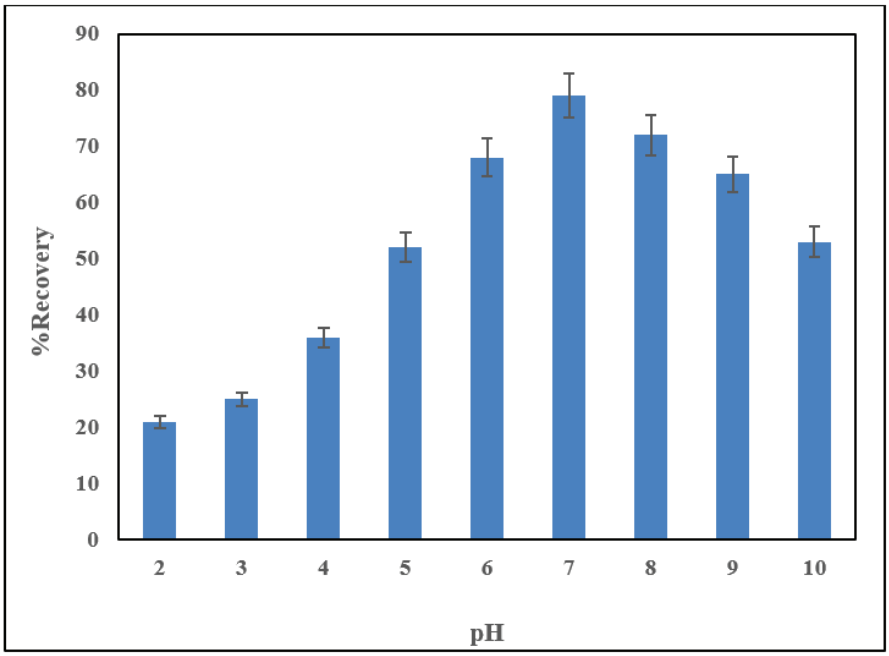

Fig. 2. Effect of pH on recovery of levofloxacin by pipette-tip solid-phase extraction technique

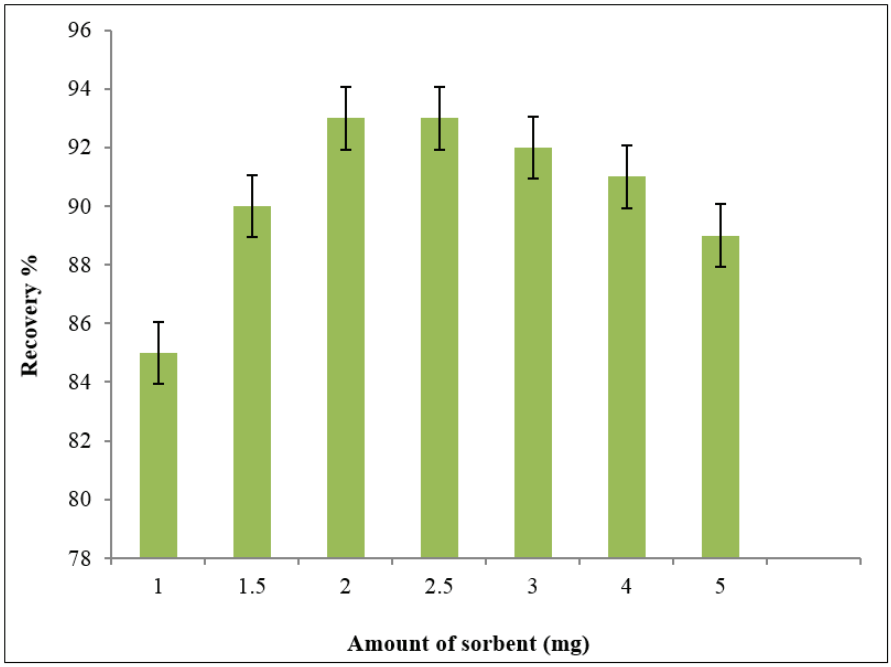

Fig.3. Effect of amount of adsorbent on recovery of levofloxacin based on Co-MOF adsorbent by pipette tip solid-phase extraction procedure (PT-SPE)

3.1.4.Effect of volume of eluting solvent

We tried to obtain the smallest volume of eluent solvent which provides the highest enrichment factor. Volumes between 5 to 50 µL of a mixture of methanol- acetonitrile were examined. As shown in Figure 4, between 15 and 30 µL of the eluting solvent, the recovery of levofloxacin is at its highest value, which means a larger volume of eluting solvent provides a better elution. Therefore, the eluting volume of 20 µL was selected for further experiments.

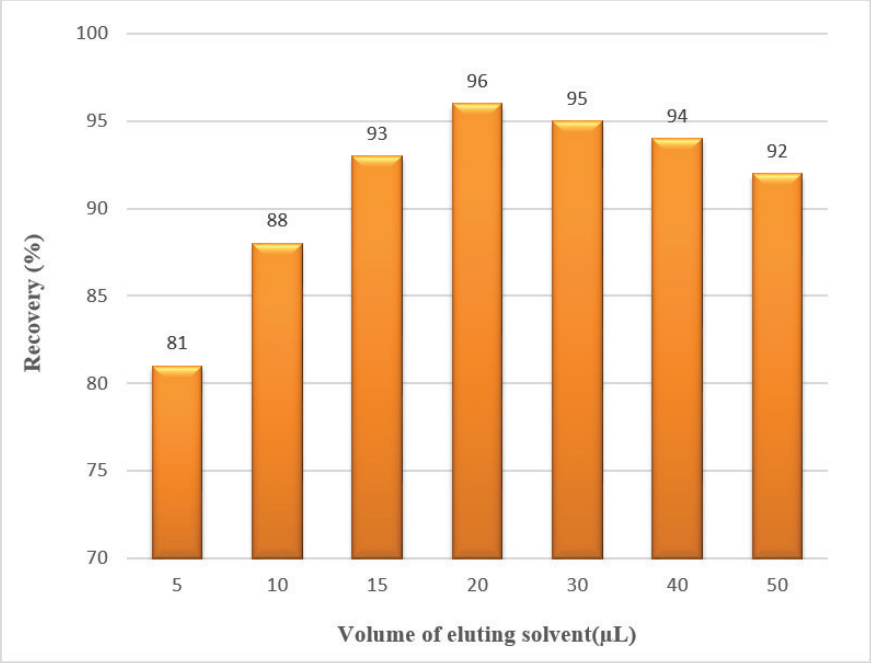

Fig. 4. Effect of eluent volume on recovery of levofloxacin based on Co-MOF adsorbent by pipette tip solid-phase extraction procedure (PT-SPE)

3.1.5. Effect of volume of sample solution

The volume of sample solution is an important factor in pipette- tip solid phase extraction. Different volumes of sample solution were evaluated in the range of 300 to 5000 µL. Figure 5 shows that with increasing the sample solution, extraction recovery of levofloxacin is also increased up to 3800 µL. Hence, this point of sample solution was selected as optimized volume. So, considering 20 µL of eluent, and extraction efficiency of 100 %, a preconcentration factor of 200 was achieved

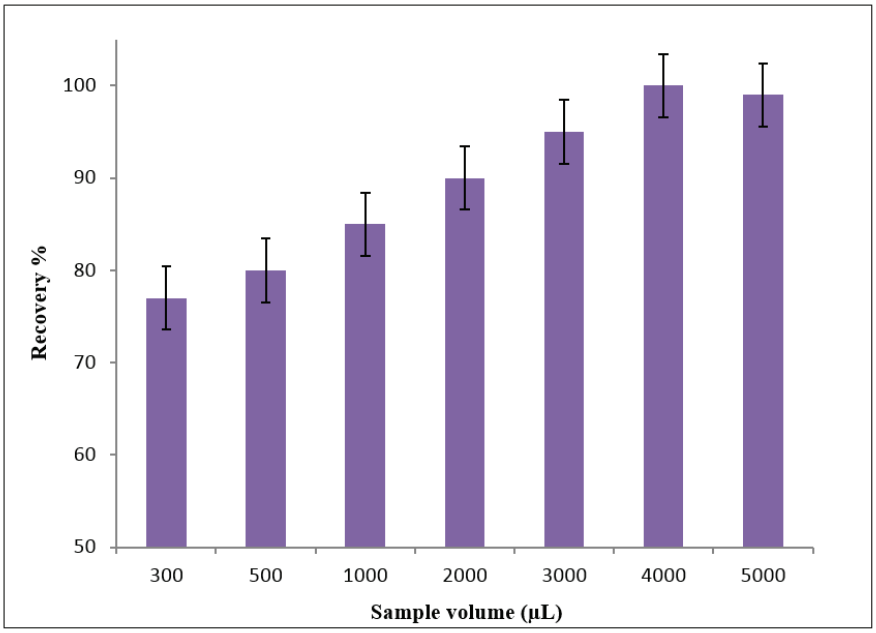

Fig. 5. Effect of sample volume on recovery of levofloxacin based on Co-MOF adsorbent by pipette tip solid-phase extraction procedure (PT-SPE)

Table 1. Analytical performance of proposed PT-SPE method

Parameter	Analytical feature
Dynamic range (µg L^{-1})	0.70-150
Repeatability	0.99
Repeatability[b] (RSD %)	2.75
Limit of detection (µg L^{-1})	0.041
Enrichment factor (fold)	200
Total extraction time (min)	≤ 10

3.1.6.Effect of number of aspirating/dispensing of sample

The number of aspirating/dispensing cycles is another important in the pipette-tip extraction. The time of extraction depends on the number of cycles and the volume of solution that passed through the extractor. The results show that the highest extraction efficiency for levofloxacin was 10 cycles, while using a 4000 µL of the sample. At a higher number of cycles, the back extraction of analytes from adsorbent into the sample solution might occur, causing a decrease in the recovery. The optimal number of aspirating/dispensing cycles used for desorption of levofloxacin was found to be 11 cycles at 9.5 min.

3.2. Analytical performance

The analytical performance of the suggested pipette-tip extraction coupled with HPLC–UV was investigated, and the results are summarized in Table 1. Limit of detection (LOD) was obtained based on a signal-to-noise ratio of 3. The linearity range was studied by varying the concentration of the standard solution from 0.1 to 200 µg L^{-1}. The repeatability of the method, expressed as relative standard deviation (RSD), was calculated for seven replicates of the standard at an intermediate concentration (100 µg L^{-1}) of the calibration curve.

3.3. Application of proposed method in real samples

The suggested pipette-tip procedure was applied for three hospital wastewater real samples. All samples were filtered through 0.45 µm nylon membranes before analysis and were sonicated for 10 min and the slurry was centrifuged at 3500rpm for 5 min. The extraction procedure was repeated three times on each wastewater sample. For evaluation of the analytical performance of the proposed method in reaa samples, the samples were spiked with 3 different concentrations to investigate the matrix effect on its determination. The results are shown in Table 2. As can be seen, recoveries of are adequate; therefore, we can justly this assumption that matrix effect is negligible for the analysis of the target analyte.

4. Conclusion

In this study, pipette-tip solid phase extraction with a novel sorbent based on Co-MOF followed by high performance liquid chromatography (HPLC) has been developed for the determination of levofloxacin in wastewater samples. Due to very high surface areas and short diffusion rate, high adsorption capacities can obtain in a very short time at pH=7. The optimized method is found to be fast, economical, sensitive, accurate and simple. The LOD, linear range (LR) and mean absorption capacity of Co-MOF was obtained 0.041 µgL^{-1}, 0.1 to 200 µgL^{-1} and 156.7 mg g^{-1}, respectively for 10 analyses. The range adsorption capacity of Co-MOF adsorbent for levofloxacin was obtained at 114.9-176.8 mg g^{-1}. Therefore, the efficient extraction and separation of levofloxacin in water and wastewater samples were obtained by the pipette tip solid-phase extraction procedure (PT-SPE) before being determined with HPLC.

5. Acknowledgements

Authors hereby thanks from health laboratory of Zabol University for cooperation to perform experiments.

Table 2. Validation of proposed method in real hospital wastewater based on Co-MOF adsorbent by pipette tip solid-phase extraction procedure (PT-SPE)

Wastewater Sample #	Added ($\mu g.L^{-1}$)	Found ($\mu g.L^{-1}$)	Recovery (%)	RSD % (n=7)
Sample 1	0	25.0	-	-
	50	89.1	98.2	3.5
	100	124.3	74.3	4.2
Sample 2	0	41.0	-	-
	50	89.2	98.7	1.3
	100	140.1	98.1	2.5
Sample 3	0	55.0	-	-
	50	104.01	98.7	4.1
	100	154.2	98.5	5.6
Sample 4	0	95.5	-	-
	50	147.4	103.8	2.8
	100	192.1	96.6	3.3
Sample 5	0	0.58	-	-
	0.5	1.06	96.0	2.7
	1.5	2.11	102.0	3.9

6. Conflict of Interest

The authors have declared no conflict of interest.

7. References

[1] M.R.R. Kahkha, G. Ebrahimzadeh, A. Salarifar, Removal of Metronidazole residues from aqueous solutions based on magnetic multiwalled carbon nanotubes by response surface methodology and isotherm study, Anal. Methods Environ. Chem. J., 2020. 3 (2020) 44-53. https://doi.org/10.24200/amecj.v3.i03.110

[2] M.R.R. Kahkha, Magnetic bentonite nanocomposite for removal of amoxicillin from wastewater samples using response surface methodology before determination by high performance liquid chromatography, Anal. Methods Environ. Chem. J., 3 (2020) 25-31. https://doi.org/10.24200/amecj.v3.i03.108

[3] E. Peterson, P. Kaur, Antibiotic resistance mechanisms in bacteria: relationships between resistance determinants of antibiotic producers, environmental bacteria, and clinical pathogens, Front. Microbiol., 9 (2018) 2928. https://doi.org/10.3389/fmicb.2018.02928

[4] F. Huang, Recognition of typical antibiotic residues in environmental media related to groundwater in China (2009− 2019), J. Hazard. Mater., 399 (2020) 122813. https://doi.org/10.1016/j.jhazmat.2020.122813

[5] S.M. Zainab, Antibiotics and antibiotic resistant genes (ARGs) in groundwater: A global review on dissemination, sources, interactions, environmental and human health risks, Water Res., 187 (2020)116455. https://doi.org/10.1016/j.watres.2020.116455

[6] P. Dhiman, G. Rana A. Kumar , G. Sharma, Nanostructured magnetic inverse spinel Ni–Zn ferrite as environmental friendly visible light driven photo-degradation of levofloxacin, Chem. Eng. Res. Des., 175 (2021) 85-101. https://doi.org/10.1016/j.cherd.2021.08.028

[7] S.M. Alwan, Al-Akidi Therapeutic Protocol for Severe Infections Associated with Covid-19: Potential and Effective Treatment by Levofloxacin and Vitamin D3 and Zinc (Part 1), J. Pharm. Pharmacol., 10 (2022) 105-118. https://doi.org/10.17265/2328-2150/2022.04.001

[8] G. Huang, M. Su, Y. Liu, W. Zhang, Comparative Study of Hyper-crosslinked Polymer-Solid Phase Microextraction and Stir Bar Fabric Phase Sorptive Extraction for Simultaneous Determination of Fluoroquinolones in Water, Chromatogr., 85 (2022) 539-549. https://doi.org/10.1007/s10337-022-04165-9

[9] E. Tsanaktsidou, C. Markopoulou, P. D. Tzanavaras, C. K. Zacharis, Homogeneous liquid phase microextraction using hydrophilic media for the determination of fluoroquinolones in human urine using HPLC-FLD, Microchem. J., 172 (2022)106906. https://doi.org/10.1016/j.microc.2021.106906

[10] M. Shamsipur, N. Mafakheri, N. Babajani, A natural deep eutectic solvent–based Ultrasound-vortex-assisted dispersive liquid–liquid microextraction method for ligand-less pre-concentration and determination of traces of cadmium ions in water and some food samples, Food Anal. Methods, 15 (2022) 1203-1213. https://doi.org/10.1007/s12161-021-02222-x

[11] J. Hu, , S. Zhu , S.-E. Chen , R. Liu , J. Sun , X.-En Zhao , H. Liu, Multiplexed derivatization strategy-based dummy molecularly imprinted polymers as sorbents for magnetic dispersive solid phase extraction of globotriaosylsphingosine prior to UHPLC-MS/MS quantitation, Microchim. Acta, 187 (2020) 1-11. https://doi.org/10.1007/s00604-020-04341-4

[12] L. P. Zhang, X.-X. Tan, Y.-P. Huang , Z.-S. Liu, Floating liquid crystalline molecularly imprinted polymer coated carbon nanotubes for levofloxacin delivery, Eur. J. Pharm. Biopharm., 127 (2018) 150-158. https://doi.org/10.1016/j.ejpb.2018.02.012

[13] J. Meng, X. Wang, Microextraction by packed molecularly imprinted polymer combined ultra-high-performance liquid chromatography for the determination of levofloxacin in human plasma, J. Chem., 2019 (2019) 4783432. https://doi.org/10.1155/2019/4783432

[14] W. Ma, K.H. Row, Simultaneous determination of levofloxacin and ciprofloxacin in human urine by ionic-liquid-based, dual-template molecularly imprinted coated graphene oxide monolithic solid-phase extraction, J. Sep. Sci., 42 (2019) 642-649. https://doi.org/10.1002/jssc.201800939

[15] H. Liu, Pian Jin, Fucheng Zhu, A review on the use of ionic liquids in preparation of molecularly imprinted polymers for applications in solid-phase extraction, TRAC Trends Anal. Chem., 134 (2022) 116132. https://doi.org/10.1016/j.trac.2020.116132

[16] M.P.G. de Llasera, M. Hernández Camarillo , A. Rodrigo García Cicourel, Semi-continuous monitoring of HMWPAH in microalgae cultures by PT-SPE/HPLC/FD-UV: Estimation of the degradation constant, Anal. Biochem., 633 (2021) 114415. https://doi.org/10.1016/j.ab.2021.114415

[17] H. Shirkhanloo, M. Osanloo, M. Ghazaghi, H. Hassani, Validation of a new and cost-effective method for mercury vapor removal based on silver nanoparticles coating on micro glassy balls, Atm. Pollut. Res., 8 (2017) 359-365. https://doi.org/10.1016/j.apr.2016.10.004

[18] H. Shirkhanloo, A. Khaligh, HZ. Mousavi, A. Rashidi, Graphene oxide-packed micro-column solid-phase extraction combined wif flame atomic absorption spectrometry for determination of lead (II) and nickel (II) in water samples, Int. J. Enviro. Anal. Chem., 95 (2015) 16-32. https://doi.org/10.1080/03067319.2014.983437

[19] M. Ghazaghi, HZ. Mousavi, H. Shirkhanloo, A. Rashidi, Ultrasound assisted dispersive micro solid-phase extraction of four

tyrosine kinase inhibitors from serum and cerebrospinal fluid by using magnetic nanoparticles coated with nickel-doped silica, Microchim. Acta, 183 (2016) 2779-2789. https://doi.org/10.1007/s00604-016-1927-z

[20] S. Golkhah, H. Zavvar Mousavi, H. Shirkhanloo, A. Khaligh, Removal of Pb (II) and Cu (II) Ions from Aqueous Solutions by Cadmium Sulfide Nanoparticles, Int. J. Nanosci. Nanotechnol., 13 (2017) 105-117. http://www.ijnnonline.net/article_25609.html

[21] H. Shirkhanloo, SD. Ahranjani, A lead analysis based on amine functionalized bimodal mesoporous silica nanoparticles in human biological samples by ultrasound assisted-ionic liquid trap-micro solid phase extraction, J. Pharm. Biomed. Anal. 157 (2018) 1-9. https://doi.org/10.1016/j.jpba.2018.05.004

[22] B. Paknejad, H. Shirkhanloo, M. Aliomrani, Is their any relevance between serum heavy metal concentration and BBB leakage in multiple sclerosis patients, Biol. Trace Elem. Res., 190 (2019) 289-294. https://doi.org/10.1007/s12011-018-1553-1

[23] I. E. Uflyand, V. A. Zhinzhilo, Recent strategies to improve MOF performance in solid phase extraction of organic dyes, Microchem. J., 168 (2021) 106387. https://doi.org/10.1016/j.microc.2021.106387

[24] S. Tajik, Y. Orooji, F. Karimi, Z. Ghazanfari, H. Beitollahi, High performance of screen-printed graphite electrode modified with Ni–Mo-MOF for voltammetric determination of amaranth, J. Food Meas. Charact., 15 (2021) 4617-4622. https://doi.org/10.1007/s11694-021-01027-0

[25] Z. Wang, S. Wang, A. Wang, X. Liu, J. Chen, Q. Zeng, L. Zhang, W. Liu, Covalently linked metal–organic framework (MOF)-polymer all-solid-state electrolyte membranes for room temperature high performance lithium batteries, J. Mater. Chem. A, 6 (2018)17227-17234. https://doi.org/10.1039/C8TA05642K

[26] M.R.R. Kahkha, M. Kaykhaii, Fast determination of bisphenol a in spiked juice and drinking water samples by pipette tip solid phase extraction using cobalt metal organic framework as sorbent, Bull. Chem. Soc. Ethiopia, 32 (2018) 595-602. https://doi.org/10.4314/bcse.v32i3.17

Anal. Methods Environ. Chem. J. 5 (2) (2022) 60-75

AMECJ

Research Article, Issue 2
Analytical Methods in Environmental Chemistry Journal
Journal home page: www.amecj.com/ir

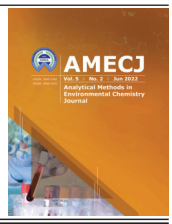

Magnetic solid-phase extraction based on the Carbonized cotton fabric/zeolite imidazolate framework-71/Fe_3O_4/ polythionine followed by atomic absorption spectrometry for cadmium monitoring in water, tomato and cabbage samples

Yasaman Sanaei[a], Mohsen Zeeb*[,a], Seyed Saied Homami[a], Amirhossein Monzavi[b] and Zahra Khodadadi[a]

[a] *Department of Applied Chemistry, Faculty of Science, South Tehran Branch, Islamic Azad University, Tehran, Iran.*
[b] *Department of Polymer and Textile Engineering, South Tehran Branch, Islamic Azad University, Tehran, Iran.*

ARTICLE INFO:

Received 17 Feb 2022
Revised form 20 Apr 2022
Accepted 6 May 2022
Available online 29 Jun 2022

Keywords:
Magnetic solid-phase extraction,
Flame atomic absorption spectrometry,
Cadmium,
Carbonized cotton fabric,
Zeolite imidazolate framework-71/ Fe_3O_4 / Polythionine

ABSTRACT

Carbonized cotton fabric/zeolite imidazolate framework-71/Fe_3O_4/ polythionine (CCF/ZIF-71/Fe_3O_4/PTh) was fabricated, characterized, and applied as efficient magnetic sorbent in magnetic solid-phase extraction (MSPE) of cadmium from water and food samples before determination by flame atomic absorption spectrometry (FAAS). This modification of carbonized cotton fabric led to making a great surface area and porosity, increase extraction efficiency, and acceptable selectivity. The characterization of this proposed sorbent was performed by X-ray diffraction (XRD), field-emission scanning electron microscopy (FE-SEM), and Fourier transform-infrared (FT-IR) spectroscopy analysis techniques. The impact of several analytical parameters including pH, sorbent dosage, time of extraction, desorption condition, chelating agent concentration, the amount of salt and effect of potentially interfering ions on the selectivity and extraction recoveries of cadmium, were evaluated and optimized. In this proposed methodology, the limit of detection (LOD), the limit of quantification (LOQ), and relative standard deviation (RSD, n = 3) were found to be 0.21 ng mL^{-1}, 0.6 ng mL^{-1} and lower than 3.0%, respectively. The validation and accuracy of the new advanced procedure were confirmed by applying the proposed procedure for certified reference materials (SRM1570A). Eventually, CCF/ZIF-71/Fe_3O_4/PTh can be utilized as a selective sorbent, for the rapid, accurate and sensitive determination of Cd (II) by magnetic solid-phase extraction tandem flame atomic adsorption spectroscopy (MSPE-FAAS) in water, tomato and cabbage samples.

1. Introduction

Heavy metal ions are classified as toxic contaminants for environmental and life-threatening pollution for human beings. However, some of them like zinc, iron, cobalt, nickel, copper and manganese are considered essential for human health, except when they are above their maximum acceptable limit concentrations. The other heavy metals for instance As, Cd, Hg and Pb are significantly toxic for living species even at ultra-low concentrations. [1-3] Heavy metals have non-biodegradable nature which is inclined to be concentrated inside the living organisms [3]. One of the most toxic heavy metals is cadmium, which exists in the environmental samples and recent years, because of the developing world, its concentration has

*Corresponding Author: Mohsen Zeeb
Email: zeeb.mohsen@gmail.com
https://doi.org/10.24200/amecj.v5.i02.186

considerably increased [1]. Cadmium can adversely affect the lungs, liver, and kidneys [2]. It can also cause cancer of the prostate and pancreas [1]. For all these reasons, it is necessary to monitor trace amounts of heavy metals in various real samples [4]. A variety of instrumental methods, such as total reflection X-Ray fluorescence spectroscopy (TXRF) [5], inductively coupled plasma-mass spectrometry (ICP-MS) [6], inductively coupled plasma-optical emission spectrometry (ICP-OES) [7], electrothermal atomic absorption spectrometry (ETAAS) [8], flame atomic absorption spectrometry (FAAS) [9] and inductively coupled plasma atomic emission spectroscopy (ICP-AES) [10], have been employed for the determination of various kind of heavy metals. Real samples have complicated matrices with relatively low concentrations of heavy metals. Therefore, these issues are problematic in the extraction procedure, so for solving these issues, it is required to utilize the preconcentration methods [4]. For preconcentration of heavy metals, the different types of methods including solid phase extraction (SPE) [10], dual-cloud point extraction (d-CPE) [11], dispersive liquid-liquid microextraction (DLLME) [12], and magnetic solid-phase extraction (MSPE) have been applied [13]. MSPE, a more sensitive and practical type of SPE, has a lot of benefits such as low-cost, easier and faster route, decreased consumption of perilous solvent, desirable enrichment factors and better recoveries [13,14]. In addition, the greatest enrichment values and superior recoveries can only be accessed when an advanced sorbent is applied. This sorbent should have reasonable reusability and stability, notable selectivity, huge surface area-to-volume ratio, acceptable porosity and cost-efficient synthesis [14,15]. Fe_3O_4 nanoparticles (Fe_3O_4-NPs) are commonly utilized in hybrid sorbents, which have ultra-high magnetic characteristics and allow the sorbent to be easily separated from the sample solution by external magnetic force [16].

Within carbon-based materials, carbonized cotton fabric (CCF) seems to be a unique element for utilizing as sorbent, due to its notable extraction ability, porous structure, and cost-effective and environmentally-friendly fabrication. [14,17] Furthermore, its fabrication can be carried out by using cotton, felt or cloth, which are inexpensive and simply available materials and due to their economics and compatibility with green chemistry, have attracted the attention of many researchers [18]. In the literature survey, to increase the performance of the CCF, it has been modified by various materials like Fe_3O_4 [14], cobalt metal-organic framework [19], Co_3O_4/Ni-based MOFs [20], and metal-organic framework/sulfonated polythiophene [21]. Metal-organic frameworks (MOFs) as tunable porous structures have several specific features like large internal surface area, reasonable stability and simple synthesis routes which made them a convenient choice for various utilization in energy and gas adsorption, catalysis, sensor and also separation [21,22]. Zeolitic imidazolate frameworks (ZIFs), a subcategory of MOFs, are composed of metal centers (e.g., Zn, Co) and organic imidazolate linkers with three-dimensional networks. [23,24]. Zeolitic imidazolate framework-71 (ZIF-71), classified among a subclass of ZIFs, offers many attractive properties including high surface to the volume ratio, acceptable chemical and thermal stability, simple, and low-cost synthesis at room temperature [25,26]. Thus, ZIF-71 was selected to be employed as a modifier in this study. Over the last few years, conductive polymers (CPs) have been employed widely in the separation and preconcentration of heavy metals [27-29]. Polythionine (PTh), as part of a large family of CPs, was employed in various studies due to many benefits, for instance large surface area, high thermal and chemical strength, hydrophobicity, good flexibility, and π-interactions [9,30-35]. From our overview of the literature, 2-(2-benzothiazolylazo) orcinol (BTAO) is one of the most popular chelating agents which is utilized for metal ions, has not been used in combination with carbonized cotton fabric to determine and pre-concentrate Cd from real samples [36].

The aim of this research was followed by fabricating sorbent based on CCF which is employed in MSPE for preconcentration and determination of Cd from water and some food samples. Firstly, the cotton fabric was carbonized and then the growth of ZIF-

71 nanocrystals on the CCF surface was achieved. Next, Fe_3O_4 was co-precipitated on CCF/ZIF-71 for offering a unique magnetic sorbent, followed by polymerization of thionine to obtain CCF/ZIF-71/Fe_3O_4/PTh. Factors that influenced the efficiency of MSPE have been optimized and evaluated in detail. Finally, the proposed procedure was employed for real matrices analysis by flame atomic absorption spectrometry (FAAS).

2. Experimental

2.1. Chemicals and reagents

All chemicals and reagents were analytical grade and were utilized without further purification. 4,5-dichloroimidazole, zinc acetate and phosphoric acid were obtained from Sigma-Aldrich (Taufkirchen, Germany). Iron (III) chloride hexahydrate, Iron (II) chloride tetrahydrate, ammonia, hydrogen peroxide, nitric acid, hydrochloric acid, perchloric acid, chloroform, methanol, ethanol, thionine (Th) acetate (85%) and nitrate salt of analyte (Cd (II)) were bought from Merck company (Darmstadt, Germany). Commercial cotton cloth (100% cotton) with a plain weave was purchased from a nearby market. Double-distilled water was used for preparing all solutions. 2-(2-benzothiazolylazo) orcinol (BTAO) was prepared according to a reported protocol in the literature [36].

2.2. Instruments

A Shimadzu atomic absorption spectrometric device model AA-640-13 (Tokyo, Japan) with an air-acetylene flame burner was employed for the measurement of Cd, with the wavelength of lamp was 228.8 nm. The X-ray diffraction (XRD) spectra were recorded by applying Cu Kα radiation (λ=1.5406 ˚A) on the X'Pert PRO MPD X-ray diffractometer (PANalytical Company, Netherlands). Fourier transform-infrared (FT-IR) spectra were obtained using A Tensor 27 FT-IR spectrometer (Bruker, Germany). Field-emission scanning electron microscopy (FE-SEM) images were collected by utilizing a Mira 3-XMU (Tescan, Czech Republic). Carbonization of the cotton fabrics was performed by a laboratory tube furnace at 1200°C (Iran).

2.3. Preparation of Carbonized cotton fabrics

Carbonized cotton fabric (CCF) was obtained by Salehi et al [34]. The commercial cotton fabric with square-cut plain weave (6.4 × 6.4 cm^2), was washed with distilled water and non-ionic detergent, and stirred for 60 min at 60 °C, then dried at 80 ° C under vacuum. For the aim of chemical activation of cotton fabric, it was soaked in phosphoric acid with a 1.5 impregnation ratio for a day, followed by drying in an oven under a vacuum at 90 ° C. To prepare carbonized cotton fabric, the carbonization of chemical-activated cotton fabric was performed by a tube oven at 500 °C for 85 minutes under nitrogen protection at a heating rate of °٦C min^{-1}. Then CCF was cooled overnight at ambient temperature (23 ± 0.5 °C) and eluted with distilled water repeatedly. Next, it was dried in an oven under a vacuum at 80 °C for half an hour, and the carbonized cotton fabric (CCF) was obtained eventually.

2.4. Preparation of CCF/ZIF-71

ZIF-71 nanocrystals were obtained by applying a method reported in the literature [27]. Briefly, a solution of the metal center was obtained by dissolving 0.07 g zinc acetate in 15 mL of methanol, and then 0.2 g 4,5-dichloroimidazole was dissolved in 15 mL of methanol, individually. afterward, the prepared solutions were merged together in a sealed sample vial in the presence of 0.095 g fabricated CCF, and placed at room temperature (23 ± 0.5 °C) for one day. Next, the methanol was drained out from the vial utilizing a pipette. The last synthesis route was completed by soaking the remaining material in chloroform (3 × 20 ml) for 72 hours and then drying under a vacuum at 90 °C for 60 min.

2.5. Preparation of CCF/ZIF-71/Fe_3O_4/PTh

The synthesis of Fe_3O_4-NPs was done by the chemical co-precipitation method described in reported studies [33]. 0.093 g of CCF/ZIF-71 was weighed and put into a three-necked flat bottom flask. The solution of iron (II) and (III) was prepared by dissolving 0.246 g of $FeCl_3.6H_2O$ and 0.096 g of $FeCl_2.4H_2O$ in 22.5 mL distilled water. Subsequently, the obtained solution was transferred

to the above-mentioned three-necked flat bottom flask and stirred for an hour at room temperature (23 ± 0.5 °C) under a nitrogen stream. After that, the pH of the solution was adjusted at 10 using ammonia at 25 % v/v, followed by raising the temperature up to 80 °C and stirring for one hour while the nitrogen was still flowing. Eventually, by employing a strong magnet, CCF/ZIF-71/Fe_3O_4 was divided from the media, washed with distilled water and ethanol four times, and dried in an oven under vacuum at 80°C for 20 min. In the next sorbent preparation step, thionine (Th) was polymerized in the presence of CCF/ZIF-71/Fe_3O_4. For this aim, the oxidative chemical polymerization method was demonstrated in previous work [32]. First of all, 0.06 g of Th and 0.03 g of $FeCl_3.6H_2O$ as a catalyst were dissolved in 12.5 mL water in a round bottom flask and then poured with an interval time of 2 min into a beaker containing 0.09g of fabricated CC/ZIF71/Fe_3O_4 and 22.5 mL of water. Subsequently, 0.6 mL of H_2O_2 as an oxidizing agent was slowly added to the resultant mixture, when it was stirred. Then, for the complete fabrication of polythionine, the temperature of the mixture was growing to 50 °C and stirred for an hour to disappear the purple color of the reaction media. Finally, the CCF/ZIF-71/Fe_3O_4/PTh was separated by an external magnet, rinsed by deionized water multiple times, and dried at room temperature (23 ± 0.5 °C) for 12 h. The diagram of all fabrication steps is illustrated in Figure 1.

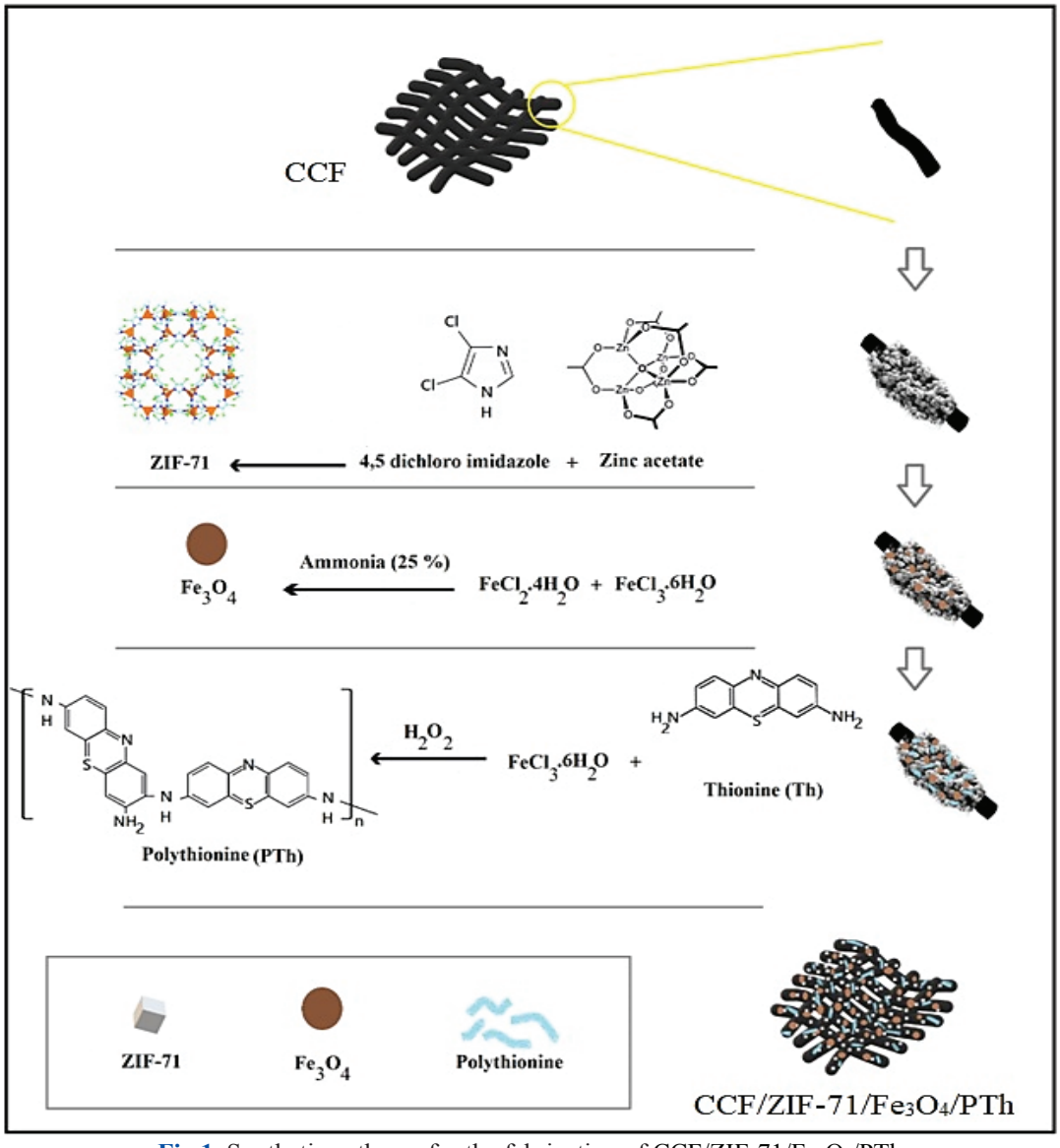

Fig.1. Synthetic pathway for the fabrication of CCF/ZIF-71/Fe_3O_4/PTh

2.6. Preparation of real samples

water samples were prepared to validate the applicability of the novel proposed method. Bottled mineral water was bought from a nearby store and tap water was taken from the water faucet in the research laboratory in Tehran, Iran. Every water sample was filtered applying a 0.45 µm Millipore filter before utilization in the proposed process. Tomatoes and cabbages samples were purchased from a local market in Tehran, Iran. Tomatoes and cabbages were washed with detergent, water and distilled water, respectively. After that, they were cut into small pieces, and then 1 g of each sample was weighed and dried at 120°C to constant weight. The dried samples were put into a muffle furnace, turned to ashes by heating to 400°C and kept at the same temperature for 12 h. After that, the samples were cooled and digested with 10.0 mL concentrated HNO_3 and 3 mL H_2O_2 (30%, w/v), and then remained in a furnace at 400°C once again for four hours. Then, 3 mL concentrated HCl and 3 mL $HClO_4$ (70%, w/v) was added to the resultant samples and then evaporated to near dryness. Next, they were transferred into a volumetric flask, and their volume were raised to 1 L.

2.7. Magnetic solid-phase extraction procedure

The magnetic solid-phase extraction process was defined in this way: 20.0 mg of CCF/ZIF-71/Fe_3O_4 /PTh and washed with distilled water. Then 30.0 mL of the samples/standard solution, containing 55 µM BTAO, with adjusted pH at 7 utilizing buffer was prepared, in addition for real samples, 90 µ of M BTAO was added as an additional dose to eliminate potential interference caused by other species, and added to the glass tube which had the prepared CCF/ZIF-71/Fe_3O_4 /PTh. The glass vessel was placed into an ultrasonic bath and sonicated for 5 min to make the further adsorption of Cd^{2+} onto the surface of CCF/ZIF-71/Fe_3O_4 /PTh sorbent. The CCF/ZIF-71/Fe_3O_4 /PTh was collected from sample media via an external magnetic field (neodymium, iron and boron (0.8 tesla) and the water phase was sucked by a pipette. The elution of the isolated phase was carried out by 500 µL of HNO_3 (50%V/V2 , M) in ethanol in the presence of ultrasound for 2 min. Finally, the sorbent was separated by employing the external magnet once again and desorbed analyte determined with a FAAS. A Schematic of the MSPE-FAAS process is shown in Figure 2.

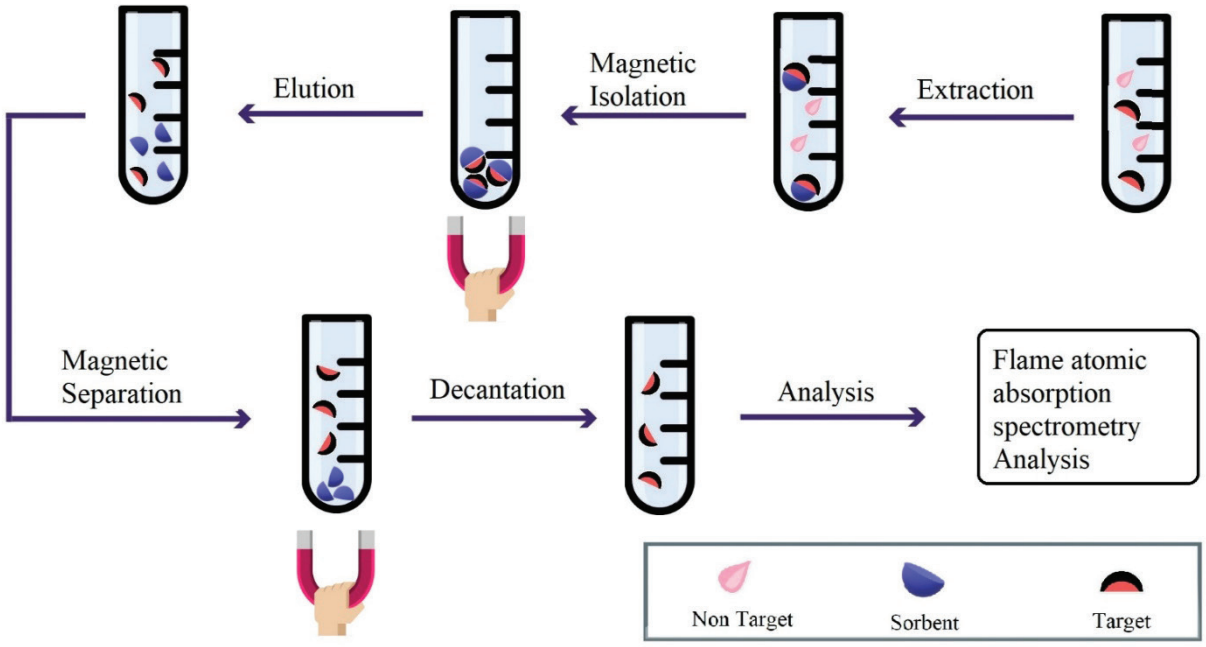

Fig.2. Graphical representation of the MSPE - FAAS procedure for determination of Cd .

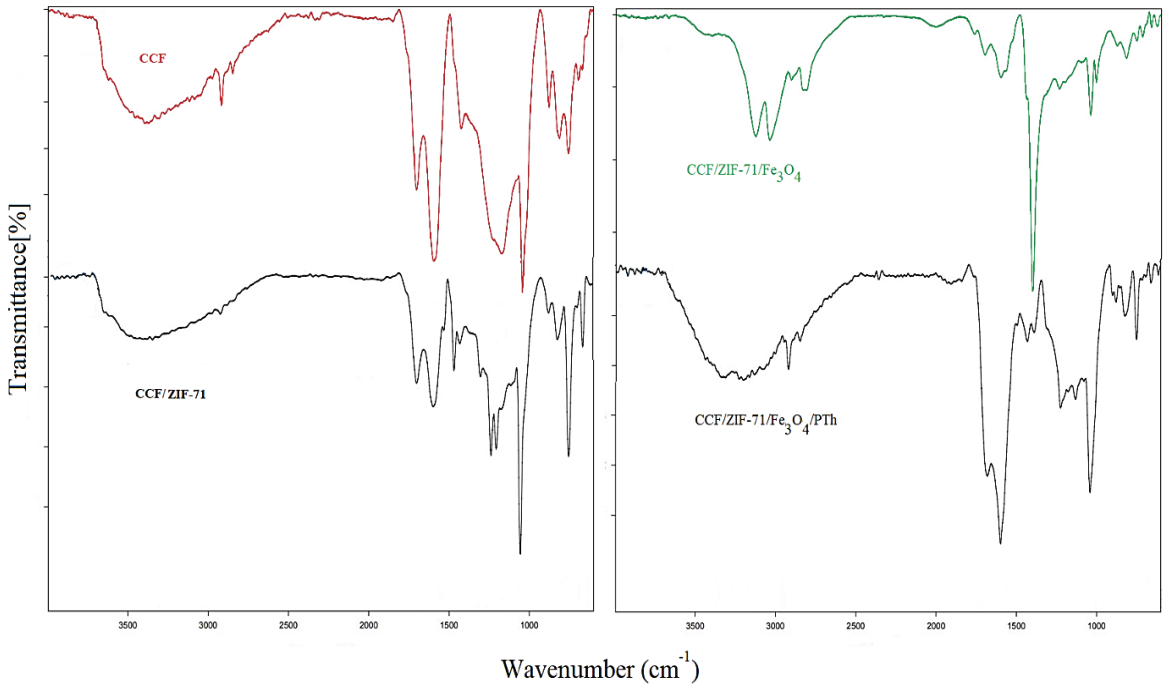

Fig.3. FTIR spectra of sorbent through all the preparation steps.

3. Results and discussion

3.1. Characterization studies

3.1.1. Fourier transform-infrared spectra analysis

For the aim of chemical confirmation of the sorbent structure and the surface modification of that: The CCF, CCF/ZIF-71, CCF/ZIF-71/Fe_3O_4 and CCF/ZIF-71/Fe_3O_4/PTh structures were investigated by employing the FT-IR spectroscopy in the range of 400–4000 cm^{-1} (Fig. 3). The band of O–H stretching vibration of CCF was situated at 3393 cm^{-1}; While, a stretching vibration of the ester group, asymmetric and symmetric stretching vibrations of carboxylate groups in the structure of CCF are laid at 1702 cm^{-1}, 1595 cm^{-1}, and 1423 cm^{-1}, respectively. a band at 755 cm^{-1} was associated with methylene's (-CH_2-) bending vibrations of CCF. the imide´s peaks in ZIF-71 structure revealed at 1300 cm^{-1}, 1594 cm^{-1}, and 1697 cm^{-1} were referred to as C–N, symmetric C=O, and asymmetric C=O stretches, respectively. The medium band for C–Cl stretching vibration of 4,5-dichloroimidazole ligand in the ZIF-71 structure appeared at 663 cm^{-1}. In addition, the band at 3342 cm^{-1} was attributed to free non-hydrogen bonded N–H bonds and the bands at 1428 and 1464 cm^{-1} were assigned to N–H bonds of secondary amine nanocrystalline formation of ZIF-71. Two peaks were evident in the range 623–660 cm^{-1} and 3039 cm^{-1} which linked to the stretching vibrations of Fe-O in the magnetic nanoparticles. The IR spectrum of CCF/ZIF-71/Fe_3O_4/PTh indicates the presence of PTh, by revealing the peak at 3198 cm^{-1} due to the N-H stretching vibration and the C-S group revealed a peak at 800 cm^{-1}. The presence of 1041 and 2918 cm^{-1} bands, characterize C-N stretching vibrations and aromatic C-H stretching vibrations of polythionine, respectively. The peaks at 1680 and 1598 cm^{-1} were attributed to the N-H scissoring of the primary amino moieties and also the peaks at 1431 cm^{-1} were associated with the aromatic C=C stretching vibration of polythionine.

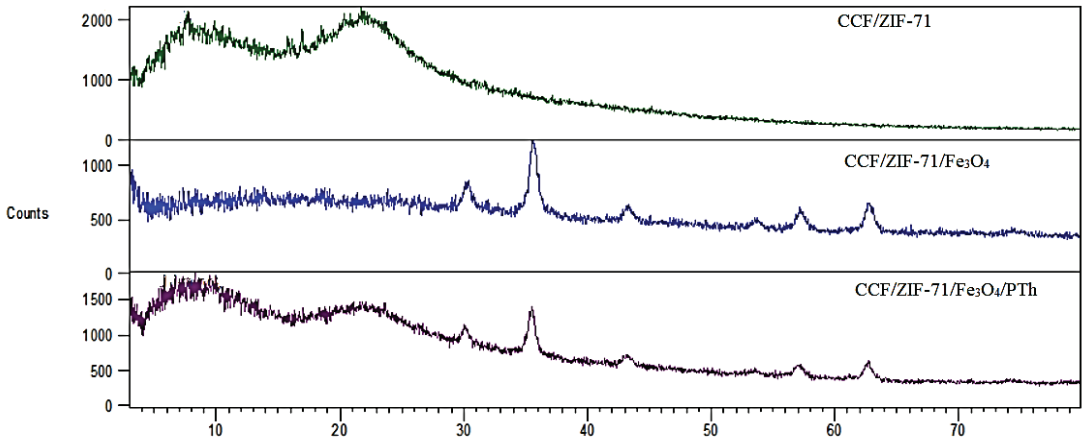

Fig. 4. XRD patterns CCF/ZIF-71 (green colour), CCF/ZIF-71/Fe_3O_4 (blue colour) and CCF/ZIF-71/Fe_3O_4/PTh (purple colour).

3.1.2. X-ray diffraction analysis:

The XRD patterns of the CCF/ZIF-71, CCF/ZIF-71/Fe_3O_4, and CCF/ZIF-71/Fe_3O_4/PTh are demonstrated in Figure 4. the diffraction peaks at 2θ values at 9° and 22.2° are attributed to the graphite carbon and the peaks are about 2θ = 5° and 15° ascribed to nanocrystal structures of zeolitic imidazolate framework-71 in CCF/ZIF-71 pattern. In addition, seven obvious diffraction peaks corresponded to pure cubic spinel crystal of Fe_3O_4-NPs (at 2θ values 30.30°, 35.63°, 43.31°, 53.64°, 57.20°, 62.76° and 74.42°). By comparing CCF/ZIF-71/Fe_3O_4 and CCF/ZIF-71/Fe_3O_4/PTh patterns, it is observed the remarkable diffraction peak of CCF shifted down to 8.2° 2θ, which indicated the great magnetic property of fabricated sorbent. That makes the fabricated sorbent a great choice for applying in magnetic solid-phase extraction.

3.1.3. Field-emission scanning electron microscopy:

A Field-emission scanning electron microscopy (FE-SEM) was utilized for the purpose of verification of the surface morphology of fabricated samples. FE-SEM images of the products in different zooms are shown in Figure 5 (A, B, C and D), respectively. The FE-SEM image of CCF (Fig. 5A) shown that the plain weave fabric structure of CCF had uniform surface morphology. After the crystallization of ZIF-71 on the CCF, the surface of CCF was not smooth anymore and the crystals of ZIF-71 were formed on the surface of CCF with size of about 91-118 nm and appropriately distributed which can be clearly seen in Figure 5B. Also, Figure 5C was depicted, the cubic spinel crystal Fe_3O_4-NPs framed with the around particle size of 20 nm were properly composed on the CC/ZIF-71 with a less aggregate and more. According to the Figure 5D, the average particle size changed to about 30 nm, so it can be concluded PTh was successfully coated on CCF/ZIF-71/Fe_3O_4. These outcomes illustrated that the modification of CCF by ZIF-71, Fe_3O_4-NPs, and PTh can be the cause of the jagged surface of prepared sorbent which prepared a good condition for applying this sorbent in enrichment, isolation, and determination of cadmium.

3.2. Effect of sorbent amount

A suitable amount of sorbent is absolutely essential for the favorable quantitative recoveries of analytes due to interaction between analytes and sorbent in the reaction media [34]. Because of this, the various amounts of CCF/ZIF-71/Fe_3O_4 /PTh between the range from 1 to 40 mg were utilized in recoveries to determine the best sorbent amount. Figure 6 indicated that the quantitative recoveries for metal ions in the range of 1 to 20 mg were enhanced significantly with the grow of the dosage of sorbent, at amounts higher than 20 mg the signals remained constant with slightly decreasing which is due to insufficient desorption of the analyte from the CCF/ZIF-71/Fe3O4 /PTh surface. So, 20 mg of CCF/ZIF-71/Fe_3O_4 /PTh was enough to gain a reasonable outcome.

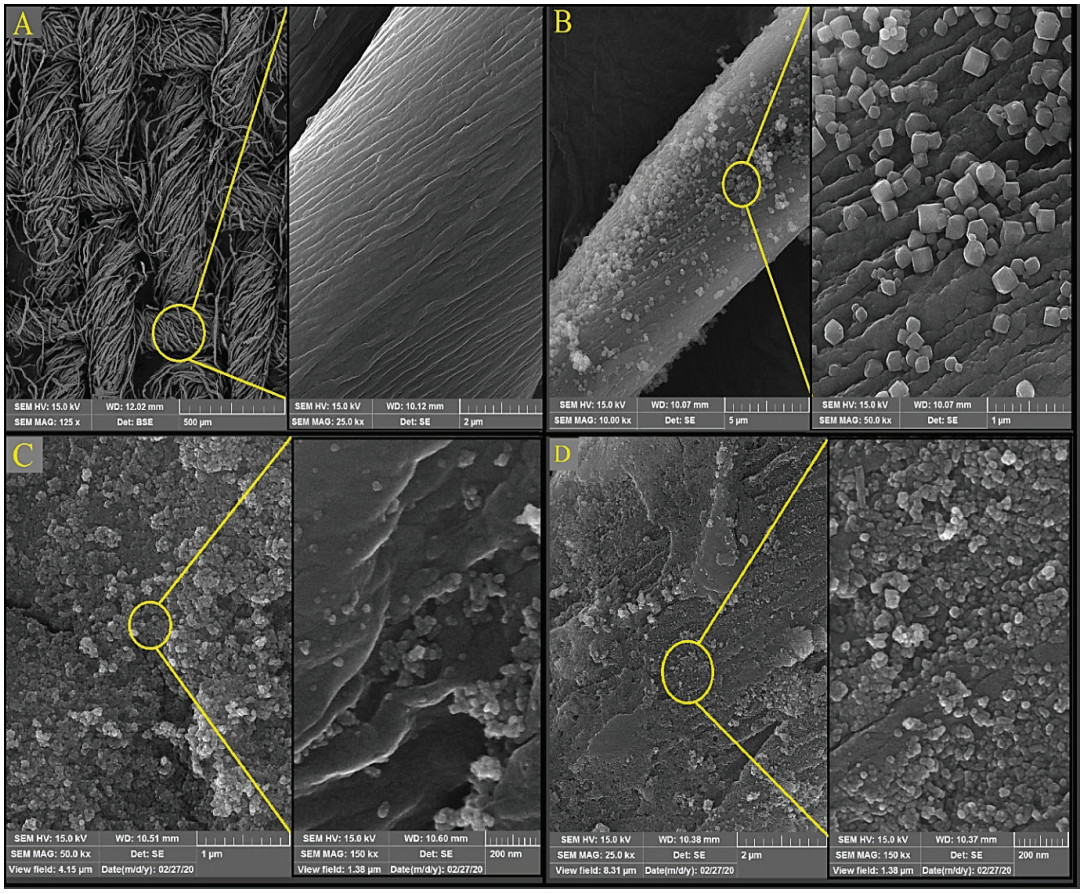

Fig. 5. Field–emission scanning electron microscopy (FE-SEM) images of (A) CCF (B) CCF/ZIF-71 (C) CCF/ZIF-71/Fe_3O_4 (D) CCF/ZIF-71/Fe_3O_4/PTh. Inset: The enlarged view of the nano-array substances and CCF.

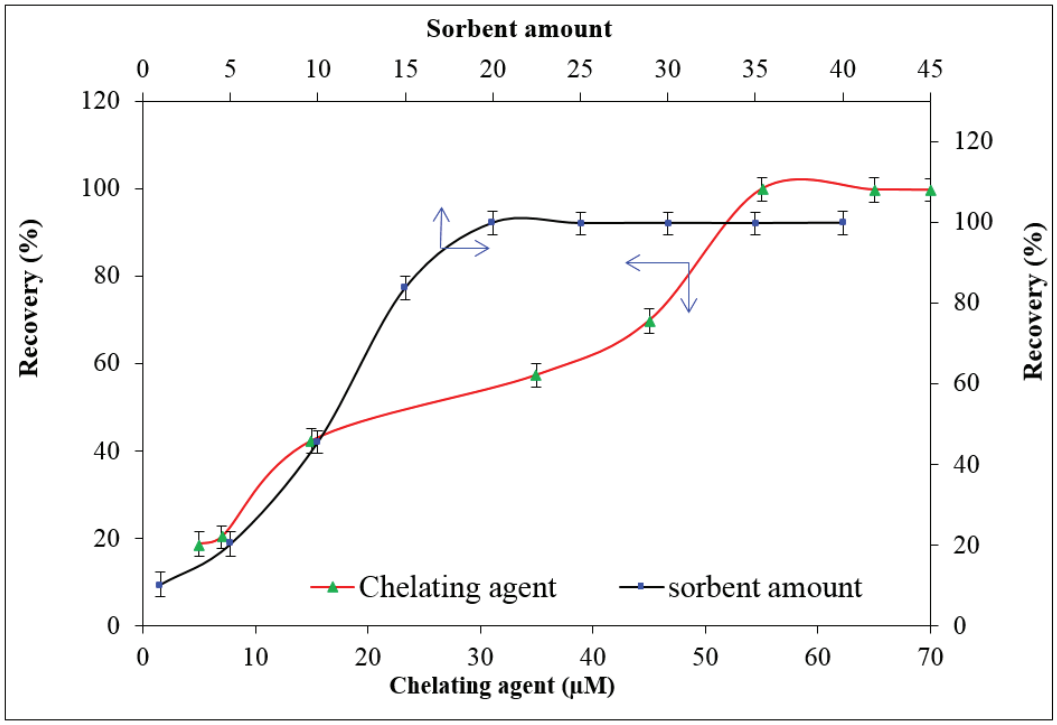

Fig. 6. Effect of CCF/ZIF-71/Fe_3O_4/PTh amount and chelating agent (BTAO) dosage on extraction recovery.

3.3. Effect of pH

In solid-phase extraction studies, the pH of the aqueous solutions is an important parameter which has influence in the formation of metal complexes. To identify the optimum pH value, the impact of pH on the recovery value of cadmium was studied over the pH range 2.0 -12.0. The results are shown in Figure 7 indicated that the recoveries of cadmium were considerably influenced by pH. Between the pH range of 2.0 to 4.0 the adsorption quantity of cadmium was noticeably low, but when the pH exceeded than 4.0, the adsorption of analyte rises considerably and reached a peak at pH 7.0 which was considered as an optimal quantity, after that steady decline was observed. Therefore, the pH at 7.0 was selected as the optimum value for the rest of the study.

3.4. Effect of amount of chelating agent

The amount of chelating agent is an important parameter for following determinations which have influenced extraction efficiency [17]. In the current magnetic solid-phase extraction protocol, 2-(2-benzothiazolylazo) orcinol (BTAO) was chosen as the capable chelating agent. The amount of chelating agent was investigated in the range of 5–70 µM. Fig.6 demonstrated that the recoveries of cadmium were go up by increasing the amount of BTAO, however after 55 µM BTAO the recoveries of Cd declined steadily. Eventually, cadmium recovery in the 55 µM BTAO is optimal, and all further work was carried out by 55 µM BTAO.

3.5. Effect of elution conditions on recovery

The type of desorption solvent is another essential aspect in the efficiency of the preconcentration process in order to achieve the best desorption of analyte, various eluents (nitric acid (50%V/V, 2M) in ethanol, methanol, and acetonitrile) were examined and the more acceptable desorption efficiency was obtained using nitric acid (50%V/V, 2M) in ethanol. In all subsequent studies, HNO_3 (50%V/V,2 M) in ethanol was used as the suitable eluent that could desorb cadmium effectively.

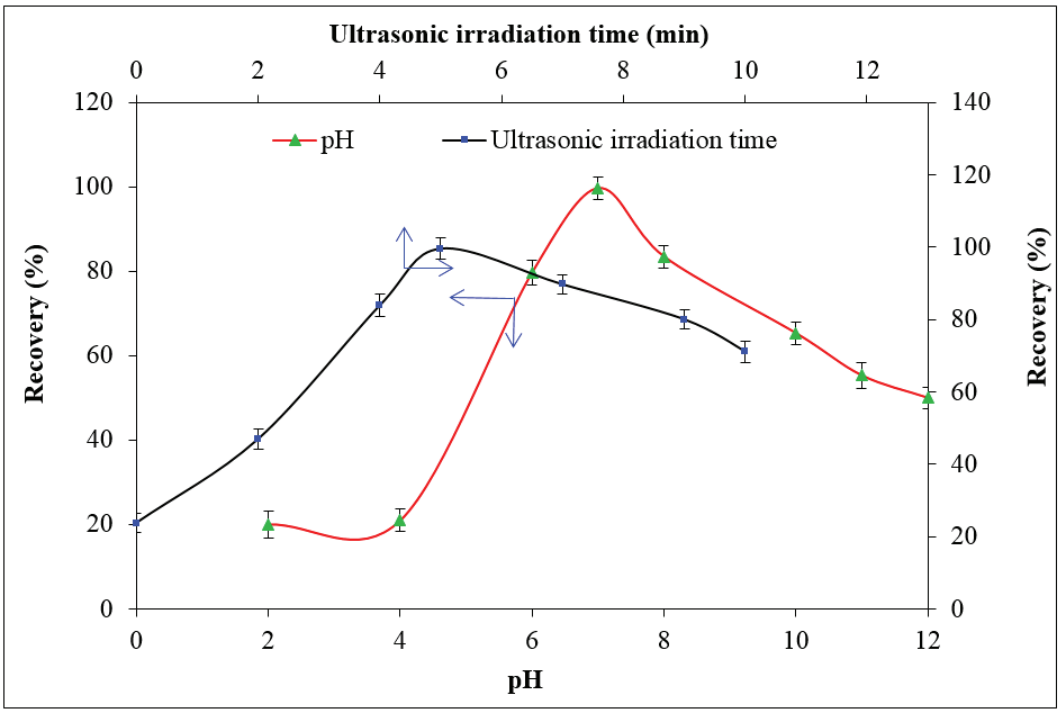

Fig. 7. Effect of ultrasonication time and pH on extraction recovery.

3.6. Effect of ionic strength

It is well known that adding NaCl as an electrolyte in the sample solutions leads to improving the extraction efficiency which is because of the salting-out effect. [37] In the current study, the influence of ionic strength in an aqueous solution on the recovery values of the analyte was evaluated by adding NaCl. By growing the amount of electrolyte, the extraction efficiency of cadmium has been dropped. The explanation for plummeting in recovery percentage is that by enhancing in electrolyte amount in sample media solution, active sites of sorbent were employed by the salt ions. Hence, no NaCl was added for the rest of the study.

3.7. Effect of ultrasonic time

The Cd ions need a particular time and ultrasonic bath to desorption from the CCF/ZIF-71/Fe_3O_4/PTh in MSPE studies. The time of ultrasonic irradiation bath is considered as the extraction time which has an important role in the recovery percentage of analyte and extraction performance. Ultrasonication was applied to the dispersion of fabricated sorbent through sample solution media and interacted with target analytes. Thus, the effect of extraction time was examined in the range from 0 to 10 min. As illustrated in Figure 7, 5 min was adequate for the quantitative determination of Cd. However, after 5 min, a steady decrease in the recovery percentage of the analyte was demonstrated which is due to the return analyte back to the aqueous solution from the sorbent. Accordingly, 5 min was selected as the optimum value.

3.8. Effect of interfering ions

There are various ions in the real samples that may cause interference in the selectivity and reduce the extraction recovery of the analyte in the proposed method [14]. The impact of different interfering ions that may react with BTAO was studied to determine the selectivity of CCF/ZIF-71/Fe_3O_4 / PTh. Therefore, different amounts of interfering ions were added to the standard solutions containing 10.0 ng mL^{-1} of cadmium, individually. The ratio of tolerance for interfering ions is shown in Table 1, The tolerance limit was determined as the largest number of interfering ions that caused alterations on the recovery percentage of the analyte less than ±5%. For the purpose of eliminating interfering ions resulting from real samples, 90 µM BTAO was used as an extra amount.

3.9. Validation of the advanced method

Several analytical aspects of the proposed method includ a limit of detection (LOD), limit of quantification (LOQ), relative standard deviation (RSD), determination coefficients (r^2), and preconcentration factor (PF) were investigated and the obtained results are listed in Table 2. The LOD and LOQ, were calculated based on LOD =$3S_b$/b and LOQ =$10S_b$/b which b is the calibration graph's slope and the standard deviation of blank solutions is illustrated as S_b, [35] were determined 0.21 and 0.6 ng mL^{-1}, respectively. The calibration curve was constructed by using the spiked sample of cadmium obtained in linear ranges from 0.6-40 ng mL^{-1} and also 0.9991 was achieved for the coefficient of

Table 1. Interference study of the interfering ions on the determination of 10 ng mL^{-1} cadmium using MSPE-FAAS

Foreign Species	Tolerance Ratios [Interference-to-Cd (II) ratio[a]]
K^+, Li^+, Na^+, CO_3^{2-}, SO_4^{2-}, NO_3^-, F^-, Cl^-	800
Ca^{2+}, Mg^{2+}	500
Al^{3+}, Pb^{2+}, Fe^{2+}	70
Co^{2+}, Fe^{3+}, Cu^{2+}, Ni^{2+}, Cd^{2+}	25

[a] Tolerance limit was defined as the largest ratio causing a relative error less than 5% in concentration level of cadmium.

determination. 60 was found as the preconcentration factor and the relative standard deviation (RSD), which was assessed from three replicates of the Cd standard solutions, was 3.0%. These results signified that the advanced procedure is a proper choice for determination of cadmium in water and food samples which has great sensitivity and acceptable accuracy. To assess the applicability and accuracy of the novel proposed methodology in real matrices, different food (tomato and cabbage) and water (tap and mineral) samples were utilized to determination and preconcentration of cadmium. These aspects were carried out by analyzing the spiked samples with varying amounts of cadmium and a certified reference material of food samples (SRM1570A). The recoveries from spiked samples and standard reference material are revealed in Table 3, as it can be seen, desirable agreement was observed between the obtained values and the certified values which pointed out that the fabricated sorbent as well as proposed method can be utilized for determination and preconcentration of Cd (II) in natural samples.

Table 2. Analytical Parameters of Cd (II) determination by of MSPE-FAAS

Parameter	Analytical data
Linear range (ng mL^{-1})	0.6-40
Determination coefficients (r^2)	0.9991
Limit of quantification (ng mL^{-1})	0.6
Limit of detection (ng mL^{-1})	0.21
Repeatability (R.S.D., %) (n = 3) ($C_{Cd(II)}$ = 10.0 ng mL^{-1})	3.0
Preconcentration factor (PF)[a]	60
Sample volume (mL)	30

[a] Preconcentration factor is defined as the ratio of sample volume to desorption solvent volume

Table 3. The determination of cadmium in water, tomato and cabbage samples by the proposed method

Sample	Added (µg g^{-1})	Found (µg g^{-1})[a]	RSD (%)	Recovery (%)
SRM1570A[b]	-	2.80 ± 0.09	3.2	96.9
Tomato	-	<LOQ	-	-
	5.0	4.6 ± 0.2	4.3	92.0
	10.0	8.9 ± 0.3	3.4	89.0
	15.0	14.1 ± 0.5	3.5	94.0
Cabbage	-	<LOQ	-	-
	5.0	4.3 ± 0.1	2.3	86.0
	10.0	10.2 ± 0.4	3.9	102.0
	15.0	13.7 ± 0.6	4.4	91.3
Sample	**Added (ng mL^{-1})**	**Found (ng mL^{-1})[a]**	**RSD (%)**	**Recovery (%)**
Bottled Mineral water	-	<LOQ	-	-
	5.0	4.8 ± 0.2	4.1	96.0
	10.0	10.1 ± 0.4	4.0	101.0
	15.0	13.5 ± 0.5	3.7	90.0
Tap water	-	<LOQ	-	-
	5.0	4.4 ± 0.2	4.5	88.0
	10.0	9.3 ± 0.4	4.3	93.0
	15.0	13.9 ± 0.7	5.0	92.7

[a]Mean ± standard deviation (n=3),
[b]Certified value**:** SRM1570A concentration, 2.89 µg g^{-1}

Table 4. The comparison of analytical parameters of the developed MSPE-FAAS method with other reported methods from some recent studies

Instrumental technique	Extraction method	Extraction phase	LOD (ng mL^{-1})	RSD (%)	sample	Refs.
FAAS	SPE	multiwalled carbon nanotubes impregnated with 4-(2-thiazolylazo) resorcinol	2.8	< 5	Macaroni, Rice and lentil	38
FAAS	US-assisted in-syringe DμSPE	Nitrogen doped nano porous graphene	0.3	4.38	human plasma, urine and saliva	39
FAAS	SPE	activated carbon cloth impregnated with PAN	1.1	NR	Soil and water	4
FAAS	SPE	poly[prothymosin-alpha -co-divinylbenzene-co-2-acrylamido-2-methylpropane sulfonic acid] (PTMA-co-DVB-co-AMPS)	1.4	≤ 2	Dried vegetable and water	40
FAAS	SPE	poly[2-(4-methoxyphenylamino)-2-oxoethyl methacrylateco-divinylbenzene-co-N-vinylimidazole] (MPAEMA-coDVB-co-VIM)	1.4	≤ 2	Tea and herbal plants	41
FAAS	MSPE	CCF/ZIF-71/Fe_3O_4 /PTh	0.21	3.0	Water, tomato and cabbage	This work

solid-phase extraction (SPE), magnetic solid-phase extraction (MSPE), flame atomic absorption spectrometry (FAAS), ultrasonic-assisted in-syringe dispersive micro solid-phase extraction (US-assisted in-syringe DμSPE), not reported (NR).

3.10. Comparison with other methods

The performance of the advanced MSPE-FAAS method employing CCF/ZIF-71/Fe_3O_4 /PTh sorbent was compared with reported methods in the literature of cadmium. Table 4 presents the comparison data, this proposed methodology has simple and faster operation, cost- effective, efficient and better performance. In addition, the proposed method does not require applying much sorbent and is also more sensitive. Due to a lower detection limit (LOD) and higher surface-to- volume ratio, the surface of CCF/ZIF-71/Fe_3O_4 /PTh has plenty of active sites, for this reason, the fabricated sorbent has a great adsorption capability. In conclusion, the MSPE method based on a CCF/ZIF-71/Fe_3O_4 /PTh coupled with FAAS utilizes as a viable choice for the determination of cadmium in real matrices.

4. Conclusion

In the current study, a novel magnetic sorbent, a sensitive, fast, and selective magnetic solid-phase extraction procedure followed by flame atomic adsorption spectroscopy, for pretreatment and determination of cadmium from water, cabbage, and tomato samples has been performed. The fabricated solid phase has notable and inherent properties like large surface area and great porous volume, simple isolation process, and cost-effective fabrication route. The fabricated novel hybrid sorbent was characterized by FT-IR, FE-SEM, and XRD. The recovery results revealed that the proposed method has excellent selectivity, satisfactory accuracy, acceptable enrichment factor, low limit of detection (LOD = 0.21 ng mL^{-1}), and essential preconcentration ability. Lastly, the proposed method can be a great offer to utilize successfully in the selective extraction, preconcentration, and determination of heavy metals in water and food samples.

5. Acknowledgment

The authors would like to gratefully acknowledge the support of this study by Islamic Azad University South Tehran Branch. We are grateful to Ms. Solmaz Karimi and Ms. Hanie Behzad Far for their kindly help in carrying out the FAAS analysis.

6. Conflict of interest

The authors declared no conflict of interest.

7. References

[1] M. Babazadeh, R. Hosseinzadeh-Khanmiri, J. Abolhasani, E. Ghorbani-Kalhor, A. Hassanpour, Solid phase extraction of heavy metal ions from agricultural samples with the aid of a novel functionalized magnetic metal–organic framework, RSC Adv., 5 (2015) 19884-19892. https://doi.org/10.1039/C4RA15532G

[2] M. Cegłowski, G. Schroeder, Removal of heavy metal ions with the use of chelating polymers obtained by grafting pyridine–pyrazole ligands onto polymethylhydrosiloxane, Chem. Eng. J., 259 (2015) 885-893. https://doi.org/10.1016/j.cej.2014.08.058

[3] K. M. Dimpe, J. Ngila, P. N. Nomngongo, Preparation and application of a tyre-based activated carbon solid phase extraction of heavy metals in wastewater samples, Phy. Chem. Earth, Parts A/B/C, 105 (2018) 161-169. https://doi.org/10.1016/j.pce.2018.02.005

[4] E. Y. Zeid A. Alothman, Mohamed Habila, Mustafa Soylak, Solid phase extraction of metal ions in environmental samples on 1-(2-pyridylazo)-2-naphthol impregnated activated carbon cloth, Ecotoxicol. Environ. Safe., 112 (2015) 74-79. https://doi.org/10.1016/j.ecoenv.2014.10.032

[5] F. Bilo, L. Borgese, A. Zacco, P. Lazo, C. Zoani, Total reflection X-Ray fluorescence Spectroscopy to evaluate heavy metals accumulation in legumes by HPTLC method, J. Anal. Bioanal. Tech., 292 (2015) 2. https://doi.org/10.4172/2155-9872.1000292

[6] S. Su, B. Chen, M. He, B. Hu, Z. Xiao, Determination of trace/ultratrace rare earth elements in environmental samples by ICP-MS after magnetic solid phase extraction with Fe3O4@ SiO2@ polyaniline–graphene oxide composite, Talanta, 119 (2014) 458-466. https://doi.org/ 10.1016/j.talanta.2013.11.027.

[7] M. Serkan Yalçın, Solid phase extraction of trace level Ag (I) using Coriolus versicolor immobilized magnetic nanoparticles and its determination by ICP-OES, Environ. Prog. Sustain. Energ., 38 (2019) e13251. https://doi.org/ 10.1002/ep.13251.

[8] V. Ivanova-Petropulos, S. Jakabová, D. Nedelkovski, V. Pavlík, Ž. Balážová, O. Hegedűs, Determination of Pb and Cd in Macedonian wines by electrothermal atomic absorption spectrometry (ETAAS), Food Anal. Methods, 8 (2015) 1947-1952. https://doi.org/ 10.1007/s12161-014-0062-x

[9] A. Babaei, M. Zeeb, A. Es-haghi, Magnetic dispersive solid-phase extraction based on graphene oxide/Fe3O4@ polythionine nanocomposite followed by atomic absorption spectrometry for zinc monitoring in water, flour, celery and egg, J. Sci. Food Agric., 98 (2018) 3571-3579. https://doi.org/ 10.1002/jsfa.8873.

[10] Z. Li, J. Li, Y. Wang, Y. Wei, Synthesis and application of surface-imprinted activated carbon sorbent for solid-phase extraction and determination of copper (II), Spectrochim. Acta Part A: Mol. Biomol. Spect., 117 (2014) 422-427. https://doi.org/10.1016/j.saa.2013.08.045

[11] A. Thongsaw, R. Sananmuang, Y. Udnan, G. M. Ross, W. C. Chaiyasith, Dual-cloud point extraction for speciation of mercury in water and fish samples by electrothermal atomic absorption spectrometry, Spectrochim. Acta Part B: Atom. Spect., 160 (2019) 105685. https://doi.org/ 10.1016/j.sab.2019.105685.

[12] S. M. Sorouraddin, M. A. Farajzadeh, H. Dastoori, Development of a dispersive liquid-liquid microextraction method based on a ternary deep eutectic solvent as chelating agent and extraction solvent for preconcentration of heavy metals from milk samples, Talanta, 208 (2020) 120485. https://doi.org/ 10.1016/j.talanta.2019.120485.

[13] S. G. Elci, Determination of cobalt in food by magnetic solid-phase extraction (MSPE) preconcentration by polyaniline (PANI)

and polythiophene (PTH) coated magnetic nanoparticles (MNPs) and microsample injection system–flame atomic absorption spectrometry (MIS-FAAS), Instrum. Sci. Technol., 49 (2021) 258-275. https://doi.org/10.1080/10739149.2020.1818577.

[14] M. B. Arain, E. Yilmaz, N. Hoda, T. G. Kazi, M. Soylak, Magnetic solid-phase extraction of quercetin on magnetic-activated carbon cloth (MACC), J. Iran. Chem. Soc., 16 (2019) 1365-1372. https://doi.org/10.1007/s13738-019-01622-5.

[15] R. S. Canlidinc, O. Kalfa, Z. Ustundag, Y. Erdogan, Graphene oxide modified expanded perlite as a new sorbent for Cu (II) and Pb (II) prior to determination by high-resolution continuum source flame atomic absorption spectrometry, Sep. Sci. Technol., 52 (2017) 2069-2078. https://doi.org/10.1080/01496395.2017.1328443

[16] Y. Yang, X. Ma, F. Feng, X. Dang, J. Huang, H. Chen, Magnetic solid-phase extraction of triclosan using core-shell Fe 3 O 4@ MIL-100 magnetic nanoparticles, and its determination by HPLC with UV detection, Microchim. Acta, 183 (2016) 2467-2472. https://doi.org/10.1007/s00604-016-1872-x.

[17] M. A. Habila, Z. A. ALOthman, E. Yilmaz, M. Soylak, Activated carbon cloth filled pipette tip for solid phase extraction of nickel (II), lead (II), cadmium (II), copper (II) and cobalt (II) as 1, 3, 4-thiadiazole-2, 5-dithiol chelates for ultra-trace detection by FAAS, Int. J. Environ. Anal. Chem., 98 (2018) 171-181. https://doi.org/10.1080/03067319.2018.1430794.

[18] J. J. Zhihong Shi, W. Pang, H. Ma, X. Chu, C. Zhou, H. Zhang, Dispersive micro-solid phase extraction using cotton based carbon fiber sorbent for the determination of three polycyclic aromatic hydrocarbons in tea infusion by gas chromatography-quadrupole mass spectrometry, Microchem. J., 151 (2019) 104209, https://doi.org/10.1016/j.microc.2019.104209

[19] Z. Wei, W. Zhu, Y. Li, Y. Ma, J. Wang, N. Hu, Y. Suo, J. Wang, Conductive leaflike cobalt metal–organic framework nanoarray on carbon cloth as a flexible and versatile anode toward both electrocatalytic glucose and water oxidation, Inorg. chem., 57 (2018) 8422-8428. https://doi.org/10.1021/acs.inorgchem.8b01106.

[20] L. Zhang, Y. Zhang, S. Huang, Y. Yuan, H. Li, Z. Jin,. J. Wu, Q. Liao, L. Hu, J. Lu, Co3O4/Ni-based MOFs on carbon cloth for flexible alkaline battery-supercapacitor hybrid devices and near-infrared photocatalytic hydrogen evolution, Electrochim. Acta, 281 (2018) 189-197. https://doi.org/10.1016/j.electacta.2018.05.162.

[21] T.-Y. Chen, Y.-J. Huang, C.-T. Li, C.-W. Kung, R. Vittal, K.-C. Ho, Metal-organic framework/sulfonated polythiophene on carbon cloth as a flexible counter electrode for dye-sensitized solar cells, Nano Energ., 32 (2017) 19-27. https://doi.org/10.1016/j.nanoen.2016.12.019.

[22] C. Zhang, J. Tian, W. Rao, B. Guo, L. Fan, W. Xu, J. Xu , Polypyrrole@ metal-organic framework (UIO-66)@ cotton fabric electrodes for flexible supercapacitors, Cellulose, 26 (2019) 3387-3399. https://doi.org/10.1007/s10570-019-02321-3.

[23] A. Modi, J. Bellare, Zeolitic imidazolate framework-67/carboxylated graphene oxide nanosheets incorporated polyethersulfone hollow fiber membranes for removal of toxic heavy metals from contaminated water, Sep. Purif. Technol., 249 (2020) 117160. https://doi.org/10.1016/j.seppur.2020.117160.

[24] Liu, Y., H. Pang, X. Wang, S. Yu, Z. Chen, P. Zhang, L. Chen, G. Song, N. S. Alharbi, S. O. Rabah, Zeolitic imidazolate framework-based nanomaterials for the capture of heavy metal ions and radionuclides: a review, Chem. Eng. J. 406 (2021) 127139. https://doi.org/10.1016/j.cej.2020.127139.

[25] W. Wei, K. M. Gupta, J. Liu, J. Jiang, Zeolitic imidazolate framework membranes for organic solvent nanofiltration: a molecular

simulation exploration, ACS Appl. Mater. Interfaces, 10 (2018) 33135-33143. https://doi.org/10.1021/acsami.8b08364.

[26] R. P. Lively, M. E. Dose, J. A. Thompson, B. A. McCool, R. R. Chance, W. J. Koros, Ethanol and water adsorption in methanol-derived ZIF-71, Chem. Comm., 47 (2011) 8667-8669. https://doi.org/10.1039/C1CC12728D.

[27] M. Rajabi, M. Hemmati, Comparison of two polythiophene nanocomposites-based dispersive micro solid-phase extraction procedures coupled with salt-induced/magnetic separations for efficient preconcentration of toxic metal ions from food samples, J. Mol. Liq., 324 (2021)114997. https://doi.org/10.1016/j.molliq.2020.114997.

[28] J. Wang, W. Zhu, T. Zhang, L. Zhang, T. Du, W. Zhang, D. Zhang, J. Sun, T. Yue, Y.-C. Wang, Conductive polyaniline-graphene oxide sorbent for electrochemically assisted solid-phase extraction of lead ions in aqueous food samples, Anal. Chim. Acta, 1100 (2020) 57-65. https://doi.org/10.1016/j.aca.2019.11.070.

[29] L. Suo, J. Zhao, X. Dong, X. Gao, X. Li, J. Xu, X. Lu, L. Zhao, Functionalization of a SiO_2-coated magnetic graphene oxide composite with polyaniline–polypyrrole for magnetic solid phase extraction of ultra-trace Cr (III) and Pb (II) in water and food samples using a Box–Behnken design, New J. Chem., 43 (2019) 12126-12136. https://doi.org/10.1039/C9NJ02038A.

[30] S. Shegefti, A. Mehdinia, F. Shemirani, Preconcentration of cobalt (II) using polythionine-coated Fe 3 O 4 nanocomposite prior its determination by AAS, Microchim. Acta, 183 (2016) 1963-1970. https://doi.org/10.1007/s00604-016-1837-0.

[31] M. Zeeb, H. Farahani, Graphene oxide/Fe_3O_4@ polythionine nanocomposite as an efficient sorbent for magnetic solid-phase extraction followed by high-performance liquid chromatography for the determination of duloxetine in human plasma, Chem. Papers, 72 (2018) 15-27. https://doi.org/10.1007/s11696-017-0253-1.

[32] M. A. Daryakenary, M. Zeeb, Trace determination of chlorpheniramine in human plasma using magnetic dispersive solid-phase extraction based on a graphene oxide/Fe_3O_4@ polythionine nanocomposite combined with high-performance liquid chromatography, RSC Adv., 7 (2017) 53210-53218. https://doi.org/10.1039/C7RA09707G.

[33] R. Salehi, F. Dadashian, M. Abedi, Preparation of activated carbon fabrics from cotton fabric precursor, IOP Conference Series, Mater. Sci. Eng., 254 (2017) 042024. https://iopscience.iop.org/article/10.1088/1757-899X/254/4/042024

[34] F. Pourbahman, M. Zeeb, A. Monzavi, S. S. Homami, Simultaneous trace monitoring of prokinetic drugs in human plasma using magnetic dispersive micro-solid phase extraction based on a new graphene oxide/metal–organic framework-74/Fe3O4/polytyramine nanoporous composite in combination with HPLC, Chem. Papers, 73 (2019) 3135-3150. https://doi.org/10.1007/s11696-019-00855-1.

[35] S. Tokalıoğlu, E. Yavuz, H. Şahan, S. G. Çolak, K. Ocakoğlu, M. Kaçer, Ş. Patat, Ionic liquid coated carbon nanospheres as a new adsorbent for fast solid phase extraction of trace copper and lead from sea water, wastewater, street dust and spice samples, Talanta, 159 (2016) 222-230. https://doi.org/10.1016/j.talanta.2016.06.022.

[36] A. A. Gouda, S. M. Al Ghannam, Impregnated multiwalled carbon nanotubes as efficient sorbent for the solid phase extraction of trace amounts of heavy metal ions in food and water samples, Food Chem., 202 (2016) 409-416. https://doi.org/10.1016/j.foodchem.2016.02.006.

[37] Y. Sanaei, M. Zeeb, S. S. Homami, A. Monzavi, Z. Khodadadi, Fabrication of ZIF-71/Fe3O 4/polythionine nanoarray-functionalized carbon cotton cloth for simultaneous extraction and quantitation of febuxostat and diclofenac,

RSC Adv., 11 (2021) 30361-30372. https://doi.org/10.1039/D1RA04670E.

[38] Z. A. ALOthman, M. Habila, E. Yilmaz, M. Soylak, Solid phase extraction of Cd (II), Pb (II), Zn (II) and Ni (II) from food samples using multiwalled carbon nanotubes impregnated with 4-(2-thiazolylazo) resorcinol, Microchim. Acta, 177 (2012) 397-403. https://doi.org/10.1007/s00604-012-0789-2.

[39] Z. Lotfi, H. Zavvar Mousavi, S. M. Sajjadi, Nitrogen doped nano porous graphene as a sorbent for separation and preconcentration trace amounts of Pb, Cd and Cr by Ultrasonic assisted in-syringe dispersive micro solid phase extraction, Appl. Organometal. Chem., 32 (2018) e4162. https://doi.org/10.1002/aoc.4162.

[40] T. Daşbaşi, H. Muğlu, C. Soykan, A. Ülgen, SPE and determination by FAAS of heavy metals using a new synthesized polymer resin in various water and dried vegetables samples, J. Macromol. Sci., Part A, 55 (2018) 288-295. https://doi.org/10.1080/10601325.2018.1424556.

[41] T. Daşbaşı, C. Soykan, N. Çankaya, A. Ülgen, Determination of some trace metals with a new synthesized polymer resin by FAAS in various tea and herbal plants samples, J. Macromol. Sci., Part A, 55 (2018) 466-473. https://doi.org/10.1080/10601325.2018.1470464.

Anal. Methods Environ. Chem. J. 5 (2) (2022) 76-89

AMECJ

Research Article, Issue 2
Analytical Methods in Environmental Chemistry Journal
Journal home page: www.amecj.com/ir

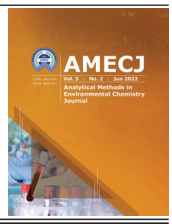

Determination of mercury values in urine and air of chloralkali workers by copper nanoparticles functionalized in carboxylic carbon nanotubes and the effects of mercury exposure on oxidative stress

Ali Faghihi-Zarandi[a], Somayyeh Karami-Mohajeri[b], Morteza Mehdipour Rabouri[a], Abbas Mohammadhosseini- Heyran[a] and Zahed Ahmadi [c,*]

[a] *Department of Occupational Health, School of Public Health, Kerman University of Medical Sciences, Kerman, Iran*
[b] *Pharmaceutics Research Center, Institute of Neuropharmacology, Kerman University of Medical Sciences, Kerman, Iran*
[c] *Department of Occupational Health Engineering, School of Public Health, Iranshahr University of Medical Sciences, Iranshahr, Iran*

ARTICLE INFO:

Received 30 Feb 2022
Revised form 2 May 2022
Accepted 28 May 2022
Available online 30 Jun 2022

Keywords:
Mercury,
Air, and Urine,
Magnetic solid-phase extraction,
Oxidative stress,
Copper functionalized carbon nanotubes,
Cold vapor atomic absorption spectrometer

ABSTRACT

Mercury exposure can produce toxic organic compounds in the body. Also, mercury can potentially cause oxidative damage and cellular disorders. In this study, the determination of mercury values in urine and air of chloralkali workers based on copper nanoparticles functionalized in carboxylic carbon nanotubes (CuNPs@CNT-COOH) were obtained by cold vapor atomic absorption spectrometer (CV-AAS). The urine samples were determined by magnetic solid-phase extraction (MSPE) at pH 8.0. By measuring the mercury level in the air and the urine sample of workers, the level of oxidative stress (Malondialdehyde (MDA), Superoxide Dismutase (SOD) and Catalase (Cat)), Interleukin-6 (IL-6), and Tumor Necrosis Factor α (TNF-α) as the proinflammatory cytokines were measured in the subject group. The results revealed statistically significant differences in the mercury level of the urine samples in the case and control groups ($p<0.001$). Similarly, the malondialdehyde (MDA) level was significantly different between the two research groups ($p<0.001$). Catalase concentration was not significantly different in the two groups ($p=0.059$). The LOD and linear range for mercury determination in urine were achieved at 0.012 µg L^{-1} and 0.05-7.0 µg L^{-1}, respectively. Workers' exposure to mercury can significantly increase oxidative stress and inflammatory cell signaling molecules such as cytokines.

1. Introduction

In the biogeochemical system of the earth, there are metallic mercury, organic and non-organic compounds. Exposure to any of the three can produce toxic compounds in the body[1]. Heavy metals are important factors in environmental pollution and mercury is one of the most toxic and threatens human health [2]. The greatest effect of mercury in elemental and organic form in the central nervous system and the greatest effect of mineral mercury on the digestive and excretory systems [3]. Mercury has been extensively investigated due to its wide range of applications, high toxicity, long-term ecological effects, aggregation in the food chain and adverse effects (in exposure to the low concentration of the liquid metal) [1, 4, 5, 6].

*Corresponding Author: Zahed Ahmadi
Email: zahedahmadi68@yahoo.com
https://doi.org/10.24200/amecj.v5.i02.188

Between 40 and 70% of the existing mercury in the atmosphere is estimated to be induced by human activities. Direct and indirect exposure of more than 2 million occupations to this pollutant is considered a global concern [4, 7, 8]. At work, exposure to mercury vapor through respiration is more common [9]. Yet, the alkali form (methyl/ethyl mercury) is highly soluble in fatty tissues and also highly volatile. Thus, it can be easily absorbed in the lungs and then the blood, and is 10 times as toxic [1]. Occupational mercury exposure can occur in petrochemical, and chloralkali industries, fluorescent lamps, thermometer manufacturing companies, glass production and dentistry (tooth amalgam) [10-12]. Chloralkali processing is a large industry worldwide in electrochemistry. The main products are cholera, sodium hydroxide, carbonate sodium, hydrochloric acid and potash [13]. The common chloralkali processes include mercury cell, membrane cell and diaphragm cell. In the mercury cell process, the anode (carbon electrode) is hung above the cell and the mercury flows on the container surface as the cathode [5, 14].When the electricity is on, the chloride ion dissolved in saline water turns into the chlorine oxide at the anode side. Sodium ions are revived as sodium at the cathode side. Sodium is then solved in mercury and sodium amalgam (sodium-mercury) is produced. Next, the amalgam is analyzed. Thus, mercury returns to the cycle and sodium are turned into sodium hydroxide [14]. Among the disadvantage of this method are ecological issues, low efficiency in terms of the voltage used, exposure to mercury and the high cost [1]. Despite the presence of several metals in the body such as iron, magnesium, zinc, copper, cobalt, molybdenum and selenium, the toxicity of mercury is incomparably high [6]. A body of research explored the threats to health caused by exposure to mercury. Instances are disorders in the nervous system especially the brain, cardiovascular diseases, metabolic disorders, pulmonary issues, damage to the immune system, liver, reproduction system, thyroid, and optical, auditory, tactile and verbal disorders [4, 7, 12, 15-20]. These studies showed that the disorders induced by exposure to mercury produce oxygen radicals in the body. The cytotoxic effects of mercury (Hg^{+2}) can be due to the oxidative stress in cells. Hg^{+2} interacts with thiols and produces mercaptans. Thus, the cellular antioxidant buffers based on glutathione thiol are reduced. Though the exact mechanism of the production of these radicals is yet unknown, probably, an increase in reactive oxygen species (ROS) is the main cause, which results from the reduced rate of glutathione [21]. Several studies show that mercury can cause oxidative damage to multiple organs and systems [21, 22]. Greater production of ROS can lead to oxidative stress and may induce dysfunctions and structural damages such as mutagenesis, carcinogenesis, oxidation, and deterioration of proteins, carbohydrates, lipids and DNA [23]. Numerous studies have also identified a significant positive relationship between the dose of mercury exposure in hair samples and high blood pressure [24]. In the cardiovascular system, the endothelium functioning is essential to the maintenance of the blood flow and the antithrombotic capacity. Vascular endothelial is highly sensitive to oxidative stress. This stress can be the main cause of disorders in this tissue in cardiovascular diseases including hypertension and atherosclerosis [4, 17]. Measuring changes in the activity of antioxidant enzymes such as superoxide dismutase (SOD) and catalase (CAT) is typically done to act as a biological index in examining cellular oxidant damages [4, 25, 26]. In cells, SOD takes charge of analyzing superoxide anions (O_2) into oxygen and hydrogen peroxide (H_2O_2). Catalase is in charge of analyzing H_2O_2 in water and oxygen [26]. Today, measuring the level of cytokines or low-weight glycoproteins is another index for cellular disorders. These hormones interlink cells and the inner body environment especially the immune and inflammatory systems [21]. Striking a balance between the two groups (i.e., the proinflammatory and anti-inflammatory cytokine groups) is key to human hemostasis. Measuring proinflammatory cytokines is significant, for example, interleukin 6 (IL-6) and the tumor necrosis factor alpha (TNF alpha), both known as major biological indices in

diagnosing cellular damage [27, 28]. The present research aimed to explore the effects of exposure to mercury on oxidative stress and proinflammatory cytokines in the body of workers in the chloralkali industry. In-addition the mercury values were determined in air (NIOSH 6009) and human urine samples based on CuNPs@CNT-COOH by MSPE procedure at pH 8.5.

2. Materials and Methods

2.1. Instrumental and reagents

A cold vapor atomic absorption spectrometer (AAS) was used to determination of mercury in water samples (CV-AAS, HG-3000, GBC, Aus). The background correction (D_2 lamp) the hollow cathode lamp (HCL, Hg), $SnCl_2/NaBH_4$ reagents and a reaction loop were used for the generation of mercury vapor and the mercury concentration determination by CV-AAS. The standard of inorganic mercury [Hg^{2+}, 1000 mg L^{-1} in 1% nitric acid) was prepared from Sigma Aldrich (CAS N: 7487-94-7, Germany). The different standard solutions of mercury were made by diluting deionized water (DW, Millipore, USA).

2.2. Design and Sampling

The present cross-sectional research was case-control in type, and was conducted in 2020 in a chloralkali factory in Tehran. The participants were 179 in number (84 blue-collar workers and 95 white-collar workers). Screening of different units showed that 114 participants were directly exposed to mercury. These workers were significantly exposed to mercury as chlorine was produced by traditional mercury cell processes. Considering the exposure criteria, among the 114 workers, 84 were found to be directly exposed and were, thus, selected as the case. For the control group, 95 white-collar workers were recruited. The inclusion criteria were: full-time work and at least two years' work experience in the unit. The exclusion criteria were: consuming antioxidant supplements (e.g., vitamin E or C) and drugs containing mercury, having renal diseases, and being non-smokers yet being unwilling to participate in the study. According to the inclusion criteria, the final sample was selected to include workers who consumed antioxidant supplements and drugs (n=7), had less than two years' work experience and were non-smokers (n=14). Those unwilling to participate (n=9) were excluded from the study. The final remaining 84 blue-collared workers were included in the research. Thus, the sampling can be called a consensus. The control group consisted of office workers who were not exposed to mercury. All the participants agreed to participate in the study by signing an informed letter of consent. A demographic questionnaire was also filled out by all participants to include their age, weight, height, work experience, smoking status and type of work shift. The human urine samples were collected in 114 participants based on Helsinki Declaration as revised in 2013. The information, including names, initials, and hospital numbers don't publish in text or any other document. (https://www.wma.net/policies-post/wma-declaration-of-helsinkiethical-principles-for-medical-research-involving- ansubjects/).

2.3. Measurement of mercury level in the air sample

Occupational mercury exposure was measured by air samples in the participants' breathing zoon using the NIOSH 6009 method. The solid sorbent tubes with 200 mg Hopcalite in a single section were used as samplers and were connected by Tygon tubing to the personal pumps calibrated before and after sampling. The flow rate was adjusted to 2 L min^{-1} and the sampling duration was set at 3 hours of a normal work shift. The sorbent tubes were capped and packed securely for shipment. The Hopcalite sorbent and the front glass wool of each sample were placed in separate 50 volumetric flasks and 2.5 mL of HNO_3. Then, 2.5 mL of HCl was added to each volumetric flask. The sorbent was dissolved and diluted to 50 ml with deionized water. 20 mL of the sample was transferred to a BOD bottle containing 80 mL of deionized water. All samples were analyzed using a cold vapor atomic absorption (GBC-936, 3000, Australia) at a wavelength of 253.7 nm (Fig. 1). The amount of mercury (C) in

the sampled air volume (V) was calculated using the following Equation 1:

$$C\ (mg/m3\ ) = W\ (\mu g) \times Vs\ (mL)\ Va/(mL) - B\ (\mu g)\ V\ (L) \quad \text{(Eq. 1)}$$

W is the amount of mercury in the sample aliquot from the calibration graph. Vs represents the original sample volume (50 mL). Va stands for the aliquot volume (20 mL), and B is the average amount of mercury in the media blanks.

2.4. Measurement of mercury concentration in the human urine sample

The most practical and sensitive method of measuring the level of mercury in the body is the urine sample. That is because mercury exits the body primarily in the urine. The concentration of the metal in urine samples shows the exposure within the past 2-3 months. In this research, mercury in the urine samples was extracted based on copper nanoparticles functionalized in carboxylic carbon nanotubes (CuNPs@CNT-COOH) by magnetic solid-phase extraction (MSPE) at pH 8.5 before being determined by cold vapor atomic absorption spectrometer (CV-AAS). Urine samples were collected in the field using a 100 mL sterile plastic container before the participants' work shift. The samples were sealed and packed in an ice bath. The mercury in 10 mL of urine samples was extracted with the COOH group of CuNPs@CNT-COOH at pH=8.0 and then the solid phase was separated by an external magnetic accessory in the bottom of the tube. After back-extraction of mercury from CuNPs@CNT-COOH in acidic pH and dilution with DW up to 1 mL, the concentration of mercury in urine samples was determined by CV-AAS (GBC-936, HG-3000, Australia), equipped with a Hg lamp at a wavelength of 253.7 nm. The extraction of toxic mercury with 25 mg of CuNPs@CNT-COOH was obtained more than 95% in 10 mL of urine samples by MSPE (Fig.2)..

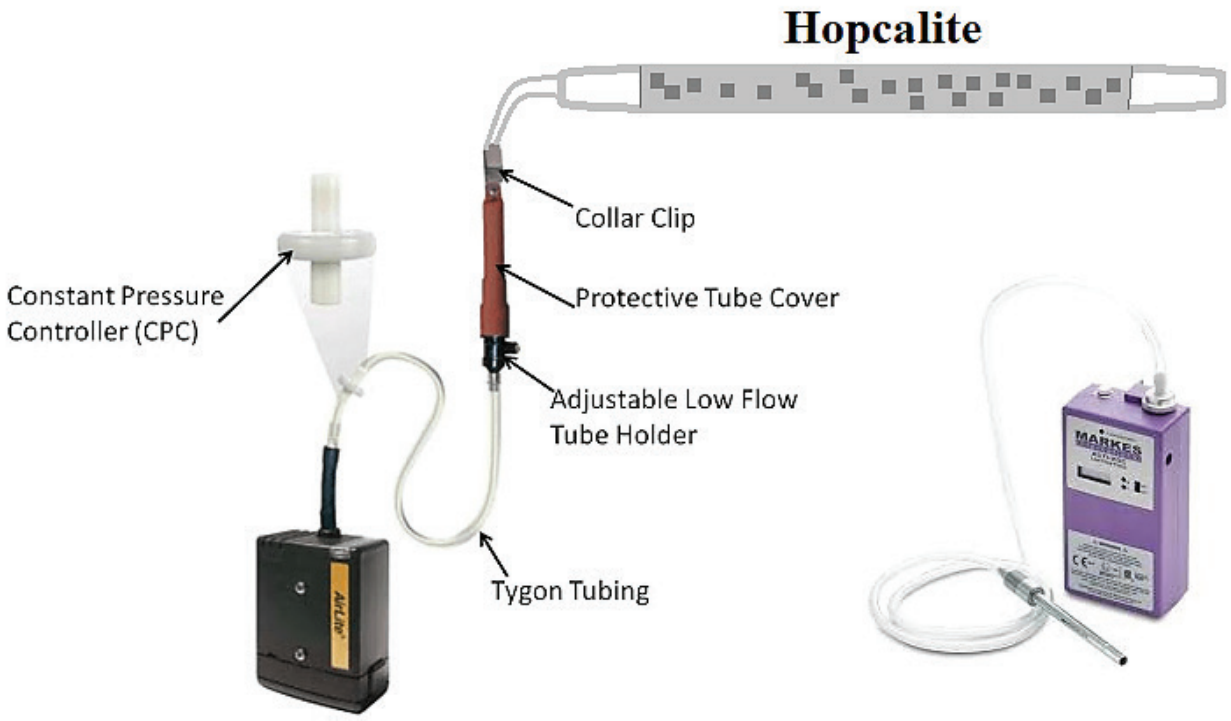

Fig. 1. Measurement of mercury level in the air sample in the participants' breathing zoon using the NIOSH 6009 method.

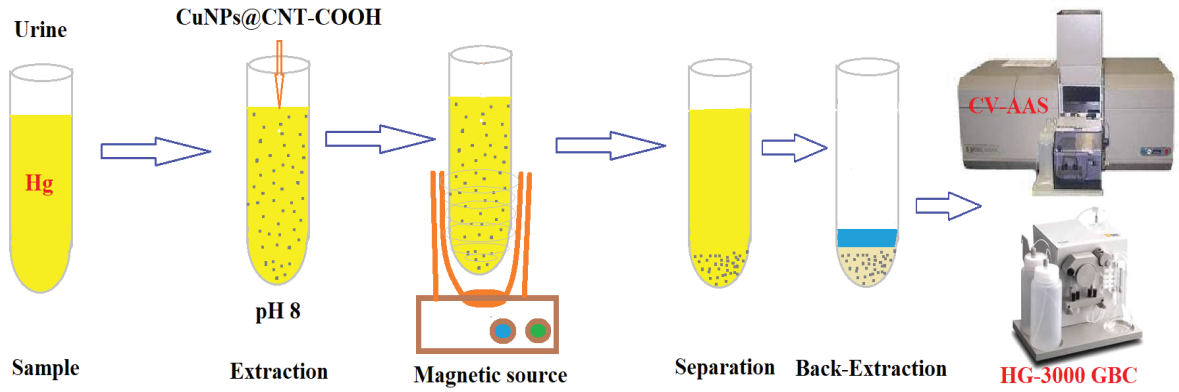

Fig.2. Measurement of mercury concentration in the human urine sample based on CuNPs@CNT-COOH by MSPE procedure at pH 8.5

2.5. Measurement of Oxidative Stress

In the present research, the level of Malondialdehyde (MDA), Superoxide Dismutase (SOD) and Catalase (Cat) as the oxidative stress indices and Interleukin-6 (IL-6) and Tumor Necrosis Factor α (TNF-α) as the proinflammatory cytokines were measured in the collected samples. Five milliliters of the venal blood were taken from the participants in both groups before their work shift. These samples were transferred into sterile tubes and were allowed to clot. After tube centrifuging (1600 × g for 10 minutes), the serum samples were separated and stored at -50 °C before analysis. The oxidative stress and proinflammatory cytokines were measured using Hangzhou Eastbiopharm kits (Hangzhou, China) by Double Antibody Sandwich (DAS) ELISA. The mean value of three repetitions for each sample was reported.

2.6. Statistical Analysis

Descriptive statistics were used including frequency (percentage) and median (inter-quartile range) to summarize demographic variables, oxidative stress indices and proinflammatory cytokines. The normality and the equality of variances were analyzed by the Kolmogorov Smirnov test and the Levene's test. Demographic variables were compared in the exposed and unexposed groups via the chi-square test. To compare the median of oxidative stress indices, proinflammatory cytokines and the level of mercury in urine samples (urine Hg) in two groups, the Mann Whitney U-test was run. Predictors of oxidative stress and proinflammatory cytokines were tested using multiple linear regression (backward). Variables with more than two categories entered the regression model after dummy coding. The variables that did not meet the normality assumption were normalized according to the method recommended by Templeton (2011) before entering the final model [29]. All statistical tests were run in SPSS v25 (IBM SPSS, Chicago, IL) at the significance level of < 0.05.

3. Results and discussion

3.1. Optimization and validation of mercury analysis

By the MSPE procedure, the extraction of mercury in urine samples was achieved by CuNPs@CNT-COOH nanoparticles. The various mercury concentration between 0.05–7.0 µg L^{-1} were used for the optimization of parameters. The mercury was extracted and separated in urine samples based on the COOH groups of CuNPs@CNT-COOH adsorbent at optimized conditions. The effective parameters such as the pH, amount of CuNPs@CNT-COOH adsorbent, the eluents, and the sample volume were studied.

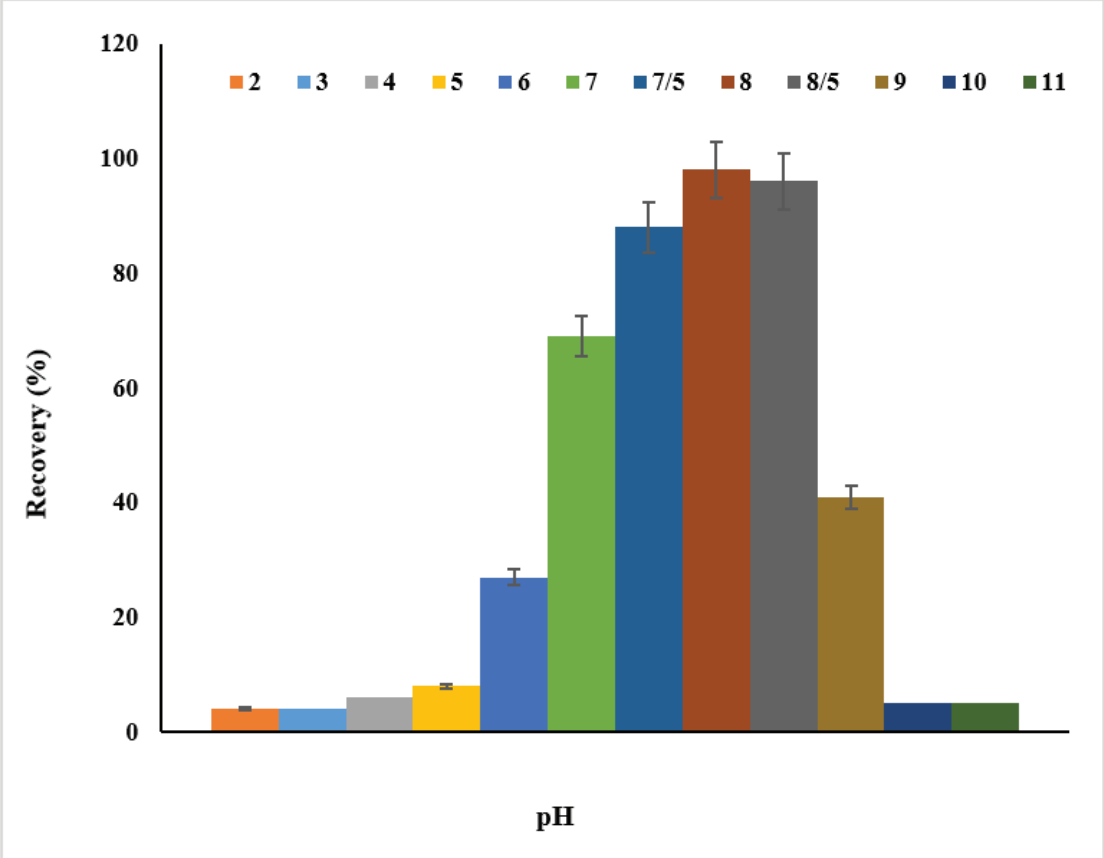

Fig. 3. The effect of pH on mercury extraction in urine samples based on CuNPs@CNT-COOH by MSPE procedure at pH 8.5

3.1.1.pH effect

For efficient extraction of mercury in urine samples, the pH sample must be optimized. So, the different values between 2 and 11 were studied. The pH is the critical parameter that was affected by efficient extraction and absorption capacity by the CuNPs@CNT-COOH adsorbent. Therefore, the various pH was selected for Hg(II) extraction in urine samples using a buffer solution. The results showed that the high recovery based on the CuNPs@CNT-COOH adsorbent for mercury extraction was obtained at a pH of 7.5-8.5. So, the efficient mercury extraction was obtained at pH 8.0 and the recovery was decreased at $8.5 < pH < 7.0$. So, the pH of 8.0 was used as optimized pH in this study (Fig. 3). The extraction mechanism occurred based on COOH groups of CuNPs@CNT-COOH adsorbent as an excellent leaving group

$$(Hg^{2+} \longleftarrow [:COOH\text{-}R])$$

with the positively charged mercury at pH 8. At lower pH the COOH groups have positively charged (+). So, the electrostatic repulsion occurred between Hg^{2+} and +COOH groups. In addition, at more than pH 8.5, the mercury ions participated as $Hg(OH)_2$.

3.1.2.Optimized CuNPs@CNT-COOH amount

For maximum extraction of mercury in water samples, the amount of the CuNPs@CNT-COOH adsorbent must be optimized in mercury concentration between 0.05–7.0 µg L^{-1}. So, the various amounts of the CuNPs@CNT-COOH between 5-40 mg were used for Hg(II) extraction in urine samples by the MSPE procedure. The efficient extraction was obtained at more than 20 mg of the CuNPs@CNT-COOH adsorbent for the extraction of mercury by the proposed procedure. Therefore, 25 mg of the CuNPs@CNT-COOH was used for further work at pH=8 (Fig. 4).

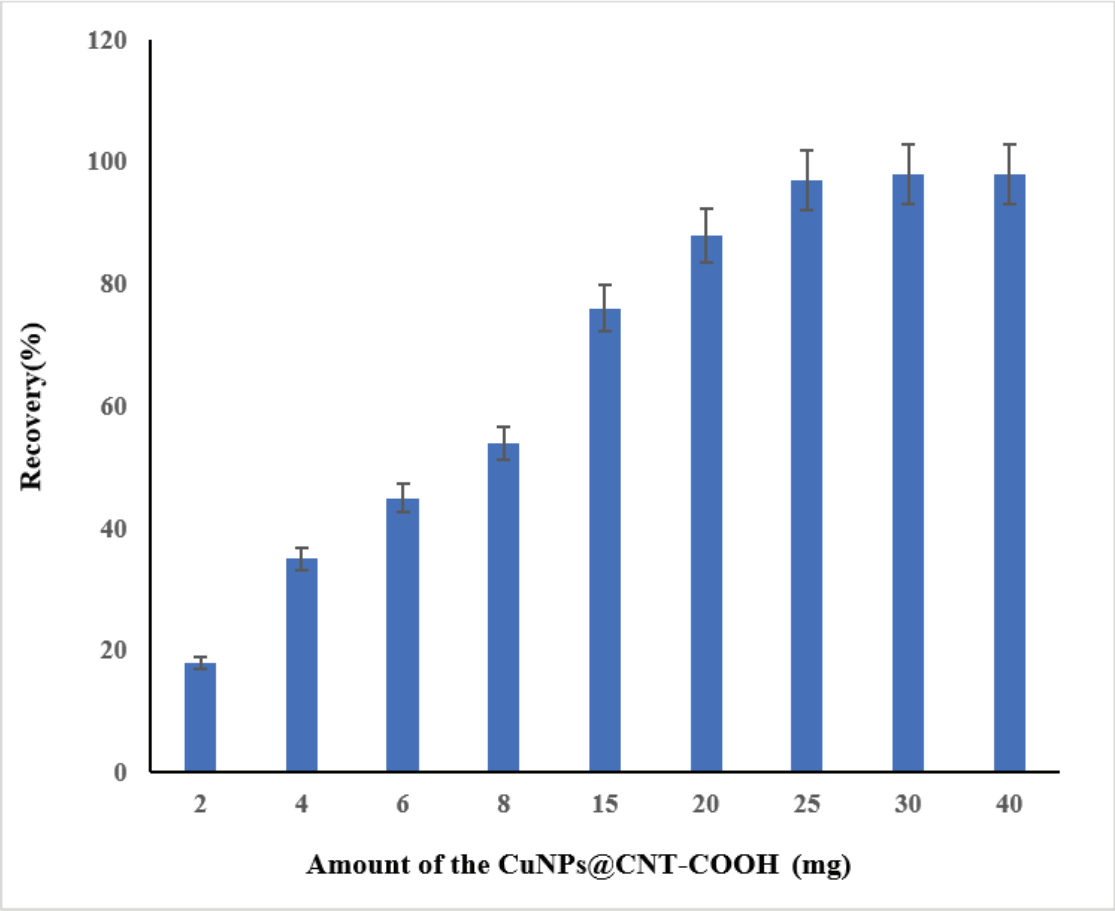

Fig. 4. The effect of amount of adsorbent on mercury extraction in urine samples based on CuNPs@CNT-COOH by MSPE procedure at pH 8.5

3.1.3.Elution process, shaking time and Sample volume

After extraction of mercury by CuNPs@CNT-COOH adsorbent, the mercury loaded on the CuNPs@CNT-COOH must be released from COOH groups by changing pH. Therefore, the different eluents such as, HCl, HNO_3, and H_2SO_4, were used for the back-extraction of mercury (Hg^{2+}) from the CuNPs@CNT-COOH adsorbent. The mercury loaded on the CuNPs@CNT-COOH adsorbent was easily determined by the CV-AAS after back extraction with inorganic acid at low pH. In this study, the different eluents (HCl, HNO_3, H_2SO_4) based on volumes and concentrations were used for back extraction of Hg(II) in urine samples. The results showed us that the Hg(II) ions were back-extracted from the CuNPs@CNT-COOH adsorbent by the nitric acid solution (0.3 mol L^{-1}; 0.5 mL). Also, the shaking time is the main parameter for the extraction of mercury in urine samples. So, the different time was studied from 1 to 10 minute for mercury extraction at pH 8. The maximum extraction was obtained in more than 4 min. So, 5 minutes was used as the optimum shaking time. In addition, the effect of sample volume for mercury extraction was studied at pH=8. The results showed us that the mercury can be extracted in 12 mL at the optimized conditions. So, the 10 mL of urine samples were selected as the optimum volume for mercury extraction for further works.

Table 1. Demographic variables of the exposed group (n=84) vs. unexposed group (n=95)

Variable	Classification	Frequency (%)		P-value*
		Exposed group	Unexposed group	
Age	<30	33 (39.3)	43 (45.3)	0.674
	30-40	37 (44)	36 (37.9)	
	>40	14 (16.7)	16 (16.8)	
Experience	≤10	47 (56)	56 (58.9)	0.686
	>10	37 (44)	39 (41.1)	
BMI	Underweighted	4 (4.7)	7 (7.4)	0.392
	Normal	75 (89.3)	78 (82.1)	
	Obesity	5 (6)	10 (10.5)	
Shift work	Yes	23 (27.4)	20 (21.1)	0.323
	No	61 (72.6)	75 (78.9)	

* Chi-square

3.2. Comparing exposed and unexposed groups

Table 1 summarizes the two research groups' demographic information. More than half of the participants in both groups had less than 10 years of work experience. Most of the participants had a normal BMI. There was no statistically significant difference between demographic variables in the exposed and unexposed groups. The median (inter-quartile range) of mercury concentration in air and urine samples, oxidative stress indices and proinflammatory cytokines are shown in Table 2. The level of mercury in the urine samples of the exposed group was significantly different from the unexposed group (p<.001). In addition, the lipid peroxidation products were measured as MDA and showed to diverge significantly between the two groups (p≤.001). The results also showed that the level of all oxidative stress indices (except for catalase) and inflammatory cytokines were significantly higher in the exposed group than the unexposed. Catalase concentration did not account for any statistically significant difference between the two groups (p=.059). The concentration of mercury in urine samples was the most significant

Table 2. Mercury level in air and urine samples, oxidative stress and proinflammatory cytokines in the exposed vs. unexposed groups

Variables	Median (inter-quartile range)		P-value*
	Exposed group (n=84)	Unexposed group (n=95)	
Air Hg ()	18.49 (13.75)	-	-
Urine Hg (μg L^{-1})	15.44 (19.85)	4.62 (3.64)	<0.001
Malondialdehyde (μmol L^{-1})	6.65 (4.88)	2.41 (3.06)	<0.001
Superoxide Dismutase (U L^{-1})	312.97 (244.67)	242.82 (144.35)	0.004
Catalase (U L^{-1})	1.16 (1.68)	1.31 (0.32)	0.059
Interleukin 6 (pg mL^{-1})	1.79 (1.41)	0.51 (0.62)	<0.001
Tumor Necrosis Factor α (pg mL^{-1})	8.13 (7.88)	4.77 (3.89)	<0.001

* Mann Whitney U

Table 3. Predictors of oxidative stress and proinflammatory cytokines in the exposed group

Variable		β	95% CI		P-value
Independent	**Dependent**		**Lower**	**Upper**	
MDA	Age Group (>30 vs 30-40)	1.33	0.066	2.61	0.039
	Urine Hg	0.123	0.069	0.178	<0.001
SOD	BMI Group (Underweight vs Normal)	182.22	54.21	310.23	0.006
	Urine Hg	4.22	1.51	6.92	0.003
Cat	Shift Work (No vs Yes)	-1.39	-2.72	-0.057	0.041
	Urine Hg	0.094	0.041	0.146	0.001
IL-6	Urine Hg	0.028	0.12	0.45	0.001
TNF-α	Urine Hg	0.145	0.056	0.233	0.002

predictor of oxidative stress and proinflammatory cytokines based on a multiple backward linear regression. As the results showed, an increase for 1 mg of mercury in the urine was followed by significant changes in the oxidative stress and proinflammatory cytokines. The regression analysis results (Table 3) show that a 1 mg L^{-1} of increase in urine mercury was followed by about a 12% of the increase in MDA level. Also, any 1 mg of increase in urine mercury showed to be followed by a four-fold increase in SOD. Similarly, any 1 mg of increase in urine mercury was found to predict a 14% of the increase in TNF-a. However, the same amount of increase in mercury showed to a predict 9% and 2% of increase in CAT and IL-6, respectively. These were the lowest levels of predicted variance in the present findings.

3.3. Discussion

The overall findings showed that among the chloralkal unit workers, the levels of oxidative stress and proinflammatory cytokines were higher in the exposed group than the control. All the variables except for the catalase were significantly different between the two groups (Fig.5). These findings point to the increase in oxidative stress and body immune responses in this population. The maximum permitted level of mercury in blood and urine is 3 and 4-5 mg L^{-1}, respectively [30]. The present findings, however, showed that the mercury concentration was more than these limits in the sampled population. Similarly, in their research, Neghab et al. found a higher (than the standard level) concentration of mercury in the exposed group, and they found a statistically significant difference between the two groups with this regard. This study not only measured and compared the mercury concentration but also the oxidative stress and proinflammatory cytokines [22]. Different mechanisms have been suggested to explain the biological toxicity of mercury, such as the oxidative stress and inflammatory mechanisms. Yet, the precise mechanism of producing ROS and inflammatory mediators by mercury is unknown. Oxidative stress is a primary lead-induced mechanism. The present findings attested to the capability of mercury to generate free oxidative species through increasing the level of LPO. MDA is a main product of non-oxidized unsaturated fatty acids. An increase in MDA content is a key indicator of LPO [31]. Mahboub et al. investigated this issue and showed that HgCl2 manages to increase the MDA level in tissues [32]. In this research, the MDA level was significantly different between the exposed and non-exposed groups. Moreover, the urine mercury level was a strong predictor of the MDA level. In another study, Hasan et al. showed that the MDA level was significantly increased along with the increased mercury concentration [33].

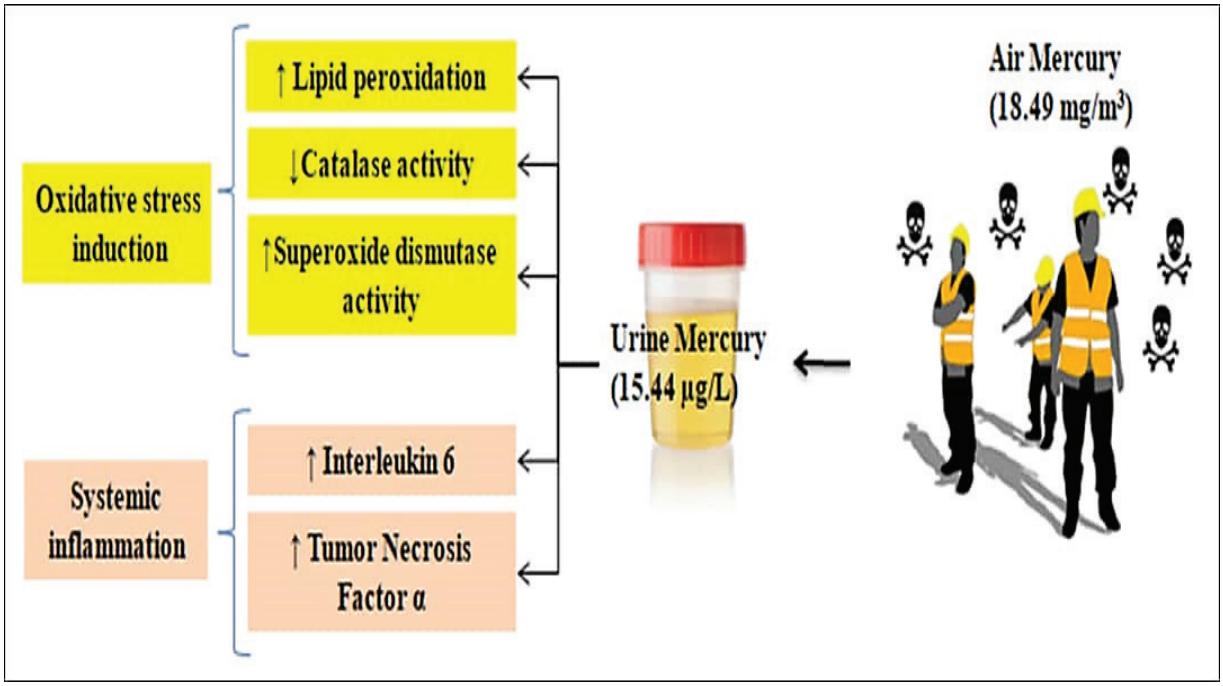

Fig.5. Flow diagram effects of mercury exposure on oxidative stress and proinflammatory cytokines

Lipid peroxidation is a chemical mechanism that can disrupt the structure and functioning of biological membranes by the free radicals attacking the lipids. The higher peroxidation rate of serum lipids in exposed workers to mercury is indicative of serious oxidative damages [31]. As a metallic compound, mercury reacts to thiols (SH-) and leads to chelate antioxidant proteins such as glutathione. Finally, reducing the antioxidant capacity of the tissues induces oxidative stress [34] the overproduction of ROS by mercury indicates its capability of making mitochondrial changes by blocking the mitochondrial permeability transition pore [35]. The Overabundance of ROS induced by mercury correlates to the incidence of neurodegenerative diseases such as amyotrophic lateral sclerosis, Parkinson's, or Alzheimer's. The recent research showed that within the past decades, the toxic effects of mercury have been correlated, probably, with the central nervous system [36]. Several studies, similar to the present research, showed that exposure to lower concentrations of mercury, firstly, induces oxidative stress and increases the number of free oxygen radicals compared to the existing serum antioxidant mechanisms [6, 37]. An increased number of free oxygen species can be one reason for the analysis of proteins, lipid peroxidation, and cellular damage or mortality [23]. As also raised by Neghab et al., mercury can damage cellular membrane through lipid peroxidation and finally disturbs the balance of synthesis and, consequently, leads to enzymatic protein deterioration [22]. The present research also revealed that the level of inflammatory mediators, (e.g. IL-6 and TNF alpha) was significantly higher in the exposed group of workers than the non-exposed. This finding is consistent with Gardner et al.'s epidemiologic investigation of the mercury level among 94 workers exposed to mercury at work. Investigating the level of proinflammatory cytokines (e.g. TNF-alpha and IL-6) in the mercury exposed workers in gold mines showed that the urine mercury level correlates with an increase in IL-1B, TNF-a, and IFN-Y in the gold miner population. Exposure to mercury in these mines can disrupt the immune body and inflammatory systems [40]. Furthermore, the research findings of animal models showed a significant correlation between the mercury level and proinflammatory cytokines such as TNF-a, IL-6, and IFN-y [37-39].

Several empirical and epidemiologic studies showed that mercury level was correlated with different cytokine profiles. Results of the experimental study of PBMC Gardner et al. showed that in the presence of LPS, the antigenic stimulus of non-organic mercury can increase the propagation of proinflammatory cytokines IL-1B and TNF-a. Simultaneously, it reduces the propagation of anti-inflammatory cytokines, IL-1Ra, and IL-10 [40]. Yet, in another study, Monastero et al. aimed to explore the correlation between exposure to a low mercury concentration, immunologic indices, and several cytokines such as TNF-a, IL-10, IL-4, IL-1B, IL-1ra, IFN-y, and IL-17. Results showed that the serum mercury level and the antinuclear antibody (ANA) or cytokine did not correlate in seafood consumers in the U.S. The Association between exposure to low concentrations of mercury and immunologic indices is unknown. Monastero et al. found a high mercury concentration in urine and blood samples of subjects exposed to a low level of mercury. However, in this research, the concentration of mercury in workers' blood and urine exceeded the recommended level [41, 42].

4. Conclusion

The present findings revealed that workers exposed to mercury have significantly more oxidative and inflammatory mediator damages. These observations highlight the essentiality of preventive measures at the workplace and checking the state of pollutants at work. Many studies confirmed that an increase in oxidative stress and inflammatory factors is followed by a higher risk of affliction with other diseases. The mercury in urine samples was determined based on CuNPs@CNT-COOH adsorbent by the MSPE procedure coupled to CV AAS. The absorption capacity of CuNPs@CNT-COOH for mercury was achieved at 167.5 mg g^{-1}. Also, the mercury in the air was obtained by the NIOSH method. The recovery and RSD for mercury extraction in urine were more than 96% and 1.65%, respectively.

5. Conflict of Interest

The authors have declared no conflict of interest.

6. Acknowledgment

The work supported by the Kerman University of Medical Sciences is based on a number of projects PN: 401000242, for mercury determination in air and human urine samples by supervisors. The ethical code obtained by Kerman University of Medical Sciences (E.C.:IR.KMU.REC. 1400.144).

7. References

[1] T. Mihaiescu, R. Mihaiescu, A. Odagiu, Environmental issues within the Chlor-alkali manufacturing industry-mercury cell process, Bull. Univ. Agric. Sci. Vet. Med., 69 (2012) 168-176. https://doi.org/10.15835/buasvmcn-agr:8746

[2] D. Soleymani-ghoozhdi, R. Parvari, Y. Jahani, M. Mehdipour-Raboury, A. Faghihi-Zarandi, A new analytical method based on Co-Mo nanoparticles supported by carbon nanotubes for removal of mercury vapor from the air by the amalgamation of solid-phase air removal, Anal. Methods Environ. Chem. J., 50.1 (2022) 22-35. https://doi.org/10.24200/amecj.v5.i01.163

[3] F. Golbabai, A. Ebrahimi, H. Shirkhanloo, M.R. Baneshi, A. Faghihi Zarandi, M.G. Kian, Performance comparison survey of multi-walled and single-walled carbon nanotubes for adsorption and desorption of Mercury Vapors in the air, Iran. Occup. Health, 10 (2013) 20-31. http://ioh.iums.ac.ir/article-1-813-en.html

[4] G.A. Wiggers, F.M. Peçanha, A. M. Briones, J.V. Perez-Giron, M. Miguel, D.V. Vassallo, Low mercury concentrations cause oxidative stress and endothelial dysfunction in conductance and resistance arteries, Am. J. Physiol. Heart Circ. Physiol., 295 (2008) H1033-H21043. https://doi.org/10.1152/ajpheart.00430.2008

[5] I. Garcia-Herrero, M. Margallo, R. Onandía, R. Aldaco, A. Irabien, Environmental challenges of the chlor-alkali production: Seeking answers from a life cycle approach, Sci. Total Environ., 580 (2017)147-157. https://doi.org/10.1016/j.scitotenv.2016.10.202

[6] G. Bjørklund, M. Dadar, J. Mutter, J. Aaseth, The toxicology of mercury, current research and emerging trends, Environ. Res., 159 (2017) 545-554. https://doi.org/10.1016/j.envres.2017.08.051

[7] R.M. Gardner, J.F. Nyland, I. A. Silva, A.M. Ventura, J.M. de Souza, E.K. Silbergeld, Mercury exposure, serum antinuclear/antinucleolar antibodies, and serum cytokine levels in mining populations in Amazonian Brazil, a cross-sectional study, Environ. Res., 110 (2010) 345-354. https://doi.org/10.1016/j.envres.2010.02.001_

[8] D. Winalski, S. Mayson, J. Savitz, Poison plants, chlorine factories are a major global source of mercury, Oceana publisher, 2005. https://oceana.org/wp-content/uploads/sites/18/poisonplants2FINAL.pdf

[9] J.F. Risher, H.E. Murray, G.R. Prince, Organic mercury compounds, human exposure and its relevance to public health, Toxicol. Ind. Health, 18 (2002) 109-160. https://doi.org/10.1191/0748233702th138oa

[10] J.F. Risher, R.A. Nickle, S.N. Amler, Elemental mercury poisoning in occupational and residential settings, Int. J. Hyg. Environ. Health, 206 (2003) 371-379. https://doi.org/10.1078/1438-4639-00233_

[11] E.G. Pacyna, J. Pacyna, K. Sundseth, J. Munthe, K. Kindbom, S. Wilson, Global emission of mercury to the atmosphere from anthropogenic sources in 2005 and projections to 2020, Atm. Environ., 44 (2010) 2487-2499. https://doi.org/10.1016/j.atmosenv.2009.06.009

[12] S.Y. Do, C.G. Lee, J.Y. Kim, Y.H. Moon, M.S. Kim, I.H. Bae, Cases of acute mercury poisoning by mercury vapor exposure during the demolition of a fluorescent lamp factory, Annals Occup. Environ. Med., 29 (2017) 1-8. https://doi.org/10.1186/s40557-017-0184-x

[13] L.C. Curlin, T.V. Bommaraju, C. B. Hansson, Alkali and chlorine products, chlorine and sodium hydroxide, Kirk-Othmer encyclopedia of chemical technology, 2000. https://doi.org/10.1002/0471238961.0308121503211812.a01

[14] J. Crook, A. Mousavi, The chlor-alkali process, A review of history and pollution, Environ. Forensics, 17 (2016) 211-217. https://doi.org/10.1080/15275922.2016.1177755

[15] D.G. Ellingsen, R. Bast-Pettersen, J. Efskind, Y. Thomassen, Neuropsychological effects of low mercury vapor exposure in chloralkali workers, Neurotoxicol., 22 (2001) 249-258. https://doi.org/10.1590/S0100-879X2007000300019

[16] S. Hirano, Evaluation of pulmonary toxicity of heavy metal compounds, Japan. J. Hyg., 50 (1996) 1013-1025. https://doi.org/doi:10.3233/WOR-203194.

[17] T. Takahashi, M. Fujimura, M. Koyama, M. Kanazawa, F. Usuki, M. Nishizawa, Methylmercury causes blood-brain barrier damage in rats via upregulation of vascular endothelial growth factor expression, PLOS One, 12 (2017) e0170623. https://doi.org/10.1371/journal.pone.0170623

[18] C. Bottino, M. Vázquez, V. Devesa, U. Laforenza, Impaired aquaporins expression in the gastrointestinal tract of rat after mercury exposure, J. Appl. Toxicol., 36 (2016) 113-120. https://doi.org/10.1002/jat.3151

[19] Y.S. Lin, G. Ginsberg, J.W. Lin, B. Sonawane, Mercury exposure and omega-3 fatty acid intake in relation to renal function in the US population, Int. J. Hyg. Environ. Health, 214 (2014) 465-472. https://doi.org/10.1016/j.ijheh.2013.09.004

[20] J. Anglen, S.E. Gruninger, H.N. Chou, J. Weuve, M.E. Turyk, S. Freels, Occupational mercury exposure in association with prevalence of multiple sclerosis and tremor among US dentists, J. Am. Dental Assoc., 146 (2015) 659-668. https://doi.org/10.1016/j.adaj.2015.05.016

[21] R. Zefferino, C. Piccoli, N. Ricciardi, R. Scrima, N. Capitanio, Possible mechanisms of mercury toxicity and cancer promotion, Involvement of gap junction intercellular communications

and inflammatory cytokines, Oxid. Med. Cell. Longev., 2017 (2017) 7028583. https://doi.org/10.1155/2017/7028583

[22] M. Neghab, M. Amin Norouzi, A. Choobineh, M. Reza Kardaniyan, J. Hassan Zadeh, Health effects associated with long-term occupational exposure of employees of a chlor-alkali plant to mercury, Int. J. Occup. Safe. Ergonomics, 18 (2012) 97-106. https://doi.org/ 10.1080/10803548.2012.11076920

[23] Z. Ahmadi, A. Moradabadi, D. Abdollahdokht, M. Mehrabani, M.H. Nematollahi, Association of environmental exposure with hematological and oxidative stress alteration in gasoline station attendants, Environ. Sci. Pollut. Res., 26 (2019) 20411-20417. Environ. Sci. https://doi.org/10.1007/s11356-019-05412-7_

[24] D. Soleymani, S. Zargari, A. Faghihi-Zarandi, Separation and determination of mercury from nail and hair in petrochemical workers based on silver carbon nanotubes by microwave-assisted headspace sorbent trap, Anal. Methods Environ. Chem. J., 3 (2020) 21-33. https://doi.org/10.24200/amecj.v3.i02.99

[25] B. Elsebai, M.E. Ghica, M.N. Abbas, C.M. Brett, Catalase based hydrogen peroxide biosensor for mercury determination by inhibition measurements, J. Hazard. Mater., 340 (2017) 344-350. https://doi.org/10.1016/j.jhazmat.2017.07.021

[26] O. Ighodaro, O. Akinloye, First line defence antioxidants-superoxide dismutase (SOD), catalase (CAT) and glutathione peroxidase (GPX): Their fundamental role in the entire antioxidant defence grid, Alexandria J. Med., 54 (2018) 287-293. https://doi.org/10.1016/j.ajme.2017.09.001

[27] B.B. Gump, E. Gabrikova, K. Bendinskas, A.K. Dumas, C.D. Palmer, P.J. Parsons, Low-level mercury in children: associations with sleep duration and cytokines TNF-α and IL-6, Environ. Res., 134 (2014) 228-232. https://doi.org/10.1016/j.envres.2014.07.026

[28] E.E. Kwaansa-Ansah, E.K. Armah, F. Opoku, Assessment of total mercury in hair, urine and fingernails of small–scale gold miners in the Amansie West District, Ghana. J. Health Pollut., 9 (2019)190306. https://doi.org/10.5696/2156-9614-9.21.190306

[29] G.F. Templeton, A two-step approach for transforming continuous variables to normal: implications and recommendations for IS research, Commun. Assoc. Inf. Syst., 28 (2011) 4. https://doi.org/10.17705/1cais.02804

[30] M. Azami, A. Mansouri, M. Khataee, A. Soleymani, K. Sayehmiri, A systematic review and meta-analysis of mercury concentrations in blood, urine, and area air samples among dentists in Iran, J. Maz. Univ. Med. Sci., 27 (2017) 203-216. http://jmums.mazums.ac.ir/article-1-8036-en.html

[31] A.C.B.A. Lopes, M.R. Urbano, A. de Souza-Nogueira, G.H. Oliveira-Paula, A.P. Michelin, H.C. Maria de Fátima, Association of lead, cadmium and mercury with paraoxonase activity and malondialdehyde in a general population in Southern Brazil, Environ. Res., 156 (2017) 674-682. https://doi.org/10.1016/j.envres.2017.04.036

[32] M. Mahboob M, Shireen KF, Atkinson A, Khan AT, Lipid peroxidation and antioxidant enzyme activity in different organs of mice exposed to low level of mercury, J. Environ. Sci. Health, Part B, 36 (2001) 687-697. https://doi.org/10.1081/PFC-100106195

[33] H.F. Al-azzawie, A. Umran, N.H. Hyader, Oxidative stress, antioxidant status and DNA damage in a mercury exposure workers, Br. J. Pharmacol. Toxicol., 4 (2013) 80-88. https://doi.org/10.19026/bjpt.4.5367

[34] M. Jozefczak, T. Remans, J. Vangronsveld, A. Cuypers, Glutathione is a key player in metal-induced oxidative stress defenses, Int. J. Mol. Sci., 13 (2012) 3145-3175. https://doi.org/10.3390/ijms13033145

[35] E.A. Belyaeva, T.V. Sokolova, L.V. Emelyanova, I.O. Zakharova, Mitochondrial electron transport chain in heavy metal-induced neurotoxicity: effects of cadmium, mercury, and copper, Sci. World J., 2012 (2012)136063.

https://doi.org/10.1100/2012/136063
[36] V.L. Cariccio, A. Samà, P. Bramanti, E. Mazzon, Mercury involvement in neuronal damage and in neurodegenerative diseases, Biol. Trace Elem. Res., 187 (2019) 341-356. https://doi.org/10.1007/s12011-018-1380-4
[37] L. Bagenstose, P. Salgame, M. Monestier, Mercury-induced autoimmunity in the absence of IL, Clin. Exp. Immunol., 114 (1998) 9. https://doi.org/10.1046/j.1365-2249.1998.00704.x
[38] S.H. Kim, V.J. Johnson, R.P. Sharma, Mercury inhibits nitric oxide production but activates proinflammatory cytokine expression in murine macrophage: differential modulation of NF-κB and p38 MAPK signaling pathways, Nitric Oxide, 7 (2002) 67-74. https://doi.org/10.1016/s1089-8603(02)00008-3_
[39] J.F. Nyland, D. Fairweather, D.L. Shirley, S.E. Davis, N.R. Rose, E.K. Silbergeld, Low-dose inorganic mercury increases severity and frequency of chronic coxsackievirus-induced autoimmune myocarditis in mice, Toxicol. Sci., 125 (2012) 134-143. https://doi.org/10.1093/toxsci/kfr264
[40] R.M. Gardner, J.F. Nyland, S.L. Evans, S.B. Wang, K.M. Doyle, C.M. Crainiceanu, Mercury induces an unopposed inflammatory response in human peripheral blood mononuclear cells in vitro, Environ. Health Perspect., 117 (2009)1932-1938. https://doi.org/10.1289/ehp.0900855
[41] R.N. Monastero, R. Karimi, J.F. Nyland, J. Harrington, K. Levine, J.R. Meliker, Mercury exposure, serum antinuclear antibodies, and serum cytokine levels in the long Island study of seafood consumption, A cross-sectional study in NY, USA, Environ. Res., 156 (2017) 334-340. https://doi.org/10.1016/j.envres.2017.03.037
[42] F. Golbabaei, A. Ebrahimi, Single-walled carbon nanotubes (SWCNTs), as a novel sorbent for determination of mercury in air, Global J. Health Sci., 8 (2016) 273. https://doi.org/10.5539/gjhs.v8n7p273

Anal. Methods Environ. Chem. J. 5 (2) (2022) 90-104

AMECJ

Research Article, Issue 2
Analytical Methods in Environmental Chemistry Journal
Journal home page: www.amecj.com/ir

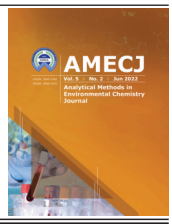

Design a continuous microfluidic flow cell for turbidimetric-flow injection technology: A new approach for routine analysis of active pharmaceutical formulations

Aktham N. Jasim [a, *], Nagham S. Turkey [b], and Hussein Fares Abd-Alrazack [b]
[a] *University of Mustansiriyah, College of Basic Education, Baghdad, Iraq*
[b] *University of Baghdad, College of Science, Department of Chemistry, Baghdad, Al-Jadriya, Iraq*

ARTICLE INFO:
Received 8 Feb 2022
Revised form 14 Apr 2022
Accepted 19 May 2022
Available online 29 Jun 2022

Keywords:
Flow injection analysis,
Microfluidic flow cell,
Promethazine,
Turbidity,
Pharmaceuticals,
Quality control analysis

ABSTRACT
In this study, a new flow injection analysis (FIA) based on a microfluidic flow cell (MFC) with a sample capacity of 40 µL is described. A Tungsten lamp directs light from a typical 2100P Portable Turbidimeter apparatus into a quartz flow cell through a round sidewall aperture of 2.0 mm and emerges through the identical aperture on the opposite side of the flow cell, where a photodiode array (light detector) detects the passing light. When compared to a traditional cuvette (25 mm x 60 mm round) with the same nominal route length, this technique improves sensitivity by around 4.0. This improvement is due to the use of a short, narrow internal diameter microfluid as the flow cell, which reduces physical dispersion. The designed flow cell has been evaluated by developing a turbidimetric method for the detection of promethazine in pure form or pharmaceutical dosages. The developed method is based on forming of a yellowish ion-pair association complex due to the reaction of promethazine and sodium tetraphenylborate (STPB) in an acidic medium. At the flow optimum conditions, the calibration curve (CC) and the limit of detection (LOD) for promethazine were obtained 0.5-90 µg mL^{-1} and 0.35 µg mL^{-1}. respectively (R^2 = 0.9955). The intra-day and inter-day precisions (RSD%) of the FIA-MFC method for measuring promethazine at concentrations of 20, and 50 µg mL^{-1} were achieved (2.0 and 1.6) and (0.8 and 1.2), respectively.

1. Introduction

Promethazine, also known as (2RS)-N, N-dimethyl-(10H-phenothiazine-10-yl) propan-2-amine, is an antihistaminic having analgesic, anticholinergic, antipsychotic and sedative effects that are utilized to treat vomiting, nausea and motion sickness in children [1]. In the wide group of phenothiazine derivatives, promethazine hydrochloride is a well-known chemical. It's a crystalline powder that's white or slightly yellowish in color, extremely soluble in water, and easily soluble in methylene chloride and alcohol. Morphine sulfate, benzylpenicillin salts, hydrocortisone sodium succinate, aminophylline, alkalis, barbiturates, heparin, and various contrast solutions are incompatible with promethazine. Tachycardia, bradycardia, transient small elevations in blood pressure, and infrequent hypotension are all side effects. Extrapyramidal symptoms have been described at high doses, such as jaundice and thrombocytopenic purpura. Excessive sedation, impaired dizziness, motor function, tachycardia, extrapyramidal symptoms, disorientation, blurred

*Corresponding Author: Aktham N. Jasim
Email: akthamjasim7@gmail.com
https://doi.org/10.24200/amecj.v5.i02.184

vision, palpitations, stomach distress, headache and constipation are all adverse effects of promethazine [2]. As a result, according to the substance act [3], promethazine is classified as a dangerous drug and is not sold over the counter. The purposeful, non-therapeutic use of a drug, even once, for its favorable psychological benefits is known as prescription drug misuse. Promethazine recreational usage among college students and high school has become a severe concern, as documented in Hong Kong, Nepal, the United States, and India [4]. Antihistamine medicines like promethazine are often abused by mixing with energy drinks, candies, soft drinks, and alcoholic beverages in cocktails [5-7]. Promethazine detection has been reported using a variety of analytical approaches. Spectrophotometry [2], gas chromatography [8], HPLC [9], electrochemical sensing [10], and capillary electrophoresis [11] are some of the techniques used. All of these approaches, however, have disadvantages for routine promethazine analysis in pharmaceutical formulations samples. Specific reagents such as 12-tungstophosphoric acid (TP) [12], potassium persulfate [13] and cerium (IV) [14] are what is the colorimetric detection based on. However, spectrophotometry instrument is not ideal for field use or on-site detection, and this method is mainly applied to samples solutions. Traditional separation procedures have significant drawbacks when it comes to separating and identifying individual components in complicated mixtures. They may necessitate time-consuming sample preparation, expensive equipment, and well-trained analysts [15, 16]. The oxidation of Promethazine can be conducted in an electrochemical flow cell rather than a chemical reaction, and the amperometric signal can be utilized to detect it. Interference is likely to be occured when there are many electroactive compounds in the sample, depending on their oxidation potential [17]. Voltammetric detection is more difficult, although it can be used when the peaks do not overlap much [18]. Because of the presence of linked pharmaceutical substances or dyes, neither approach is completely suitable for determining Promethazine in a variety of pharmaceutical formulations. In recent years, a growing number of Flow Injection Analysis (FIA) techniques for the determination of Promethazine have been described [10, 19-22]. Almost all of them investigate the practicality of in-line oxidation of the analyte by an immobilized oxidant or confluent, accompanied by spectrophotometric detection of the colored radical, stabilized under very acidic conditions, while others look into the fluorescence effect. The need for acid-resistant tubing for the flow manifold system, as well as the danger of interference from colored excipients, which can vary from one commercial formulation to the next and may absorb at the wavelength chosen for the analyte, are some of the drawbacks of spectrophotometric procedures. Although spectrometry has been used to study electrostatic interactions in phenothiazines, it has also been used to investigate analyte detection procedures that involve colored intermediates or products. However, its application for routine analytical purposes is scarce, perhaps because the cells are difficult to construct or operate, or because they were not designed for FIA [23, 24]. The turbidimetric-flow injection technique is a quicker alternative to spectrophotometric methods for evaluating active pharmaceutical ingredients, as it can produce results in as little as one minute. Moreover, the turbidimetric method has the advantages of low consumption of samples and reagents, high accuracy, simple operation and quick analysis. Therefore, several turbidimetric-FIA procedures have been developed for the determination of active pharmaceutical ingredients in different matrices [25-29]. To overcome the limitations associated with the spectrophotometric-flow injection technique, an inexpensive, very simple and long-optical-path turbidimetric-flow cell is designed and evaluated. This quartz cell is resistant to high temperatures and corrosion. The flow cell is cylindrical, 50 mm in length, and features 2 mm inside and 4 mm outer diameter input and output holes. The developed cell is compatible with an exit manifold system for interfacing to tubing and it requires only a simple

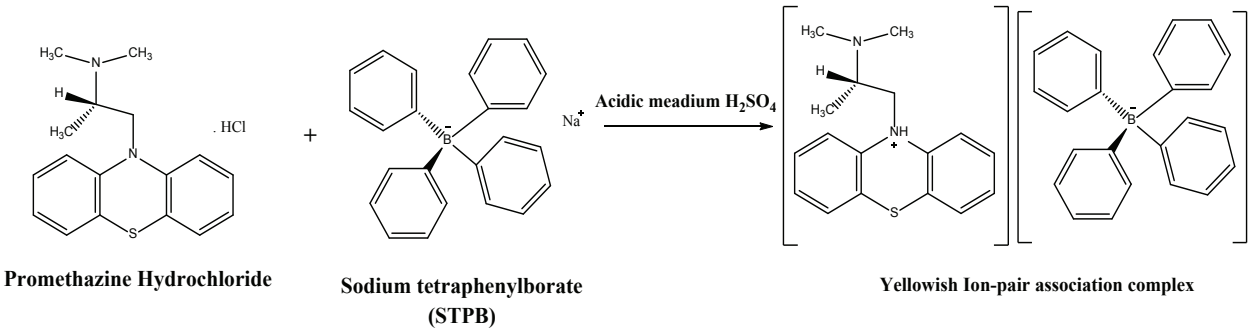

Fig. 1. The proposed mechanism of the reaction between the promethazine hydrochloride and the STPB reagent

benchtop apparatus for detecting and measuring the samples or any standard materials that pass through it. The designed flow cell was successfully used to develop and validate an analytical method for the determination of Promethazine in pure and pharmaceutical formulations to evaluate the flow cell. Also, many techniques such as LLME and SPE was used for sample preparation in human and environment.

The developed method is based on forming of a yellowish ion-pair association complex due to the reaction of promethazine and sodium tetraphenylborate (STPB) in an acidic medium, the proposed mechanism for the reaction is shown in Figure 1. The simplicity, flexibility and effectiveness of this new turbidimetric-flow cell approach opened up new avenues for investigating the current approach in analytical analysis applications, as shown here in the determination of promethazine hydrochloride. It's perfect for routine analysis of promethazine hydrochloride in pure form or dosage forms containing active substances, inert ingredients, and dyes.

2. Experiment

2.1. Reagents and solutions

All solutions and analytical grade reagents were prepared with double-distilled water. Dilution of concentrated sulfuric acid acid produced an appropriate concentration of a sulfuric acid solution (0.2 mol L^{-1}). Working solutions were prepared daily by diluting suitable aliquots of promethazine hydrochloride ($C_{17}H_{20}N_2S$, HCl, 320.9 g mol^{-1}, SDI) into double distilled water. The purity of the promethazine was determined to be 99.7 % using an official method [30]. A stock solution of Sodium tetraphenylborate (STPB), $C_{24}H_{20}BNa$, 342.22 g ml^{-1}, BDH 50 µg mL^{-1} by dissolving 4.2777g per 250 mL distilled water. Sulphuric acid, hydrochloric acid, nitric acid, acetic acid, ammonium chloride, sodium nitrate, potassium bromide and sodium chloride were purchased from Sigma Aldrich.

2.2. Preparation of standard and sample solutions

0.049 mg of promethazine was weighed and diluted in 250 mL of double-distilled water to produce the standard stock solution (200 µg mL^{-1}). After that, the stock solution was kept in an amber container for the subsequent research. Dilutions of appropriate quantities of stock solution with double-distilled water were used to create standard solution ranges. The stability of promethazine was monitored frequently using UV spectrophotometry to see if there was any decomposition during the development of the method, and the results showed that promethazine was stable for 20 days. Two distinct commercial companies of 25 mg were used in this study. The pharmaceutical preparations tested were Histazine tablets (25 mg per tablet) by United pharmaceutical Jordan and Phenergan tablets (25 mg per tablet) by GLOBAL manufacturer Sanofi United pharmaceutical UK, these tablets are available in most countries. Twenty tablets were powdered and dissolved in double-distilled water after being precisely weighed. The sample solution

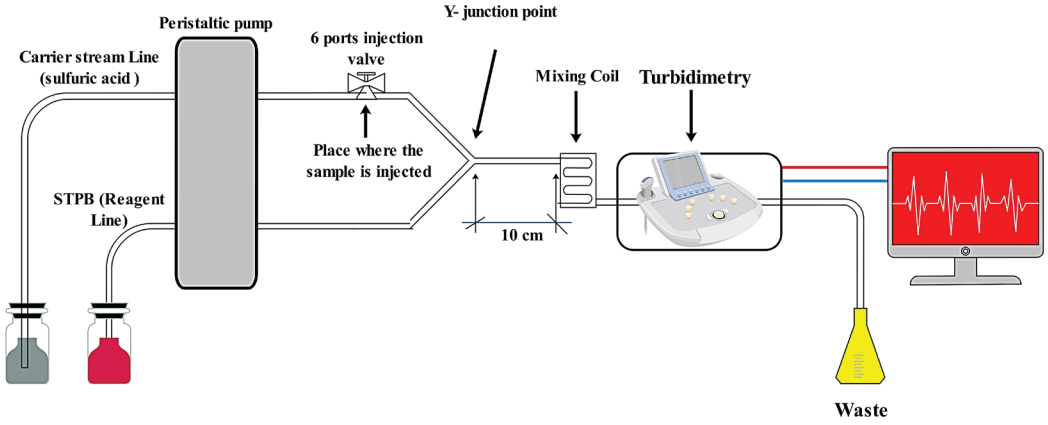

Fig. 2. The whole manifold system used to determine the promethazine hydrochloride

was then filtered after being shaken for 20 minutes. The various concentrations of the injected sample solutions were obtained by diluting the prepared stock solution appropriately. For each commercial tablet type, the method has been repeated.

2.3. Apparatus

All the turbidimetric measurements were conducted using a conventional 2100P Portable Turbidimeter (USEPA 180.1, EU), modified in the authors' laboratory and interfaced to the computer where all data and measurements are recorded and stored. The Portable turbidimeter is also interfaced with the PC controlled by software supplied by the same company (HACH). A manual rotating injector (6 ports) and an Ismatec 2 channels (ISM796, supplied with Tygon pump tubing, Switzerland) peristaltic pump were employed in the FIA experiments. All of the studies were carried out at room temperature. Figure 2 illustrates the manifold used in the promethazine hydrochloride assay. Teflon (IDEX corporation, USA) tubes were used to connect all the manifold system parts.

A flow cell was designed and used for all of the turbidimetric experiments; this quartz cell is resistant to high temperatures and corrosion. The flow cell is 50 mm long and has input and outlet ports with an interior diameter of 2 mm and an outer diameter of 4 mm. It is through this flow cell that the samples and any standards are passed for detection and measurement by the turbidimetric detector as shown in Figure 3.

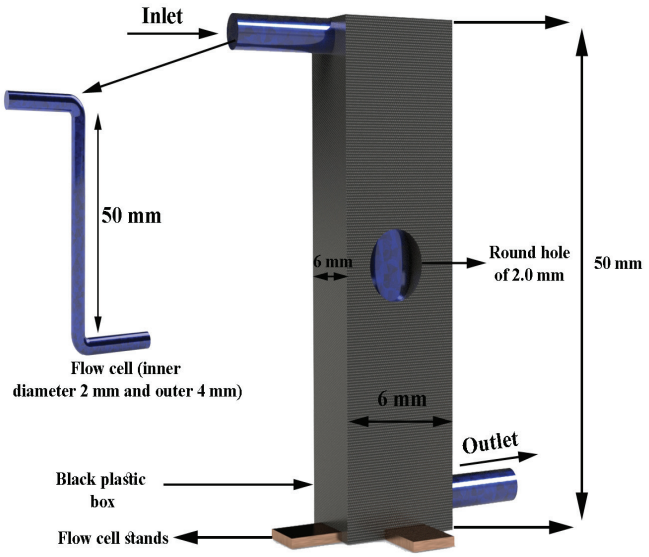

Fig. 3. The complete description of the developed flow cell

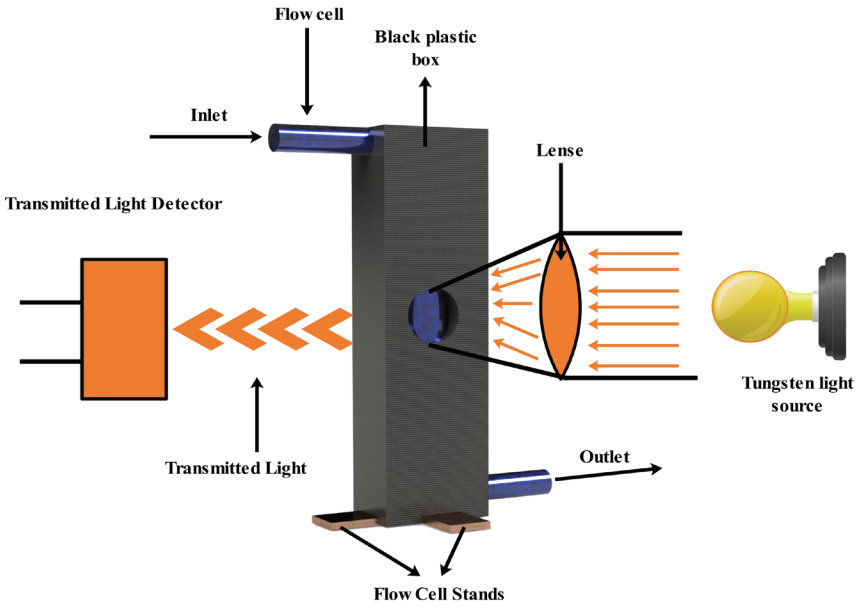

Fig. 4. The front view of the design flow cell assembly. The tungsten light source is mounted directly on the round hole of the flow cell and the radiation of the light source is concentrated on the flow cell hole using a lens. In contrast, the flow cell sits on the floor stage mounted vertically on the platform using three metal stands. The transmitted light detector is introduced on the opposite side of the flow cell.

As illustrated in Figure 4, the flow cell is inserted vertically into a black plastic box with a diameter of (50 mm (L) 6 mm (W) 6 mm (thickness)). This plastic box can occupy the entire flow cell. The sidewall of the black box contains a round hole of 2.0 mm which is suitable for the source of light that radiates from the turbidity device, the light source was fully mounted and constructed. While the opposites side of the box is supplied by the light detector (photodiode array) that is used to measure the passing light through the flow cell. A silicone rubber tubing sleeve with the necessary inner diameter was used to connect the constructed flow cell to the FIA manifold system, and the entire cell assembly was placed on a robust metal base plate and encased in a black plastic box.

2.4. General Procedure

Figure 2 illustrated the manifold flow apparatus that was used to determine promethazine in pharmaceutical preparations. This system consisted of two lines: the carrier streamline (20 Mmol L^{-1}, sulfuric acid) and the reagent line solutions (STPB 30 µg mL^{-1}). Both lines were accelerated using a two-channel peristaltic at flow rates of 2.0 ml min^{-1} for the acid line and reagent line, respectively. The injection coil of the injection valve is first loaded with (100 µL) of aliquot volume from a sample solution that contains promethazine. The injection valve's position is then adjusted from loading to the injection mode. The sample solution is injected into the acidic streamline and merged with the reagent at the Y junction point (one of the manifold system parts, made from Methyl methacrylate) to generate the yellow complex product, which is then delivered by the stream to the detector system for analysis. The formed complex's turbidity measurements will be recorded and stored continually by PC indicated by (peak). The instrument is calibrated to be set to a signal of zero for the blank signal each time it is used since the blank (STPB) has a signal that is almost zero. The calibration graph used to calculate promethazine is then shown with the corresponding peaks. The created product might adsorb on the

wall of the quartz flow cell since it is turbid, which will result in inaccurate findings being obtained. To address this issue, a washing buffer solution containing 7 g ammonium chloride, 57 mL 25 % (m/m) ammonia, and 40 g EDTA (disodium salt) was made by dissolving the various ingredients in 500 mL distilled water and diluting to 1.0 L [31]. After each sample injection, 10.0 mL of washing buffer solution is utilized to ensure that any adsorption particles on the flow cell's surface are removed.

3. Results and Discussion

The turbidimetric and spectrophotometric responses were measured concurrently in all of the experiments. The operating conditions were extensively studied and optimized, including the STBP concentrations, flow rate, injected-sample volume, carrier stream, mixing coil and analyte concentration. Studies were carried out by changing one variable at a time while keeping the others unchanged. When measuring promethazine hydrochloride in Histazine and Phenergan tablets using analytical curves or the method of standard additions, the results obtained were sufficient and reliable enough to propose the methodology as an alternative to the British Pharmacopoeia's official methods with confidence [30].

3.1. Investigation of FIA parameters

The quantitative determination of compounds using a flow system necessitates the optimization of several physical and chemical parameters, including the type of carrier stream, reagent concentration, injected-sample volume, flow rate, and mixing coil. All of these trials were optimized under flow conditions. First, a series of STPB concentrations ranging from 0.5 to 50 µg mL^{-1} were generated while other parameters such as sample volume (50 µL), flow rate (1.0 mL min^{-1}), and open valve mode were held constant. The injection valve in use has two settings: closed and open. Closed valve mode implies rotating the valve from the injection to the loaded position after some time, whereas open valve mode means leaving the valve in the injection position and allowing the carrier stream to pass through it to transport the sample to the detector. The goal of these modes is to figure out how long it takes to transfer all of the sample segments using the carrier stream. The results showed a considerable rise in the response profile up to 30.0 µg mL^{-1}, beyond which there was no increase in the detector signal. As a result, the optimal concentration of 30.0 µg mL^{-1} was used in Figure 5.

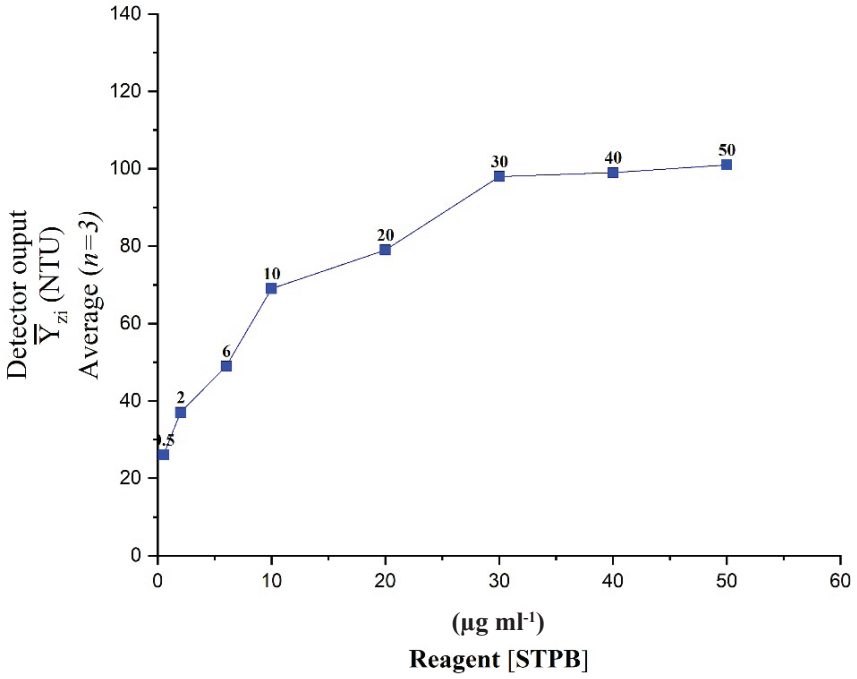

Fig.5. The effect of STPB Conc. [µg ml^{-1}] on the determination of promethazine using experimental conditions: 100 µL of promethazine (50 µg mL^{-1}), flow rate 1.0 mL min^{-1} and open valve mode

In most flow systems, double-distilled water serves as the carrier stream; however,using other solutions instead of water may enhance the detector signal; as a consequence, a series of 25.0 mmol L^{-1} solutions (H_2SO_4, HNO_3, HCl, CH_3COOH, NH_4Cl, $NaNO_2$, KBr, NaCl, KNO_3) were used as a carrier stream in place of water. These solutions were chosen at random, and some of them have an anion and cation activity, while the remainder is acid and basic medium. The major reason to use these alternatives rather than water is that the interaction between the sample solution and the organic reagent occurs in an aqueous medium (distilled water), resulting in the formation of a new colorful product. As a result, it was necessary to determine whether the new product is steady in the aqueous solution or if it will be dissolvable and some of it will solubilize in that solution, as we are always searching for a product with chemical stability in the flow system. The highest detector signals were obtained using diluted sulfuric acid as the carrier stream across all of these solutions. This result can indeed be attributed to the fact that the formed product, which is developed as a result of the reaction between both the organic reagent (STPB) and the promethazine, is more stable in sulfuric acid solution than in distilled water, and this is connected to the fact that sulfuric acid inhibits promethazine precipitation during promethazine dissociation. As a result, sulfuric acid was chosen as the carrier stream (Fig. 6).

After agreeing to employ sulfuric acid instead of water as the carrier stream, the concentration of it had to be adjusted, therefore varied concentrations ranging from 10 to 50 mmol L^{-1} were prepared and then used under previous flow conditions. Because the results revealed that 20 mmol L^{-1} sulfuric acid was adequate to achieve a strong signal, 20 mmol L^{-1} was selected in subsequent experiments (Fig.7). Sulfuric acid 20 mmol L^{-1}, promethazine 30 µg mL^{-1}, 1.0 mL min^{-1} flow rates are the flow conditions that are applied to conduct the injected-sample volume experiment; therefore, the influence of the injected-sample volume was studied, and a series of sample volumes ranging from 30-150 µL were injected into the manifold system that utilizes a 6-port injection valve. The acquired data revealed that the response profile increased up to 100 µL, but that applying more than that volume resulted in a lowering in the response profile owing to precipitation of the generated product in the flow cell and decreased incident light attenuation. As a result, as shown in

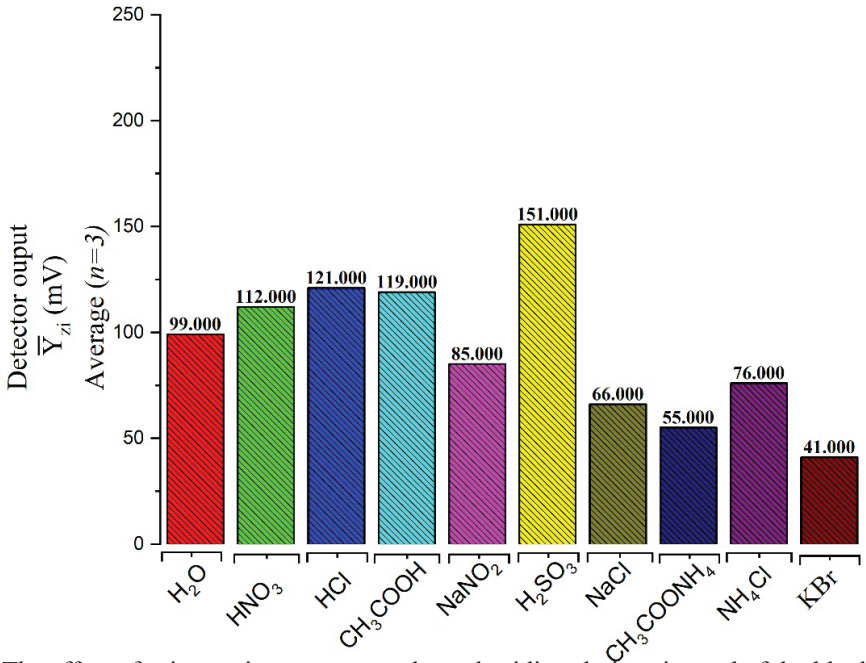

Fig. 6. The effect of using various aqueous salts and acidic solutions instead of double distilled water as a carrier stream on the detector signal under using the same initial flow conditions

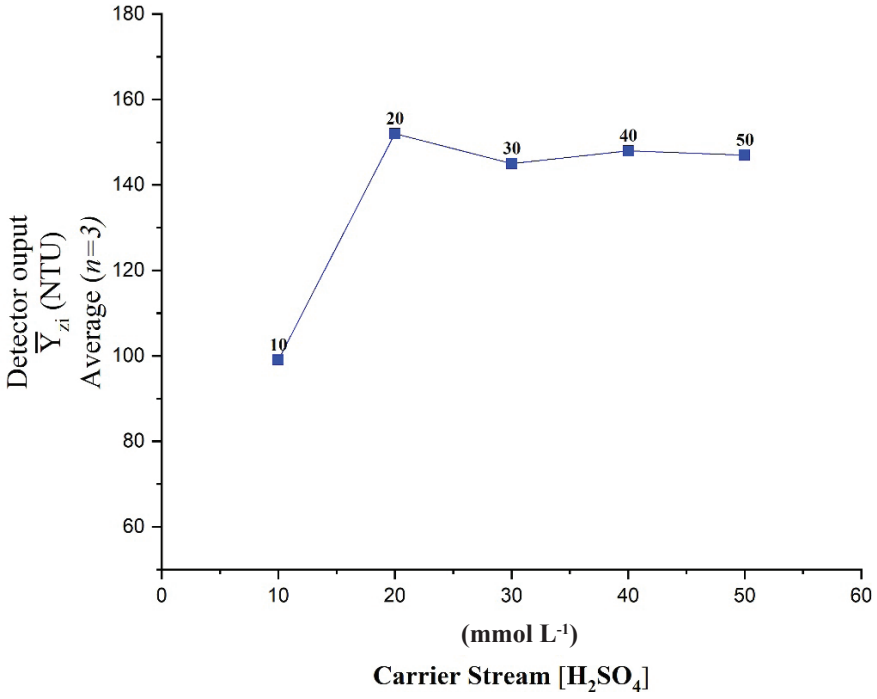

Fig.7. Optimization the concentration of sulfuric acid

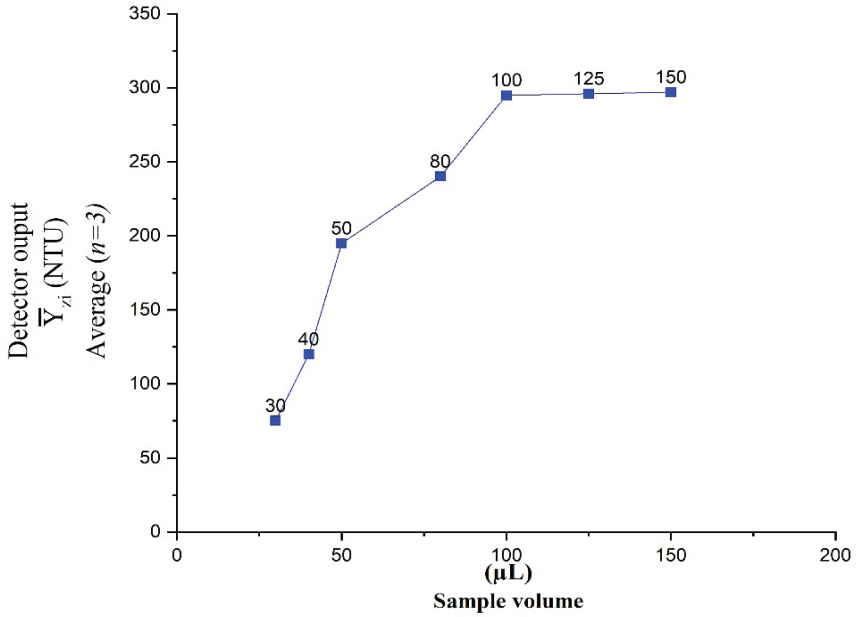

Fig. 8. The effect of the injected sample volume of promethazine [µL] on the determination of promethazine using experimental conditions: flow rate of lines 1.0 ml min^{-1}, STPB (30 µg mL^{-1}) and open valve mode.

Figure 8, 100 µL was the ideal sample segment. One of the most common physical characteristics that need to be optimized in any flow system is the flow rate. Therefore, flow rates of 0.2-4.0 mL min^{-1} were used to propel the two lines (carrier stream and reagent line). The greatest signal was attained at 2.0 mL min^{-1} based on the acquired data, as shown in Figure 9. As a result, this flow rate of 2.0 mL min^{-1}

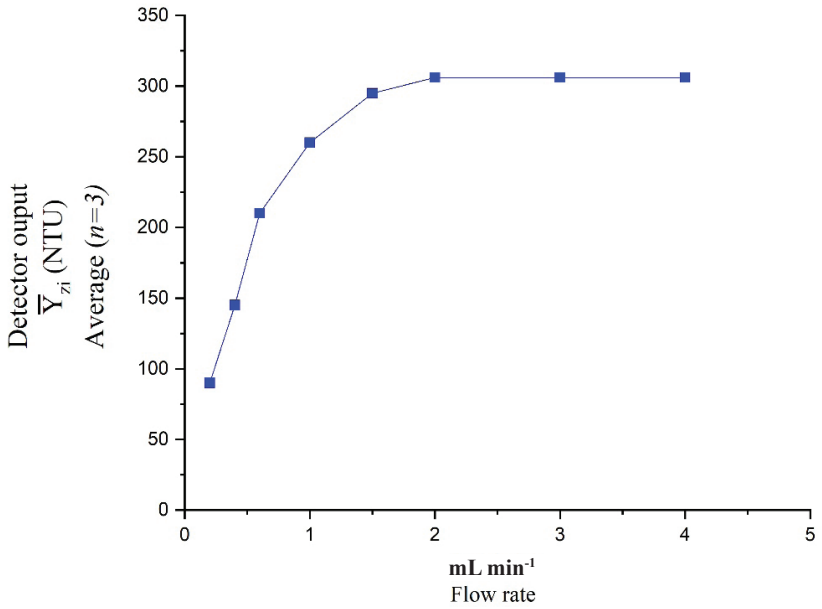

Fig. 9. The effect of the flow rate of lines [ml min^{-1}] on the determination of promethazine using experimental conditions: 100 µL of promethazine (50 µg ml^{-1}), STPB (30 µg ml^{-1}) and open valve mode.

was selected for use in further experiments.

Finally, to guarantee that the reaction between the promethazine and the organic reagent (STPB) was complete, mixing coils of various lengths (0–20 cm) were used. The highest-profile signal was seen at a distance of 10 cm; however, using mixing coils longer than 10 cm caused the peaks to spread, which is not desired in flow systems. As a result, the ideal mixing coil is 10 cm, which was employed in further studies as shown in Figure 10. Table 1 shows the optimal concentration ranges for all physical and chemical characteristics

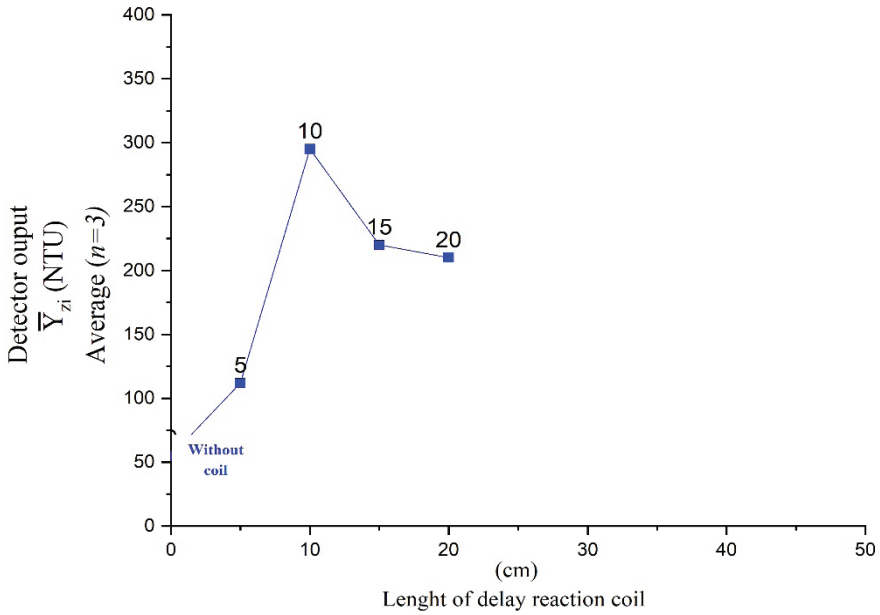

Fig.10. The effect of using variable mixing coil lengths [cm] on the determination of promethazine using experimental conditions: flow rate of lines 2.0 mL min^{-1}, open valve mode STPB (30 µg mL^{-1}) and sample volume (100 µL).

Table 1. The optimum flow characteristics for the determination of Promethazine

Studied flow parameters	Applied Ranges		Optimum value
	From	To	
STPB concentration (µg ml^{-1})	0.5	50	30
H_2SO_4 concentrations (mmol L^{-1})[a]	10	50	25
Flow rates (mL min^{-1})[b]	0.2	4.0	2.0
Mixing coil length (cm) [b]	without	20	10
Sample volume (Injected (µL)) [b]	30	150	100

[a] The carrier streamline that carries the sample segment into the manifold system
[b] The flow rates of both lines (carrier and reagent)
[c] This part is placed after the Y-junction point to ensure the reaction is completed

examined.

The following values were chosen for flow injection parameters: STPB 30.0 µg mL^{-1}, sulfuric acid 20 mmol L^{-1}, flow rate 2.0 mL min^{-1}, 100 µL injected-sample volume and 10 cm mixing coil. With this setup and to generate the analytical curves, a series of standard promethazine hydrochloride concentrations were run in triplicate. The results for the 0.5-90 µg mL^{-1} range are illustrated in Table 2. The linearity range of the flow system integrated turbidimetric method was 0.5-90 µg mL^{-1}. The statistical examination of the linear range regression equation revealed low values of RSD %, slope (b), and high values of (r) with a detection limit of 0.35 µg mL^{-1}. Table 2 summarizes the statistical studies of the calibration curve.

The flow system repeatability was examined for promethazine hydrochloride solution containing two concentrations 20 µg mL^{-1} and 50 µg mL^{-1}, across 5 injections for each concentration resulting in a total of 10 determinations (Table 3). The relative standard deviations for the turbidimetric measurements were less than 2.0 %. And it was within the acceptance limit of ICH (The International Council for Harmonisation of Technical Requirements for Human Use) and the FDA (Food and Drug Administration) [32]. The limited sample throughput, i.e., 50.0 determinations per hour, was not accounted for by the cell washing time; however, this number may be increased by running at greater flow rates, with a minor loss in

Table 2. The developed method's statistical description of the linear equation for determining Promethazine

Linear equation Parameter	Promethazine
Linearity (µg ml^{-1})	0.5-90
Linear Equation	139.61129.5441+4.1325± C[a]±0.5221
Intercept	139.6112±9.5441
Slope	4.1325 ±0.5221
r[b]	0.9967
R^2 [c]	0.9935
LOD (mmol L^{-1})[d]	(0.35 µg ml^{-1})
% RSD [e]	Less than 2.0

[a] The detector signal in NTU for the concentration of C µg ml^{-1}
[b] Correlation coefficient
[c] Coefficient of determination
[d] The limit of detection
[e] The relative standard deviation percentage for *n=3*

Table 3. The results of the proposed method's repeatability assay for determining Promethazine

[Promethazine] (µg ml^{-1})	Detector signal in NTU	RSD %
20	230.552	0.52
50	271.225	0.19

sensitivity of the absorbance peak heights.

3.2. Applications

Promethazine hydrochloride was successfully determined in pharmaceutical preparations such as Histazine tablets (25 mg/tablet) and Phenergan tablets (25 mg per tablet) using the proposed method. Table 1 summarizes the optimal assay conditions for promethazine. The analyte was quantified using typical calibration curves in a defined concentration range and the method of standard additions for both commercial tablets. The turbidimetric data has a linear response and a decent curve fitting through the same equation that was observed in the calibration curve of standard material. The results are described in Tables 4 and 5, which also include a comparison of the suggested and official spectrophotometric (measuring the absorption band at 297 nm) methods for determining promethazine in Histazine tablets (25 mg per tablet) and Phenergan tablets (25 mg per tablet). The two sets of data are nearly identical and are consistent with the nominal value (25 mg per tablet). The value of promethazine is determined by the manufacturer during manufacturing and quality control (to improve shelf time, this medicine is routinely produced with a 10 % excess of active pharmaceutical ingredients). The manufacturer employs a time-consuming multi-step extraction procedure followed by spectrophotometric analysis of the promethazine absorbance peak at 297 nm. It really should be obvious that the novel flow turbidimetric approach is quicker and does not

Table 4. Assay results for Promethazine determination in real commercial samples using official and developed methods

PCP	VL (mg)	t[a]	F[a]	Found [b] *(n=3)*	
				Developed method	**Official method**
				FIA-turbidity	**UV λmax $_{297}$**
Material A	25	0.521	0.955	25.022±•‚12	25.122±•‚32
Material B	25	1.231	1.655	24.9550.024±	25.2441±•‚•5

PCP: Promethazine Commercial product
VL: Claimed label
Material A: Histazine 25 mg, ® United pharmaceutical, Jordan
Material B: Phenergan 25 mg ® (GLOBAL manufacturer Sanofi United pharmaceutical, UK)
[a] the tabulated values of F and t at P=0.05 (95%) are (2.168) and (2.093) respectively. [33]
[b] mean test % of label claimed ± SD

Table 5. The recovery results achieved by applying the standard addition method to the developed method

Promethazine Preparations	Promethazine in solution (mg)	Added (mg)	Total found (mg)	Recovery % [a] (mg)
Material A	25.022	5	30.225	100.61
Material A	25.022	10	36.233	100.58
Material B	24.955	5	29.995	100.13
Material B	24.955	10	35.245	100.82

[a]Average of three Promethazine determinations
Material A: Histazine 25 mg, ® United pharmaceutical, Jordan
Material B: Phenergan 25 mg ® (GLOBAL manufacturer Sanofi United pharmaceutical, UK)

require any prior extraction processes.

4. Conclusion

Because the manifold system can perform 50 tests per hour, the design of this flow cell boosts its throughput, making it an effective instrument for routine analysis of active pharmaceutical ingredients. Using the design flow cell can increase the speed of measurements, minimize the number of chemical tools that must be ordered, cleaned and stored, and finally, eliminate the need for matched sample cells. The developed method for determining promethazine hydrochloride in pure form or in pharmaceutical dosage forms is straightforward, quick, and accurate. It's a great illustration of the turbidimetric approach's potential and attractiveness for analytical applications, either alone or in tandem with FIA techniques. The combined approaches (FIA and turbidity measurements) help to increase method validity by allowing for analysis of the sample in a very short time (one minute), which is important in increasingly complicated samples. Therefore, as a rule, the interfering compounds included in this sort of matrix, such as excipients (sugar, propylene glycol, dyes, ascorbic) usually do not create difficulties. Promethazine analytical recoveries varied from 100.13 to 100.81 %. At the 95 % confidence level, the levels of promethazine estimated by the proposed approach and amounts obtained by the official method were not considerably different. The proposed approach is low-cost, simple, and safe to use, uses little sample and reagent, and allows for quantitative measurement of the target analyte in both pure and dosage forms. The proposed flow cell is acid-resistant and does not require special care by the analyst. So, the presented technique has better sensitivity and the capacity to perform the reaction under the high acidity of the reaction medium. The apparatus is readily available in any analytical laboratory, and the manifold system cell may be constructed from affordable components, resulting in little reagent usage.

5. Funding and Conflicts of Interest

This work was supported by the authors and the authors declare no conflicts of interest

6. Acknowledgments

The authors are grateful to Professor Dr. Issam M. A. Shakir for his support and his help in typing the manuscript

7. References

[1] A.A. Ensafi, P. Nasr-Esfahani, B. Rezaei, Synthesis of molecularly imprinted polymer on carbon quantum dots as an optical sensor

for selective fluorescent determination of promethazine hydrochloride, Sensors and Actuators B: Chem., 257 (2018) 889-896. https://doi.org/10.1016/j.snb.2017.11.050

[2] M.J. Saif, J. Anwar, A new spectrophotometric method for the determination of promethazine–HCl from pure and pharmaceutical preparations, Talanta, 5 (2005) 869-872. https://doi.org/10.1016/j.talanta.2005.03.034

[3] T. Potaros, S. Yeephu, Recognition of tramadol abuse, dispensing practices, and opinions about its control policy among community pharmacists in Bangkok, Thailand, Asian Biomed., 12 (2018) 91-99. https://doi.org/10.1515/abm-2019-0006

[4] K.L. Lynch, B.J. Shapiro, D. Coffa, S.P. Novak, A.H. Kral, Promethazine use among chronic pain patients, Drug Alcohol Depend., 150 (2015) 92-97. https://doi.org/10.1016/j.drugalcdep.2015.02.023

[5] S.W. Gust, J. McCormally, National Institute on Drug Abuse International Program: improving opioid use disorder treatment through international research training, Curr. opin. psychiatry, 31 (2018) 287-293. https://doi.org/10.1097/YCO.0000000000000426

[6] J.A. Ford, M.S. Hinojosa, H.L. Nicholson, Disability status and prescription drug misuse among US adults, Addict. Behav., 85 (2018) 64-69. https://doi.org/10.1016/j.addbeh.2018.05.019

[7] P.J. Joudrey, G. Bart, R.K. Brooner, L. Brown, J. Dickson-Gomez, A. Gordon, Research priorities for expanding access to methadone treatment for opioid use disorder in the United States: A National Institute on Drug Abuse Clinical Trials Network Task Force report, Subst. abuse, 42 (2021) 245-254. https://doi.org/10.1080/08897077.2021.1975344

[8] A. Phonchai, S. Pinsrithong, B. Janchawee, S. Prutipanlai, O. Botpiboon,N. Keawpradub, Simultaneous determination of abused prescription drugs by simple dilute-and-shoot gas chromatography–flame ionization detection (GC-FID), Anal. Lett., 4 (2021) 716-728. https://doi.org/10.1080/00032719.2020.1779738

[9] N.M. Njuguna, K.O. Abuga, F.N. Kamau, G.N. Thoithi, A liquid chromatography method for simultaneous determination of diphenhydramine, promethazine, chlorpheniramine and ephedrine in cold-cough syrups, Pharm. Chem. J., 2 (2017) 153-158. https://doi.org/10.1016/j.jpba.2007.06.003

[10] P.F. Pereira, M.C. Marra, R.R. Cunha, W.P. da Silva, R.A.A. Munoz, E.M. Richter, Two simple and fast electrochemical methods for simultaneous determination of promethazine and codeine, J. Electroanal. Chem., 713 (2014) 32-38. https://doi.org/10.1016/j.jelechem.2013.11.031

[11] R.R. Cunha, M.M.A.C. Ribeiro, R.A.A. Muñoz, E.M. Richter, Fast determination of codeine, orphenadrine, promethazine, scopolamine, tramadol, and paracetamol in pharmaceutical formulations by capillary electrophoresis, J. Sep. Sci., 40 (2017) 1815-1823. https://doi.org/10.1002/jssc.201601275

[12] P. Chen, X. Hu, S. Liu, Z. Liu, Y. Song, Study on the resonance nonlinear scattering spectra of the interactions of promethazine hydrochloride and chlorpromazine hydrochloride with 12-tungstophosphoric acid and their analytical applications, Spectrochim. Acta Part A: Mol. Biomol. Spect., 77 (2010) 207-212. https://doi.org/10.1016/j.saa.2010.05.009

[13] A. Lantam, W. Limbut, A. Thiagchanya, A. Phonchai, A portable optical colorimetric sensor for the determination of promethazine in lean cocktail and pharmaceutical doses, Microchem. J., 159 (2020) 105519. https://doi.org/10.1016/j.microc.2020.105519

[14] J.M. Calatayud, V.G.J.A. Mateo, Cerium (IV) arsenite as a solid-phase reactor for use in flow-injection analysis. Spectrophotometric determination of promethazine, Anal.

Chim. Acta, 264 (1992) 283-9. https://doi.org/10.1016/0003-2670(92)87016-E

[15] S. Thumma, S.Q. Zhang, M.A. Repka, Development and validation of a HPLC method for the analysis of promethazine hydrochloride in hot-melt extruded dosage forms, Die Pharmazie-An Int. J. Pharm. Sci., 63 (2008) 562-567. https://doi.org/10.1691/ph.2008.08.8022

[16] O.A. Saleh, A.A. El-Azzouny, H.Y. Aboul-Enein, A.M. Badawy, A validated HPLC method for separation and determination of promethazine enantiomers in pharmaceutical formulations, Drug Dev. Ind. Pharm., 35 (2009) 19-25. https://doi.org/10.1080/03639040802130095

[17] R. Sakthivel, S. Kubendhiran, S.M. Chen, Facile one-pot sonochemical synthesis of Ni doped bismuth sulphide for the electrochemical determination of promethazine hydrochloride, Ultrason. Sonochem., 54 (2019) 68-78. https://doi.org/10.1016/j.ultsonch.2019.02.013

[18] P. Xiao, W. Wu, J. Yu, F. Zhao, Voltammetric sensing of promethazine on a multi-walled carbon nanotubes coated gold electrode, Int. J. Electrochem. Sci., 2 (2007) 149-157. http://www.electrochemsci.org/papers/vol2/2020149.pdf

[19] D. Daniel, I.G.R. Gutz, Flow injection spectroelectroanalytical method for the determination of promethazine hydrochloride in pharmaceutical preparations, Anal. Chim. Acta, 494 (2003) 215-224. https://doi.org/10.1016/S0003-2670(03)00903-6

[20] A.K. Hassan, B. Saad, S.A. Ghani, R. Adnan, A.A. Rahim, N. Ahmad, Ionophore-based potentiometric sensors for the flow-injection determination of promethazine hydrochloride in pharmaceutical formulations and human urine, Sensors, 11 (2011) 1028-1042. https://doi.org/10.3390/s110101028

[21] H.S. Jabbar, A.T. Faizullah, Flow injection analysis with chemiluminescence detection for determination of two phenothiazines, Int. J. Pharm. Sci. Res., 6 (2015) 474-481. http://www.ijpsr.info/

[22] I.M.A. Shakir, N.S. Turkey Flow injection analysis for the photometric determination of promethazine-HCl in pure and pharmaceutical preparation via oxidation by persulphate using Ayah 3SX3-3D solar micro photometer, Baghdad Sci. J., 10 (2013)1190-1202. https://doi.org/10.21123/bsj.2013.10.4.1190-1202

[23] J.S. Mayausky, R.L. McCreery, Spectroelectrochemical examination of charge transfer between chlorpromazine cation radical and catecholamines, Anal. Chem., 55 (1983) 308-312. https://doi.org/10.1021/ac00253a029

[24] J. López-Palacios, A. Colina, A. Heras, V. Ruiz, L. Fuente, Bidimensional spectroelectrochemistry, Anal. Chem., 73 (2001) 2883-2889. https://doi.org/10.1021/ac0014459

[25] N.S. Turkey, J.N. Jeber, Flow injection analysis with turbidity detection for the quantitative determination of mebeverine hydrochloride in pharmaceutical formulations, Baghdad Sci. J., 19 (2022) 141-154. https://doi.org/10.21123/bsj.2022.19.1.0141

[26] N.S. Turkey, J.N. Jeber, Light scattering detector based on light-emitting diodes-Solar cells for a flow analysis of Warfarin in pure form and pharmaceutical formulations, J. Phys. Conf. Ser., 2063 (2021) 012006. https://doi.org/10.1088/1742-6596/2063/1/012006/meta

[27] J.N. Jeber, N.S. Turkey, An optoelectronic flow-through detectors for active ingredients determination in the pharmaceutical formulations, J. Pharm. Biomed. Anal., 201 (2021) 114128. https://doi.org/10.1016/j.jpba.2021.114128

[28] N.S. Turkey, J.N. Jeber, A flow analysis system integrating an optoelectronic detector for the quantitative determination of active ingredients in pharmaceutical formulations, Microchem. J., 160 (2021) 105710. https://doi.org/10.1016/j.microc.2020.105710

[29] J.N. Jeber, N.S. Turkey, A turbidimetric method for the quantitative determination of cyproheptadine hydrochloride in tablets using an optoelectronic detector based on the LEDs array, Int. J. Pharm. Res., 12 (2020) 2911-2924. https://doi.org/10.31838/ijpr.2020.12.04.401

[30] British Pharmacopoeia BP. The stationary office. London; 2008. https://www.worldcat.org/title/british-pharmacopoeia-2009/oclc/246965234

[31] H.R. Silva, M.A. Segundo, A.O.S.S. Rangel, Use of a mixing chamber for sample preparation and multiple collection in sequential injection analysis: determination of sulfate in wines, J. Brazil. Chem. Soc., 14 (2003) 59-64. https://doi.org/10.1590/S0103-50532003000100010

[32] S. Walfish, Analytical methods: a statistical perspective on the ICH Q2A and Q2B guidelines for validation of analytical methods, BioPharm. Int., 19 (2006) 40-45. https://www.biopharminternational.com/view/analytical-methods-statistical-perspective-ich-q2a-and-q2b-guidelines-validation-analytical-methods

[33] P.C. Meier, RE. Zünd Statistical methods in analytical chemistry, John Wiley and Sons, 456 pages, 2005. https://www.wiley.com/en